Ultra-high performance fiber-reinforced concrete in incremental bridge launching

A study on the application of UHPFRC in the superstructure of an incrementally launched box girder bridge in The Netherlands

Master's Thesis – Main Study

A.J. Oostra

18-08-2015

Ultra-high performance fiber-reinforced concrete in incremental bridge launching

A study on the application of UHPFRC in the superstructure of an incrementally launched box girder bridge in The Netherlands

By

A.J. Oostra

Bachelor of Built Environment, Hogeschool van Amsterdam (2011).

Student number: 4183770.

Submitted to the Department of Structural Engineering
in partial fulfillment of the requirements for the degree of

Master of Science in Civil Engineering

at the Delft University of Technology,

to be defended publicly on Thursday August 27, 2015 at 11:00 AM.

Supervisor:	Dr. ir. C. van der Veen,	TU Delft
Thesis committee:	Prof. dr. ir. D.A. Hordijk (chairman),	TU Delft
	Prof. ir. A.Q.C. van der Horst,	TU Delft
	Ir. A.D. Reitsema,	TU Delft
	Ir. C.M.P. 't Hart,	Royal HaskoningDHV
	Ir. M. Kortenaar,	Royal HaskoningDHV

TU Delft Delft University of Technology

Royal HaskoningDHV
Enhancing Society Together

Preface

The findings of this thesis are the result of the graduation project on ultra-high performance fiber-reinforced concrete in incremental bridge launching. The study focuses on the application of UHPFRC in the superstructure of an incrementally launched bridge in The Netherlands and explores the competitiveness of the concept. The graduation project is the last step in completion of the Master's degree program at Delft University of Technology and has been conducted with the engineering consultancy Royal HaskoningDHV.

Completing this thesis would not have been possible without a number of people I would like to thank at this moment. First of all, I would like to thank my graduation committee: dr. ir. C. van der Veen, prof. ir. A.Q.C. van der Horst, prof. dr. ir. D.A. Hordijk, ir. A.D. Reitsema, ir. M. Kortenaar and ir. C.M.P. 't Hart for their assistance and inspiring ideas. Secondly, I would like to thank my parents for their support. And lastly, I would like to thank Marc for reviewing the report and suggesting improvements.

Arjen Oostra
Hoofddorp, August 2015

Abstract

Incremental bridge launching is one of the many ways in which a bridge can be constructed. In The Netherlands this method is not often used. This may be explained by the fact, that there are not many suitable locations for application of this method. Incremental bridge launching is profitable for long bridges and can only be used for straight bridges or when the superstructure has a constant horizontal and vertical radius throughout the length. However, when the preconditions for use of this method are met, incremental bridge launching can be a great solution for bridge design.

Ultra-high performance fibre-reinforced concrete (UHPFRC) is a new concrete. In contrast to regular reinforced concrete, UHPFRC contains fibers to provide for the capacity that is necessary when the concrete is loaded in tension. However, as for incrementally launched bridges, its application is limited as of yet. One explanation for the reluctance to use the material, is that compared to regular concrete, the cost of production are many times higher. To make economical designs using UHPFRC, the high cost of production need to be recovered by material savings, when a structure is executed or during its lifetime.

The aim of this thesis is to identify whether a superstructure designed in UHPFRC can increase the application range of incremental bridge launching in The Netherlands, and to explore whether the concept can compete with other bridge designs. In order to make a statement, a case study approach is used. It concerns the launch of the eastern approach bridge of the bridge over “Het Pannerdensch Kanaal”, designed in UHPFRC. The location suits incremental bridge launching perfectly, as there is a constant horizontal and vertical curvature in the alignment for over 550 meters.

The most favorable cross-section for incrementally launched bridges is a box girder. A comprehensive analysis on the cross-sectional capacity of a prestressed box girder, designed with different concrete strength classes, is performed to optimize the shape. The design of a box girder takes a special procedure, where both the transverse and longitudinal directions are considered separately. Transverse bending moments and shear forces, due to mobile loading, are obtained with influence surfaces and the differential equation of the Euler-Bernoulli bending beam. For the longitudinal direction, a spreadsheet is developed to identify the bending moments and shear forces that occur during launch and service life. The force method for analysis of indeterminate structures is used to determine the governing bending moments for this multiple span bridge. Also, the sheet contains parts to determine the required amount of central and continuity prestressing and to optimize the length of the steel nose to reduce the peak moments during launch.

The use of UHPFRC in the design of a structure requires a special approach. Requirements regarding quality control are strict and need to be prescribed to allow on-site production. The typical characteristics of UHPFRC have an important impact on the execution and production cycle of the incrementally launched bridge, which is therefore investigated. The case study is used to investigate the competitiveness of the design. Cost of production and execution are integrated into a price per cubic meter of concrete and compared to the design of The Zeeburgerbrug, which was launched and built with regular concrete.

Efficient use of UHPFRC allows a light box girder design, which can be launched without auxiliary supports. Conventional and shear reinforcement are not necessary. Transverse and longitudinal prestressing provide sufficient bending moment capacity, while the fibers contribute to a huge shear capacity that is more than enough to withstand the shear forces. The required amount of central and continuity prestressing does not fit in the concrete cross-section. Therefore, all tendons are applied externally. The anchors and deviators will not fit in the concrete cross-section either.

The cost comparison shows, that a lot of the higher cost of production of UHPFRC can already be compensated during the design and construction phases. The remaining part of the higher cost of production of UHPFRC need to be compensated differently, for instance by savings in maintenance cost due to better durability properties or by a lighter substructure, as we are able to generate proper savings in the amount of concrete for the superstructure.

The case study proves that when the superstructure is considered only, it might be hard to design and execute the UHPFRC box girder more economically than the design of The Zeeburgerbrug. However, when we consider the total bridge over the entire service life, we might have a competitive design. Alternative bridge designs, that use different construction techniques should be developed to assess the competitiveness of the incrementally launched UHPFRC box girder for that location.

Table of Contents

1 Introduction

1.1 Problem indication

In The Netherlands, incremental bridge launching is a construction technique that is not often used. However, in a recent Croatian study by (Mandic Ivankovic, et al., 2014), incremental bridge launching proved to be very competitive to other bridge execution methods. Also, (Rosignoli, 1997) showed that incrementally launched bridges without auxiliary supports are located in the area of transition between constant and variable height superstructures. Since variable height superstructures generally have higher construction cost and longer construction times, increasing the application range of full span incremental bridge launching is obviously beneficial. Besides that, research on the application of new concretes, like ultra-high performance fiber-reinforced concrete, is an important subject at Delft University of Technology. This study contributes to current research by providing insights on whether UHPFRC can increase the application range of incremental bridge launching and whether the combination results in an economical bridge design.

1.2 Scope

In incremental bridge launching, the superstructure of a bridge is manufactured by sections on one of the abutments. Each new segment is poured directly against the preceding one and after it has hardened, the whole structure is moved forward towards the span. Therefore, the study aims on the design and execution of the superstructure of the bridge and does not consider the substructure. The application of a new material in bridge construction requires vast expertise on material behavior. Especially development of mechanical properties during early age and properties regarding execution play a crucial role and need to be studied.

1.3 Research goal and method

The aim of the study is to explore whether the superstructure of an incrementally launched box girder bridge can be designed and executed in UHPFRC and if the concept can compete with bridge designs that use other construction techniques. A case study approach is used to make a statement and to identify the associated boundary conditions and external factors and to prescribe the requirements that apply to this situation.

1.4 Thesis outline

Chapter 2 summarizes the most important findings in reviewing the literature on UHPFRC and incremental bridge launching and provides an overview of research goals for the main study. Chapter 3 presents the results obtained from the analysis of the cross-sectional capacity of different types of beams designed with different types of concrete. In chapter 4 the hardening properties of UHPFRC and the quality of concrete are discussed, while Chapter 5 provides typical mixture compositions and preconditions for on-site production and application of the material.

Chapter 6 describes the case study with corresponding requirements, boundary conditions and design assumptions. In chapter 7 the shape of the box girder and dimensions for preliminary design are defined. Chapter 8 starts with the special procedure for box girder design and then analyzes the transverse direction. Chapter 9 investigates the force distribution in longitudinal direction.

Finally, in chapter 10 and 11, the execution of the incrementally launched UHPFRC box girder is described and the cost are compared to the design of The Zeeburgerbrug, which used normal strength concrete. Chapter 12 and 13 contain the conclusions and recommendations for further research.

2 Literature review

This chapter summarizes the most important findings obtained from the literature review on incrementally launched bridges and UHPFRC. Paragraph 2.13 presents the research goals for the main study.

2.1 The construction method of a traditional incrementally launched bridge

The superstructure of an incrementally launched bridge is made up of sections, manufactured in a fabrication yard behind one of the abutments. Conditions similar to those in a factory can be reached, making high quality production possible. Each new unit is poured directly against the preceding one and after it has hardened is pushed towards the span by a hydraulic jacking device. In all bridges that were explored during literature review (Oostra, 2014), construction of one unit took about a week after which all operations were repeated. The exact interpretation of such a cycle depends on whether the box girder will be cast in one or two phases. The weekends will be used for the concrete to harden.

The bridge supports are equipped with temporary sliding bearings to reduce friction during launch. The bearings usually consist of a high quality concrete block covered with a stressed chrome-steel plate. Steel reinforced neoprene sliding plates, with a Teflon coating on one face, should be able to be inserted without difficulty.

The conditions during erection are of great influence upon the economy of the superstructure. A lightweight nose is mounted to the cantilevering superstructure to reduce the cantilever moment during launch. Alternatively the front end can be guyed from a mast. For bridges with very long spans the use of auxiliary piers during erection may be beneficial.

During launch the superstructure is subjected to alternating bending moments. Each cross-section moves from regions of positive moments into regions of negative moments. To withstand these moments central prestressing is used. Central prestressing means that prestressing is arranged such that at all points the cross-section is equally compressed. Usually the central prestressing is positioned in the deck and floor.

When the superstructure has been completely launched, the continuity tendons are stressed. Their arrangement is designed according to the bending moments occurring in the use phase. The continuity prestressing is normally located in the webs and is anchored and stressed at buttresses on their inner faces. The continuity prestressing has a draped profile and is ideally anchored at the points of contra flexure in the bending moment diagram.

2.2 Preconditions for use of incrementally launched bridge construction

Incremental bridge launching has the following preconditions:

- Incremental bridge launching can be used for straight bridges or when the superstructure has a constant horizontal and vertical radius throughout the length.
- All segments should exactly fit into the span to achieve high repetition in lay-out of reinforcing and prestressing steel.

2.3 The cross-section of an incrementally launched box girder bridge

When a favorable cross-section has been chosen one can make considerable savings in the required amount of central prestressing. The following requirements should be met:

1. The superstructure should be designed as light as possible.
2. The ratio of moment of resistance above and beneath the neutral axis should be similar to the ratio of support moments to span moments. This requires the moment of resistance of the top part to be about twice the moment of resistance of the bottom part.
3. The core width, i.e. the ratio between moment of resistance and cross-sectional area, should be as large as possible.

These three conditions are best fulfilled by a box girder with cantilevers. The required amount of central prestressing is about equal above the support and in the span.

The width of the web in the span is dominated by the shear forces which appear when the section passes a support. The width of the web at the support is governed by the shear forces that occur in the use phase.

During launch, every cross-section of the deck is subjected to the same transitory stresses. A great uniformity of cross-section along the deck is necessary. Mid-span sections cannot be designed lighter, but would be beneficial as the span increases and is often done with other construction techniques.

The cross-section moves between the two limit configurations shown in Figure 2.1. Configuration (a) represents the use phase. In configuration (b) the superstructure has advanced by half a span. In both configurations, the cross-sections at mid-span are rarely overloaded, because the combination of lower shear forces and a lower bending moment than under live loads often only require sufficient prestressing to withstand tensile stresses in the bottom floor.

With respect to the cross-section above the support, configuration (b) is governing. In configuration (b) the cross-section is subjected to maximum negative moment and maximum shear, while in final position it will be at mid-span and needs to withstand positive moments and slight shear. These transient stresses tend to cause an oversized cross-section with respect to the use phase.

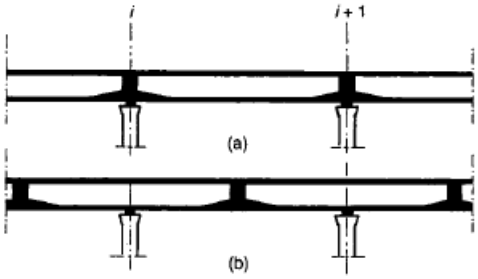

Figure 2.1: Limit configurations during launching (Rosignoli, 1997).

2.4 Loading during launch

In (Iversen, et al., 1993), the launch of the 21 span Dornoch Firth Bridge was analyzed. To investigate the effects of launch on the leading units, a six-span structure was modeled with a steel launch nose attached to the first unit and the rear support being a clamped support. Peak moments developed during launch over approximately the first 60 meters of the superstructure, as shown in Figure 2.2.

(Bourne, et al., 2009) discussed the effects of launch of the Clackmannanshire Bridge on its bending moment diagram. Figure 2.3 illustrates that even with a 35 meters long launching nose the bending moments in the first two spans were around 25% higher than in the remaining spans. Instead of the ultimate bending moment capacity, cracking appeared to be critical in the design. The engineers decided to reduce the reinforcement bar spacing to obtain a more fine cracking pattern.

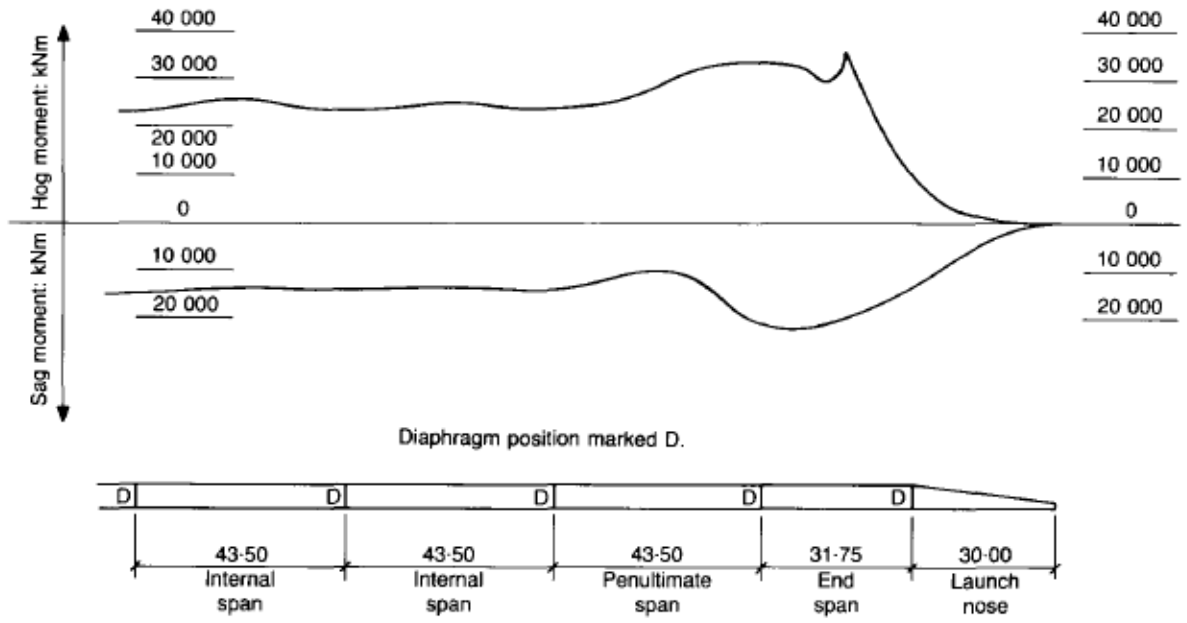

Figure 2.2: Self-weight bending moment diagram during launch (Iversen, et al., 1993).

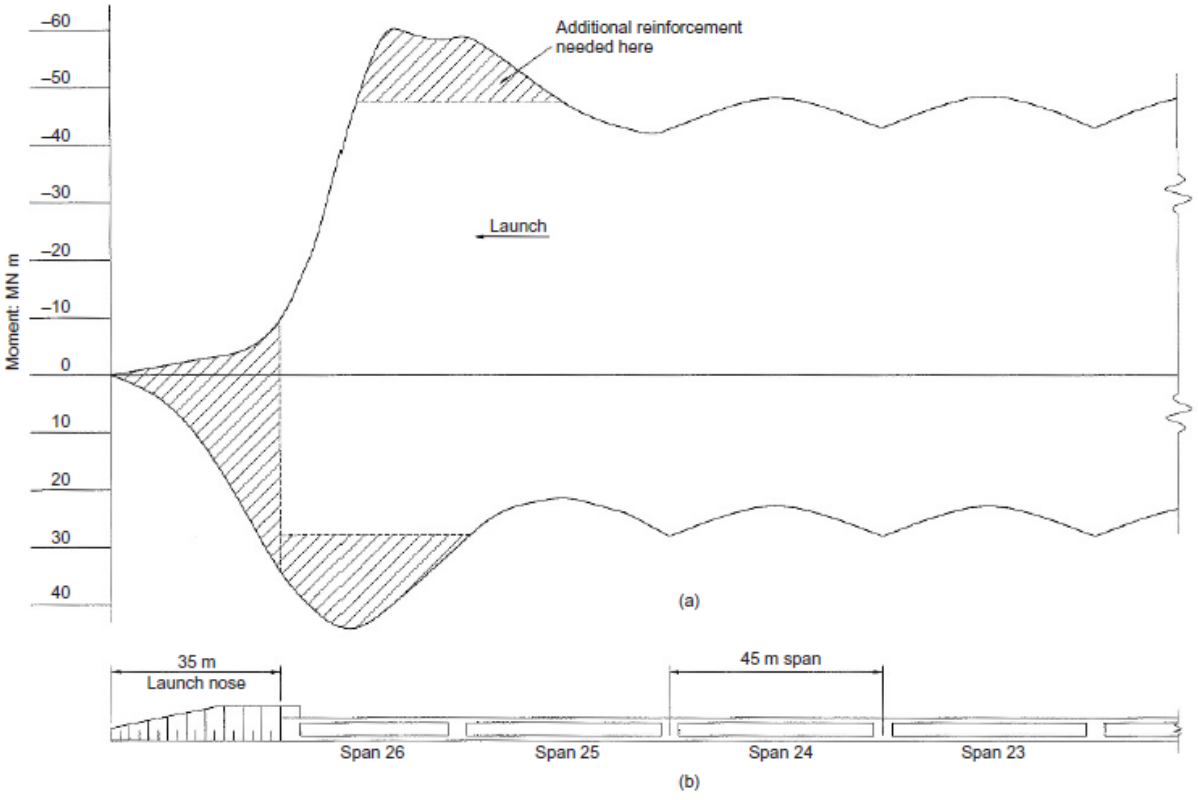

Figure 2.3: Bending moments due to launching effects (Bourne, et al., 2009).

2.5 Cost

The incremental bridge launching method saves manpower and equipment compared to other in-situ construction methods. However, the consumption of materials is higher because of the required uniformity of the cross-section and central prestressing for the launching phase. The result is a higher self-weight ρ of the superstructure.

The structural efficiency can be calculated as:

$$\rho = \frac{p_{live}}{q + p_{live}}$$

The live load p_{live} being equal, incrementally launched bridges have a lower efficiency than bridges that used other construction techniques. To increase this efficiency without an increasing consumption of materials, the moment of inertia should increase while maintaining the self-weight. This can be achieved by increasing the overall height of the cross-section to increase the internal lever arm, which, unfortunately, causes the structure to lose its slenderness.

Constant height box girders built with alternative techniques often have spans less than 40 meters. This is due to the fact that higher construction cost are found for longer spans and variable height cross-sections are more efficient.

Incrementally launched bridges without temporary piers are located in the area of transition between constant and variable height superstructures. Since variable height cross-sections usually have higher construction cost and longer construction times, increasing the application range of full span incremental bridge launching is obviously beneficial.

To reduce self-weight and consumption of materials, research on Ultra-High Performance Concrete and external prestressing may be interesting.

The optimum length of the mould can be found when assembly cost and launching cost are at their minimum.

$$K = B \times K_b + \frac{L}{B} \times K_v + C$$

B: length of the mould (m).

K_b: cost per meter of formwork.

L: total length of launching part (m).

K_v: cost per launching operation.

L/B: number of launching operations.

C: cost independent on B.

K is at its minimum when $dK/dB = 0$.

$$\frac{dK}{dB} = K_b - \frac{LK_v}{B^2} = 0 \rightarrow K_b = \frac{LK_v}{B^2} \rightarrow B^2 = \frac{LK_v}{K_b} \rightarrow B = \sqrt{\frac{LK_v}{K_b}}$$

2.6 Benefits of incremental bridge launching

Compared to other construction techniques, incremental bridge launching has the following advantages:

- The superstructure can be erected without stationary falsework that would disturb the environment. The so-called 'traffic fine' – a penalty for crossing a road and when it has to be closed temporarily – can be confined.
- The concentration of the building site and concrete batch plant behind one of the abutments keeps the transportation distances extremely short.
- Construction is safe, because the complete bridge can be erected from one of the abutments and no construction on falsework or at a balanced cantilever is necessary.
- A more sustainable superstructure can be designed compared to other construction techniques due to longer elements and thus fewer joints. Furthermore, each new segment will be poured directly onto its predecessor, which results in watertight joints. Cracking near joints will be limited due to continuous longitudinal reinforcement. All these properties may contribute to less maintenance.

2.7 Drawbacks on incremental bridge launching

There are not a lot of incrementally launched bridges built in The Netherlands. The reason may be one of the following:

- The location is not suitable for this construction method, because of: a short bridge, short spans, low road alignment (construction with precast girders will be cheaper), complex road geometry, no space for a temporary fabrication yard, environment can be disturbed (in-situ construction on scaffolding will be cheaper).
- The consumption of materials is high, because a great uniformity of cross-section and central prestressing for the launching operation are required.
- Incrementally launched bridges have a less slender superstructure than bridges built with other construction techniques.
- Web thickness at mid-span may increase for longer spans as opposed to bridges built with other construction techniques. This is due to the temporary shear forces which appear when a section passes a support.
- Due to the static scheme of a continuous beam on many supports, horizontal forces may become very large. The substructure must be designed to withstand these forces and is therefore likely to become heavy.

2.8 The competitiveness of incremental bridge launching in Croatia

In a study by (Mandic Ivankovic, et al., 2014), where the competitiveness of incremental bridge launching in Croatia was investigated, the following conclusions were made:

- Bridges built by incremental launching have the shortest construction time and cost when they are suitable for application of this construction method. Incrementally launched bridges can be economic for longer bridges, for spans over 30 meters and for higher road alignment.
- For shorter bridges and in case of complex road geometry, bridge construction on fixed scaffolding or with precast girders is more suitable.
- Due to large investment cost in equipment, erection on movable scaffolding is limited to bridges longer than 200 meters. In Croatia, this method is not often used as not many box girder bridges with spans of 35 – 50 meters with such a sufficient length were built to make this investment profitable.
- For a span of 30 meters, providing a sufficient length of the bridge, the differences in cost with respect to the chosen construction method are small, as can be seen in Figure 2.4.
- For a span of 40 meters, incremental bridge launching and bridge erection on movable scaffolding are most suitable.
- For spans over 50 meters, incremental bridge launching is the only cost-effective method.

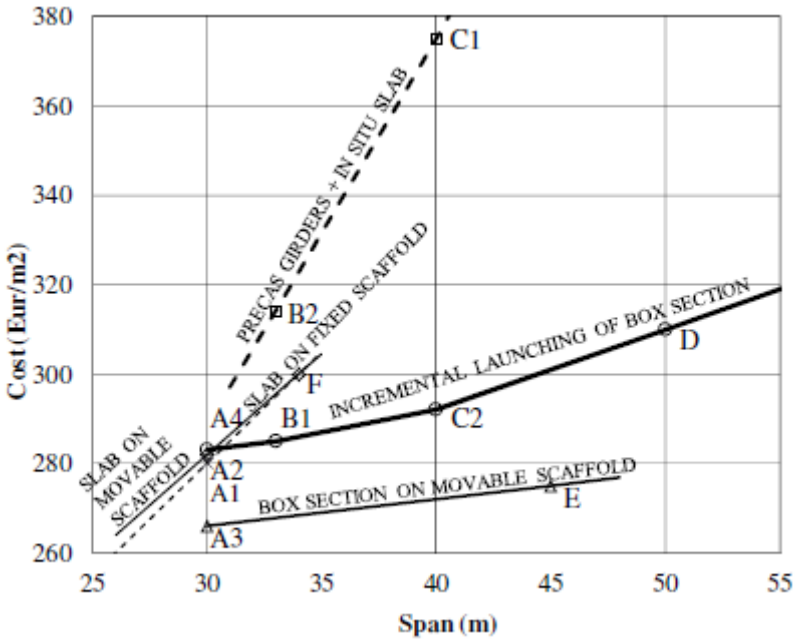

Figure 2.4: Superstructure cost according to different construction methods (Mandic Ivankovic, et al., 2014).

In The Netherlands, we have different conditions. In Croatia, almost all bridges cross deep valleys so construction on movable scaffolding will not be a good solution. It is interesting to know if, and under what conditions, incremental bridge launching could compete with other construction techniques in The Netherlands. Since the method is suitable for longer bridges and intermediate spans, it may only be used for approach bridges and long viaducts.

2.9 Internal or external prestressing of incrementally launched bridges

2.9.1 Development in prestressing

(Oostra, 2014) studied prestressing of incrementally launched bridges, and noticed a clear development in the type of prestressing used for incrementally launched bridges:

1. Traditionally, central and continuity prestressing are located inside the concrete cross-section. However, the arrangement of central prestressing is not beneficial for the use phase.
2. Central prestressing will be applied internally. Continuity prestressing will be applied externally and arranged according to the use phase.
3. Horizontal external tendons act as central prestressing. After the launching operation is completed, their arrangement is adapted in order to form an efficient lay-out for the use phase. Above the supports the cables are elevated. At mid-span the cables are pulled downwards. This operation requires the cables to elongate, which can be done by so-called *shims*. The cables should be detensioned before their rearrangement. Such a system was used in the bridge over the Rio Caroni in Venezuela.
4. A part of the external continuity tendons is installed permanently and balanced by as many temporary tendons, which have an opposite lay-out. After launching, these temporary tendons are detensioned and rearranged as final external tendons for the use phase. Such a system was used in the Sathorn Bridge in Thailand.
5. The use of partial prestressing. During launching, the load is shared between external prestressing and longitudinal reinforcement; passive reinforcement that would otherwise be ignored. The dead load should be carried by continuity tendons. The live loads will be carried by the longitudinal reinforcement. This system was used in the Clackmannanshire Bridge in Scotland.

Prestressing, which will be active in both the launch and use phase, will be most effective. When the same tendons can be used in both phases, the prestressing force doesn't have to be limited during launching and auxiliary supports may be avoided.

In a study by (Vermeulen, et al., 1993) a combination of system (3) and (4) was developed. Half of the continuity tendons will be installed permanently before launching (4). The other half will be arranged such that a central prestressing is acquired. Figure 2.5 illustrates, that after launching these tendons are rearranged for the use phase (3).

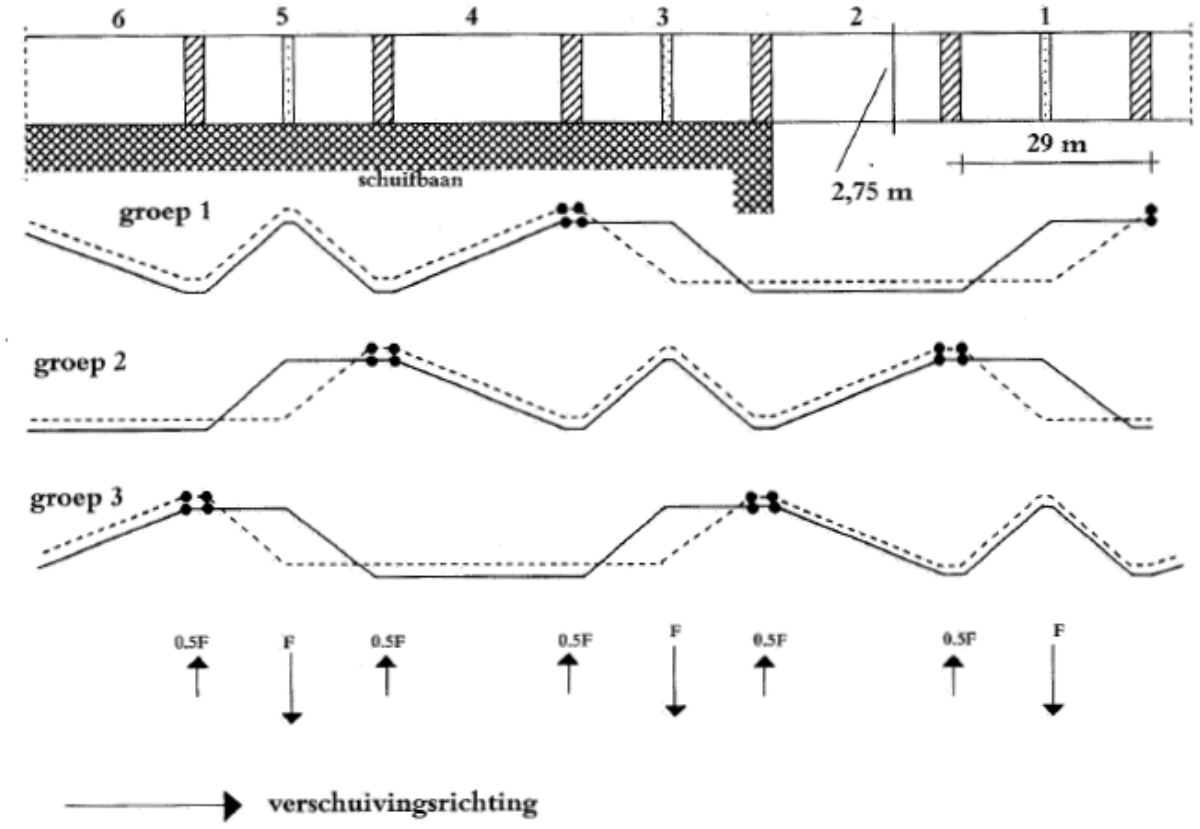

Figure 2.5: Alternative tendon lay-out Zeeburgerbrug(Vermeulen, et al., 1993).

2.9.2 Benefits of external prestressing

External prestressing has the following advantages over internal prestressing:

- With the use of external prestressing the webs of a box girder will not contain ducts. The shear capacity will not be reduced and the webs can be designed more slender. This will cause a reduction in self-weight and thus a reduction in the amount of reinforcement.
- Because of the absence of ducts in the webs, the execution gets simplified with respect to casting the concrete.
- The tendons can be inspected and repaired more easily. Therefore, the chance of not fully grouted cables is negligible. One can inject the ducts with grease to protect the cables against corrosion.
- The tendons are replaceable when the ducts and anchorage allow this replacement.
- Depending on the cable type and anchorage the prestressing force can be adjusted.
- A complicated tendon layout inside the concrete can be avoided, so friction losses will be small and unintended curvature pressures are absent.

2.10 Ultra-High Performance Concrete

Ultra-High Performance Concrete (UHPC) indicates concrete mixtures with a very high characteristic compressive strength f_{ck}between 150 and 250 MPa. These types of mixtures are characterized by a very low water/cement ratio. Their high-quality properties are based on three principles: an improved homogeneity, packing density/microstructure and ductility, providing the mixture contains fibers.

2.10.1 Fibers

When fibers are added to the concrete, one speaks of Ultra-High Performance Fiber Reinforced Concrete (UHPFRC). Short fibers bridge micro-cracks and cause an increase in concrete strength. Long fibers bridge macro-cracks and cause an increase in ductility. Two types of fibers exist: steel and synthetic fibers. Steel fibers provide and improved ductility, post-cracking strength and compressive strain limit. Synthetic fibers provide a fire resistance and reduced cracking due to plastic shrinkage.

2.10.2 Compressive strength

UHPC in compression performs elastic behavior until a maximum f_{ck} is reached. After the peak the strain does not remain uniform. A sudden drop in stress can occur when fiber content is less than the recommended value of two percent.

2.10.3 Tensile strength

Just like conventional concrete, UHPFRC exhibits linear elastic behavior until a certain peak value. However, as opposed to conventional concrete, the stress will not become zero after this peak has been exceeded. This is due to the fibers' crack-bridging properties. Different constitutive equations exist. *Strain-hardening* occurs when the post-cracking strength is higher than the capacity of the matrix itself, in concrete with high fiber content (Figure 2.6 left). *Strain-softening* occurs when the post-cracking strength is lower than the capacity of the matrix in concrete with low fiber content and inefficient fibers (Figure 2.6 right).

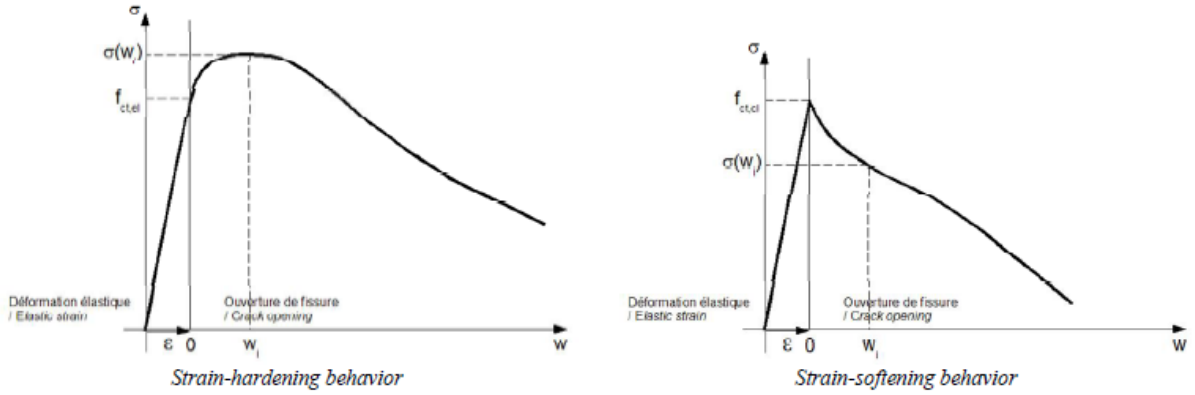

Figure 2.6: Tensile strength UHPFRC (Association Francaise de Génie Civil, 2013).

2.10.4 Fiber orientation

Fibers tend to align in the direction of flow. Fibers close to formwork walls are naturally aligned parallel to them. However, this phenomenon stops when a certain distance to the formwork is exceeded. The influence of fiber orientation on real strength values to be considered in calculations is taken into account by a certain K-factor. One can distinguish between a local and global factor. This factor is only applicable after the concrete is cracked.

2.10.5 Durability

The mixture composition of UHPC and high binder content eliminate capillary porosity of the concrete and result in good durability. Self-healing properties provide long-term maintaining of tensile strength given that crack width is controlled. The improved durability properties may lead to a reduced concrete cover and less maintenance.

2.10.6 Optimal use of UHPC

In order to make optimal use of UHPC the high compressive strength should be fully utilized. This is especially important for elements that are loaded in pure bending. When fibers are forced to act as reinforcement or when traditional reinforcement has been applied, the material cannot be used effectively, as compression strength only acts in the concrete compression zone. UHPC is suitable for high prestressing forces.

2.10.7 Reticence on a wide application for use of UHPC

One is reluctant to use the new material UHPC, because:

- Production cost for UHPC are many times higher than for NSC.
- There are still no (inter)national regulations on designing with UHPC that are acknowledged, so it is hard to prove the reliability of a structure.
- There is no proof that structures remain reliable throughout their lifetime.
- Due to the higher production cost of UHPC in comparison with NSC, it will take a long time to exploit the better durability properties and thus lower maintenance cost to reach break-even. Today's Design Build Finance and Maintain (DBFM) contracts often run for 25 years. The break-even point may lie much further away.

2.11 Building incrementally launched bridges in UHPC

All incrementally launched bridges that were discussed in the preliminary study (Oostra, 2014) were built with normal strength concrete. However, UHPC is a different material. Production of UHPC differs from production of NSC. The concrete mixture is composed differently, quality control of the production process is stricter and highly skilled personnel are required. To ensure fiber continuity, concrete should be poured without interruption. High drop heights should be avoided to minimize the probability of segregation of fibers from the cement paste or formation of fiber clusters. Fiber orientation defines the behavior of UHPC and should be monitored closely. UHPC hardens a lot quicker than NSC. Heat treatment should be carried out to minimize shrinkage and creep. Further research should be done on whether precast or in-situ UHPC units should be used in incremental bridge launching.

2.12 Why UHPC and incremental bridge launching might complete each other

Due to the high mechanical properties of UHPC, structures may have a much lighter design, which simplifies assembly and requires less central prestressing. It would then also reduce the forces that have to be carried by the substructure. Furthermore, consumption of materials may be reduced, which is usually high for incremental bridge launching in comparison with other construction techniques.

The structural efficiency can be enlarged by a lighter design. This permits the superstructure to remain slender, which is very rare for incrementally launched bridges and positive on aesthetics.

Incrementally launched bridges without temporary piers are located in the area of transition between constant and variable height superstructures. Since variable height superstructures usually have higher construction cost and longer construction times, increasing the application range of full span incremental bridge launching may be beneficial. Moreover, the length of precast girders is restricted by crane capacity and transportation.

Prestressing turned out to be most effective when it can be active in both launch and use phase. When the same tendons are used for both phases, the level of prestressing does not need to be limited during launch. UHPC can be highly prestressed and one might not need auxiliary supports.

Because of the quick hardening properties of UHPC and since passive reinforcement might be avoided, the cycle to construct a segment might be accelerated to find a shorter total construction time.

2.13 Research goals for the main study

2.13.1 The Dutch market

Infrastructural improvements in The Netherlands in the near future need to be reviewed to see if they are suitable for application of incremental bridge launching. A location and corresponding requirements and boundary conditions should be defined to examine the competitiveness of an UHPC incrementally launched bridge in The Netherlands.

2.13.2 Design and execution of an UHPC incrementally launched bridge

The influence of the use of UHPC in the design and execution of the incrementally launched bridge should be further investigated. Requirements regarding quality control of production need to be prescribed and the quick hardening properties of UHPC and the possibilities for a shortened total construction time should be studied. Finally, the production cycle needs to be defined.

2.13.3 Optimization of the cross-section

Optimization studies with respect to the cross-section for different concrete strength classes need to be performed. Normal strength concrete, high strength concrete, very high performance concrete and ultra-high performance concrete are different materials and their influence on the cross-sectional capacity need to be examined. All possible load cases and load combinations during launch and lifetime should be interpreted in order to perform checks regarding the bending moment capacity, shear force capacity and crack width criterion.

2.13.4 Prestressing in incremental bridge launching

The type and amount of prestressing for the launch and use phase must be determined. In order to use UHPC effectively a huge amount of prestressing may be required. The fitting of a lot of anchors inside a light UHPC cross-section may cause problems and needs to be sorted out. Force introduction must be checked, as well as the preconditions for possible re-use of central prestressing.

2.13.5 An optimal span length

The lightweight nose has an optimal length that should be determined. The limiting factors for maximum span length should be defined. The case study should be used to determine if the bridge can be launched without auxiliary supports and which span length gives the lowest cost.

2.13.6 Alternative execution method

Finally, the bridge must be compared to the best alternatively executed bridge for that location to determine whether we have an economical bridge design.

3 Designing with UHPFRC

This chapter discusses the differences in design calculations between regular reinforced concrete and UHPFRC. Three design guidelines are compared on the stress-strain relationships that they use for the design. Finally, the cross-sectional capacity of several types of beams, designed with different types of concrete, is analyzed to identify the parameters that influence the bending moment and shear capacity to start the optimization process.

Designing with UHPFRC differs from designing with NSC and HSC, due to differences in stress-strain diagrams. The stress-strain relation in compression has a similar shape for UHPFRC (Figure 3.2) and NSC/HSC (Figure 3.1), but the fibers cause a different stress-strain relation in tension. NSC and HSC have a small tensile capacity that will be neglected whenever the concrete has cracked and the reinforcement is activated. However, the fibers in UHPFRC provide a tensile capacity that co-operates with (shear) reinforcement and prestressing.

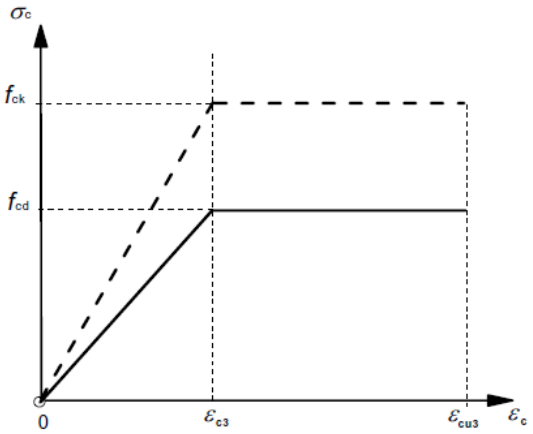

Figure 3.1: bi-linear stress-strain relation for NSC and HSC in compression (NEN-EN 1992-1-1).

Figure 3.2 shows two stress-strain diagrams that have been developed by (Association Francaise de Génie Civil, 2013) for UHPC design in the ultimate limit state. The left one illustrates strain hardening behavior, while the right one illustrates strain softening behavior.

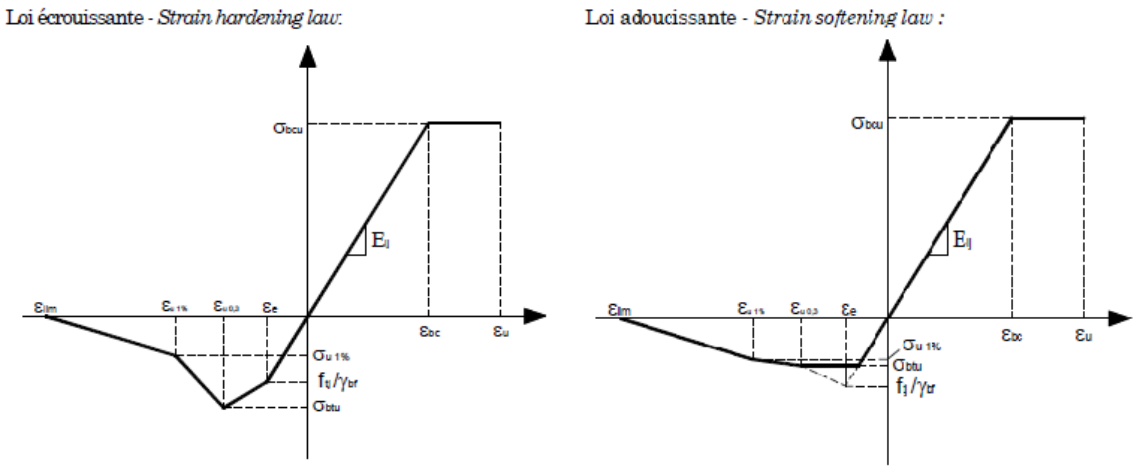

Figure 3.2: stress-strain diagrams for UHPC ULS design (Association Francaise de Génie Civil, 2013).

Figure 3.3 shows a stress-strain design curve for Ductal UHPC in compression and was obtained from measurements taken in a standard compression test on a 70 mm diameter cylinder (Behloul, 1999). The ascending part OA can be assumed to be linear up to the peak stress. The plateau AB represents the ductility provided by the steel fibers. The shape of the plateau and the descending part depend on the type and amount of fibers. For design purposes, (VSL Australia, 2000) has developed an idealized stress-strain relationship as shown in Figure 3.4.

When the concrete compressive strength of UHPC increases, the linear elastic part extends and the length of the plastic phase decreases: $f_{ck} \uparrow \rightarrow \varepsilon_{cmax} = 0.85 f_c'/E_c \uparrow$. Similar behavior can be noticed for NSC and HSC: $f_{ck} \uparrow \rightarrow \varepsilon_{c3} \uparrow$.

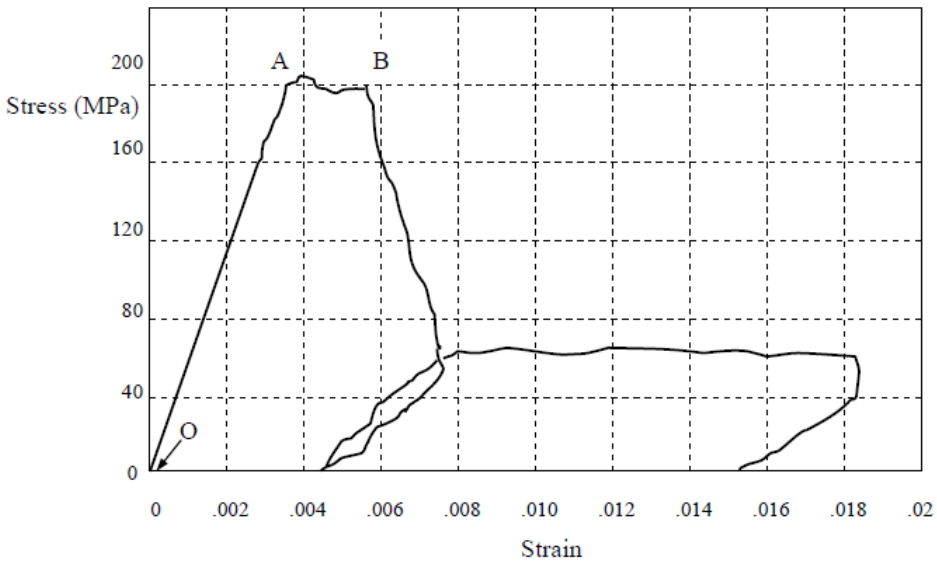

Figure 3.3: typical stress-strain relationship in compression (Behloul, 1999).

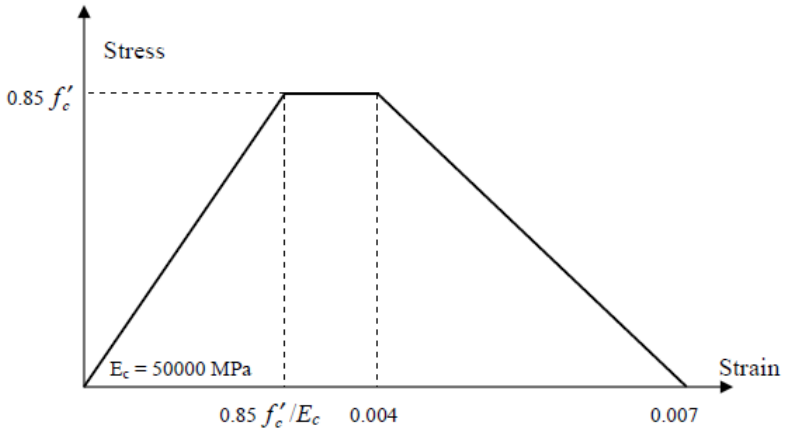

Figure 3.4: design stress-strain relationship in compression (VSL Australia, 2000).

The behavior of Ductal UHPC in tension is illustrated in Figure 3.5. It was obtained from measurements in a direct tensile test on a 70 mm diameter notched cylinder (Behloul, 1999). The behavior after cracking highly depends on the type, amount and orientation of the steel fibers bridging the cracks. An important observation that can be made from Figure 3.5 is, that the average tensile stress on the cracked surface increases after first cracking before starting to decrease at a crack width of 0.2 – 0.3 mm. This is typical strain hardening behavior. For design purposes, (VSL Australia, 2000) has developed an idealized stress-strain relationship in tension as shown in Figure 3.6.

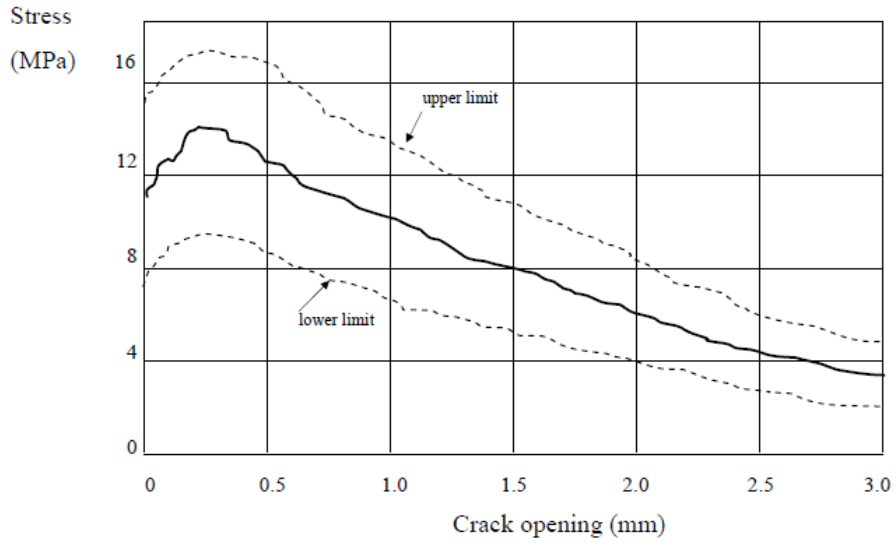

Figure 3.5: behavior in direct tension (Behloul, 1999).

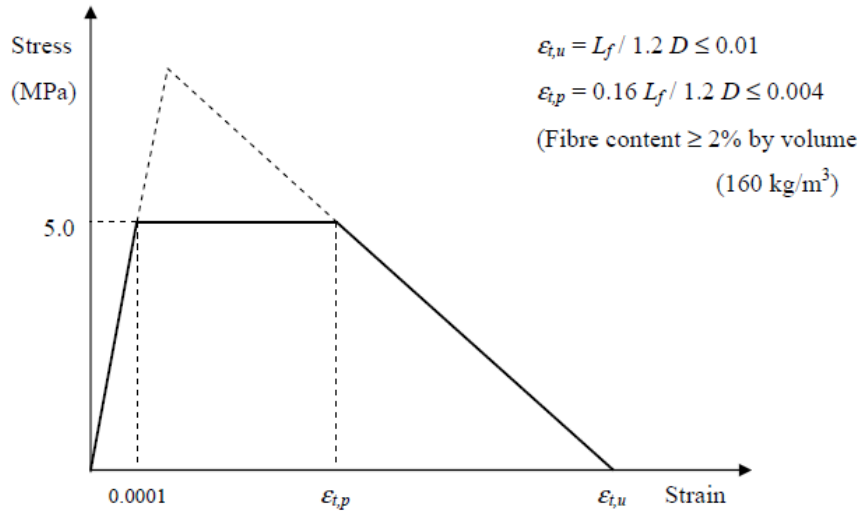

Figure 3.6: design stress-strain relationship in tension (VSL Australia, 2000).

The end of the plateau in the stress-strain relationship for UHPC in tension is given by: $\varepsilon_{t,p} = 0.16L_f/1.2D \leq 0.004$. This means that for longer fibers and for more slender cross-sections the length of the plateau will increase and thus the ductility of the member increases.

The ultimate tensile strain is given by: $\varepsilon_{t,u} = L_f/1.2D$, which means that slender members having longer fibers have the largest ultimate tensile strain.

Figure 3.7 shows an idealized stress-strain design curve developed by (CAE Nederland B.V., 2011) for UHPC design in the ultimate limit state. It is based on(Association Francaise de Génie Civil, 2013). To simplify calculations and to incorporate safety, the hatched area is neglected and a design curve similar to the (VSL Australia, 2000) one is obtained.

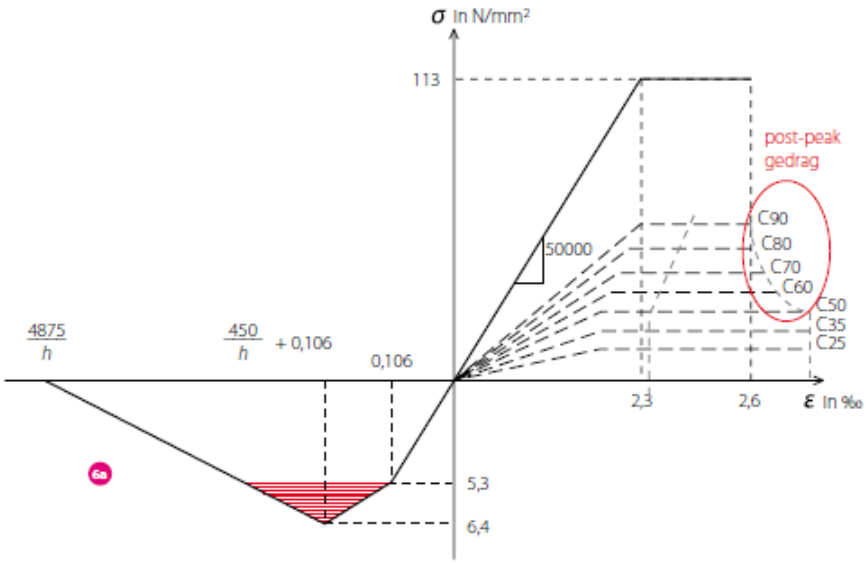

Figure 3.7: idealized stress-strain diagram for ULS design (CAE Nederland B.V., 2011).

The (VSL Australia, 2000) design stress-strain relationships will be used for the analysis of a design in UHPFRC. They apply to structural members made of DUCTAL that have the following properties:

- a characteristic compressive strength at 28 days f_c' in the range 150 – 220 MPa.
- a minimum fiber content of 2% by volume, a fiber length of 13 mm, a diameter of 0.2 mm and a minimum fiber tensile strength of 1800 MPa.
- a saturated, surface-dry density in the range 2400 – 2650 kg/m^3.
- a minimum characteristic strength at transfer of 100 MPa and a minimum modulus of elasticity at transfer of 40000 MPa.

In the guidelines that have been addressed in this paragraph, different symbols are used for the mechanical properties. Table 3.1 presents an overview.

	VSL Australia	AFGC/Setra 2002	NEN-EN-1992	CAE NL
characteristic compressive strength at 28 days	f_c'	f_{cj}	f_{ck}	-
characteristic tensile strength at first crack	f_{ct}'	f_{tj}	$f_{ctk;0,05}$	-
design value tensile strength at first crack	σ_{ctmax}*	f_{tj}/γ_{bf}	-	f_{ctd1}
ultimate compressive strain	ε_{cu}*	ε_u	ε_{cu3}	-
compressive strain at start plastic phase	ε_{cmax}*	ε_{bc}	ε_{c3}	-
modulus of elasticity	E_c	E_{ij}	E_{cm}	-
tensile strain at first crack	ε_{ctmax}*	ε_e	ε_{ct}	-
limiting tensile strain in concrete	$\varepsilon_{t,p}$	-	-	-
ultimate tensile strain	$\varepsilon_{t,u}$	ε_{lim}	ε_{ctu}	-
yield strain in prestressing steel	ε_{py}	-	f_{pd}/E_p	-
design value compressive strength	$0.85f_c'$	σ_{bcu}	f_{cd}	-
tensile strain at 0,3 mm crack width	-	$\varepsilon_{u0,3}$	-	$\varepsilon_{ct0,3}$
tensile strain at 1% crack width	-	$\varepsilon_{u1\%}$	-	$\varepsilon_{ct1\%}$
tensile stress at 1% crack width	-	$\sigma_{u1\%}$	-	-
tensile stress at fully developed crack pattern	-	σ_{btu}	-	f_{ctd2}
crack width of 0,3 mm	-	$w_{0,3}$	-	-
crack width of 1% of sample height	-	$w_{1\%}$	-	-
characteristic length	-	l_c	-	-
fiber length	L_f	l_f	-	-
fiber orientation factor	-	K	-	k

Table 3.1: a list of the symbols used in the guidelines

In order to understand the behavior of UHPFRC in design calculations, the next paragraphs present an analysis on the cross-sectional capacity of the following types of beams:

- Rectangular reinforced NSC/HSC beam;
- Rectangular doubly reinforced NSC/HSC beam;
- Rectangular doubly reinforced NSC/HSC beam + normal force;
- Rectangular prestressed NSC/HSC beam;
- Reinforced NSC/HSC box girder;
- Prestressed NSC/HSC box girder;
- Rectangular unreinforced UHPFRC beam;
- Rectangular prestressed UHPFRC beam;
- Unreinforced UHPFRC box girder;
- Prestressed UHPFRC box girder.

3.1 Rectangular reinforced NSC/HSC beam

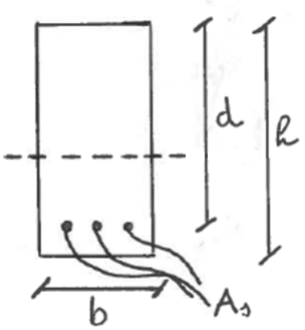

Figure 3.8: rectangular reinforced concrete beam

Figure 3.9 illustrates a typical moment-strain diagram for the rectangular normal strength reinforced concrete beam from Figure 3.8. In this case, the characteristic concrete compressive strength: $f_{ck} = 20\ N/mm^2$. The point of cracking can be clearly distinguished at a concrete compressive strain of approximately 0.35‰. The beam fails after the concrete compressive strain limit is reached: $\varepsilon_c = \varepsilon_{cu3}$, which is 3.5‰ for normal strength concrete.

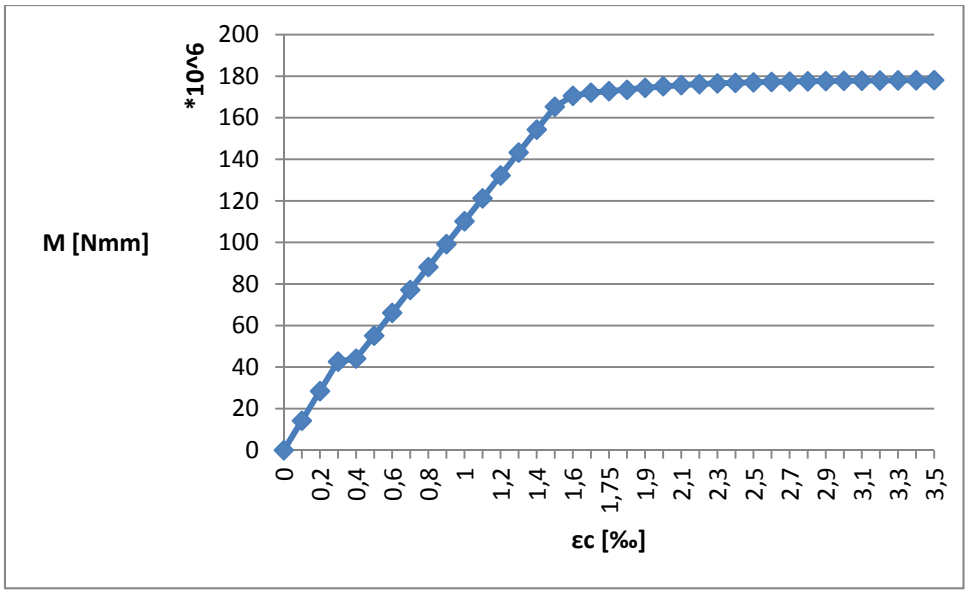

Figure 3.9: moment-strain diagram for a rectangular reinforced normal strength concrete beam

Figure 3.10 illustrates the moment-curvature diagram of the same beam. The dots represent consecutively the cracking moment, yield moment, plastic moment and ultimate moment.

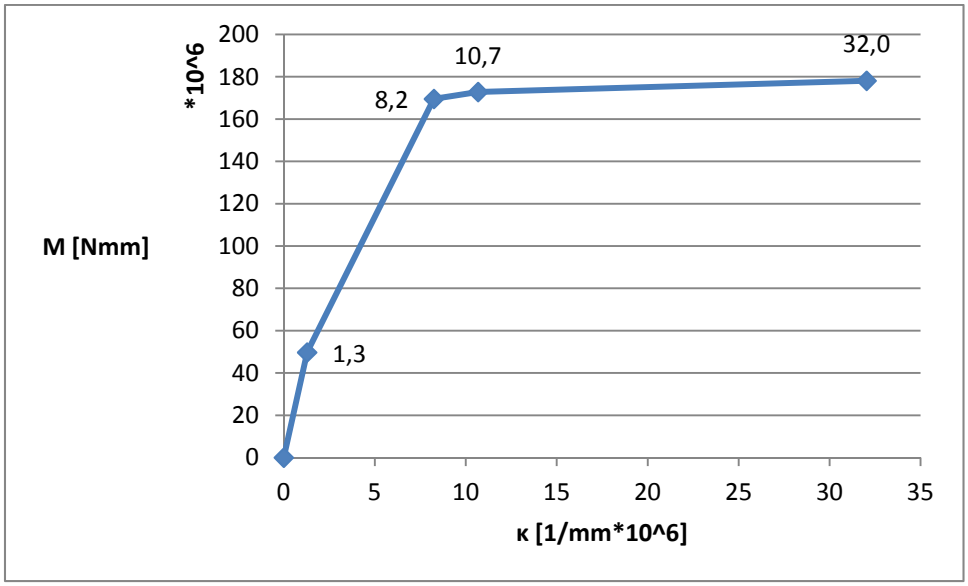

Figure 3.10: moment-curvature diagram for a rectangular reinforced normal strength concrete beam

Figure 3.11 illustrates the moment-strain diagram for a rectangular reinforced high strength concrete beam. In this case, the characteristic concrete compressive strength: $f_{ck} = 90\ N/mm^2$. For high strength concrete, the concrete compressive strain limit is lower than for normal strength concrete: $\varepsilon_{cu3} = 2.6‰$.

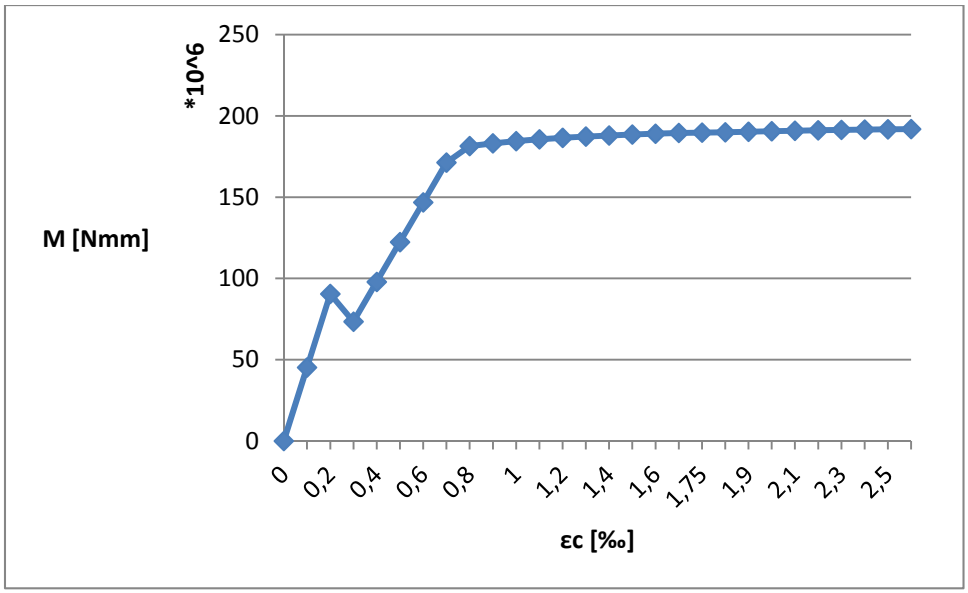

Figure 3.11: moment-strain diagram for a rectangular reinforced high strength concrete beam

For a rectangular reinforced concrete beam, which is loaded in pure bending, an increase in concrete compressive strength f_{ck} from $20\ N/mm^2$ to $90\ N/mm^2$ will only lead to a small increase in bending moment resistance. Appendix 11.1 and appendix 11.2 show an increase by a factor of: $1.91 \cdot 10^8/1.78 \cdot 10^8 = 1.07$. The shear capacity and moment capacity in SLS will increase a lot more: $6.64 \cdot 10^5/4.50 \cdot 10^5 = 1.48$ and $1.38 \cdot 10^8/9.75 \cdot 10^7 = 1.41$ respectively.

For regular reinforced concrete the shear capacity V_{Rd} consists of a concrete part V_{Rdc} and a shear reinforcement part $V_{Rd,s}$. When the shear resistance of the concrete part is exceeded, the shear reinforcement must sustain the entire shear force and the contribution of the concrete part must be ignored. The shear force is limited by crushing of the concrete compression struts: $V_{Rd,max}$. The increase in concrete compressive causes an increase in shear capacity by improving the strength of these concrete compression struts

A beam with a concrete compressive strength of $90\ N/mm^2$ can hold much more reinforcement than the same beam with a concrete compressive strength of $20\ N/mm^2$. Appendix 11.3 shows that an increase in bending moment resistance by a factor of $6{,}96 \cdot 10^8/1{,}78 \cdot 10^8 = 3.91$ is possible. So using high strength concrete instead of normal strength concrete will only be beneficial if the cross-section is heavily reinforced. However, there is a limit; the maximal number of reinforcing bars is restricted by the bar spacing.

3.2 Rectangular doubly reinforced NSC/HSC beam

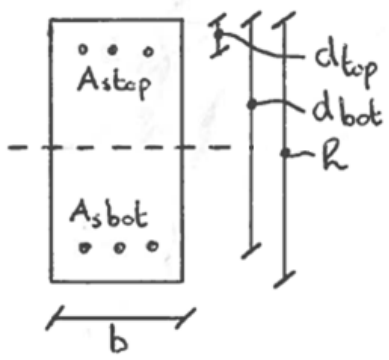

Figure 3.12: rectangular doubly reinforced concrete beam

Appendix 11.4 demonstrates that adding a top layer of reinforcement (Figure 3.12) to the concrete beam from paragraph 3.1, which only has bottom reinforcement and is loaded in pure bending, hardly affects the bending moment capacity. The same holds for the shear capacity and moment capacity in SLS.

3.3 Rectangular doubly reinforced NSC/HSC beam + normal force

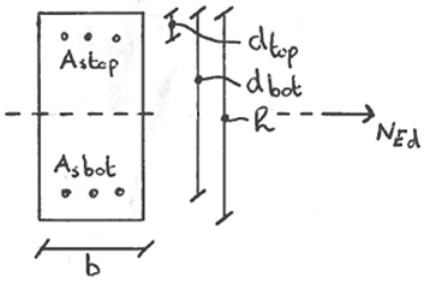

Figure 3.13: rectangular doubly reinforced concrete beam + normal force

Compared to the beam from paragraph 3.2, which is loaded in pure bending only, a beam subject to a bending moment and a compressive force N_{Ed}, as shown in Figure 3.13, will have an increased ultimate bending moment capacity. Because of the large compressive force, the plastic moment will often be reached before the yield moment. Appendix 11.6 shows an improvement in bending moment capacity of: $3.28 \cdot 10^8 / 1.81 \cdot 10^8 = 1.81$. The shear capacity only increases by a factor of: $4.87 \cdot 10^5 / 4.68 \cdot 10^5 = 1.04$.

The moment-strain diagram can be seen in Figure 3.14. The first part of the graph has negative and incorrect values, probably caused by the fact, that the cross-section is fully compressed and does not have a compressive and tensile region on which the calculation in the uncracked phase was based.

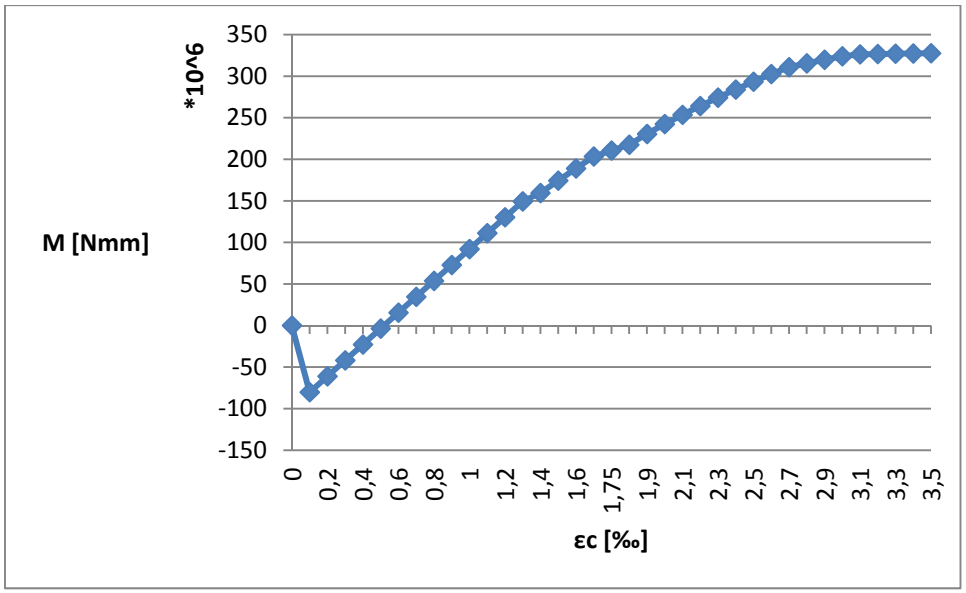

Figure 3.14: moment-strain diagram for a rectangular doubly reinforced normal strength concrete beam + normal force

The M-N-κ-diagram of the beam can be seen in Figure 3.15. The consecutive points in the graph represent the cracking moment, plastic moment, yield moment of the top reinforcement, yield moment of the bottom reinforcement and the ultimate bending moment.

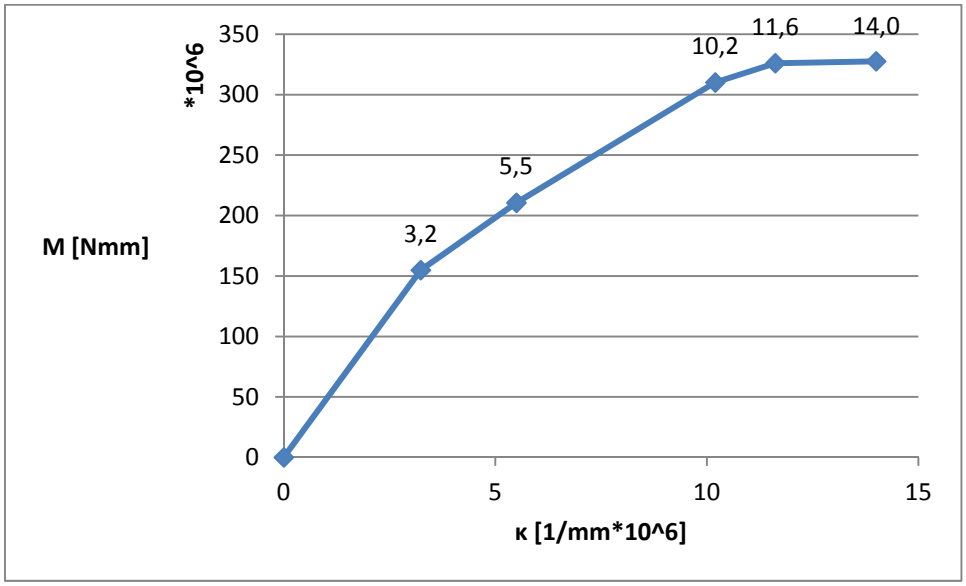

Figure 3.15: moment-normal force-curvature diagram for a rectangular doubly reinforced normal strength concrete beam

3.4 Rectangular prestressed NSC/HSC beam

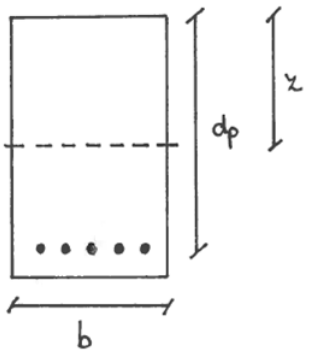

Figure 3.16: rectangular prestressed concrete beam

Appendix 11.7 illustrates, that by using three Ø16 Y1860S7 prestressing strands instead of three Ø16 B500 reinforcement bars in the rectangular normal strength concrete beam from Figure 3.16, the bending moment capacity increases with a factor: $1.99 \cdot 10^8 / 1.11 \cdot 10^8 = 1.79$. However, the shear capacity hardly increases: $4.98 \cdot 10^5 / 4.68 \cdot 10^5 = 1.06$.

If the concrete compressive strength is increased from 20 to $90\ N/mm^2$, three strands will not suffice anymore; the strain in the prestressing steel exceeds the ultimate strain $(\varepsilon_p > \varepsilon_{ud})$ and the full capacity of the concrete cannot be used (Appendix 11.8). High strength concrete can hold much more prestressing than normal strength concrete. However, there are limits with respect to strand spacing and concrete cracking at $t = 0$ when the beam is only subjected to its self-weight. When the prestressing force is too high cracking might occur at the top of the beam.

3.5 Reinforced NSC/HSC box girder

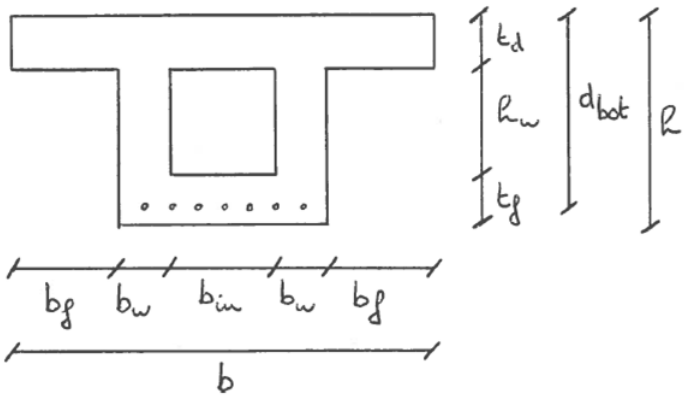

Figure 3.17: reinforced concrete single cell box girder

Box girders have, for the same amount of concrete, an increased moment of inertia and moment of resistance compared to rectangular cross-sections. Based on dimensions from (van der Veen, 2014) and (van der Meulen, 1991), a reinforced normal strength concrete single cell box girder, as shown in Figure 3.17, has been designed in Appendix 11.9.

The results show, that the ultimate bending moment capacity is reached, when the steel strain is: $\varepsilon_s = 4{,}06 \cdot 10^{-2}$. This cannot occur, because $\varepsilon_{ud} = 2{,}25 \cdot 10^{-2}$. Thus the steel reinforcement fails before $\varepsilon_c = \varepsilon_{cu3}$ and the concrete is not being used to its full potential. A solution is to apply more steel reinforcement bars. However, the bar spacing is limited to make sure that the concrete can easily flow through the bars, gets fully distributed and no weak spots will form. To economically use higher strength concretes to save weight, prestressing steel should be applied.

3.6 Prestressed NSC/HSC box girder

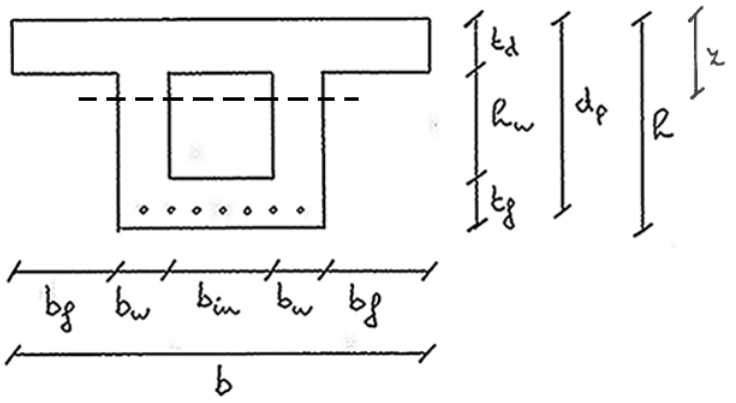

Figure 3.18: prestressed concrete single cell box girder

Based on dimensions from (van der Meulen, 1991) and (van der Veen, 2014), a prestressed normal strength concrete single cell box girder as shown in Figure 3.18 has been designed in Appendix 11.20.

The analysis demonstrates that in order to fully use the concrete compressive strength ($\varepsilon_c = \varepsilon_{cu3}$), six tendons with 55 strands should be present in the concrete cross-section $(\varepsilon_p < \varepsilon_{ud})$. These anchors need a clearance of 580 mm (Figure 3.20) and thus will never fit in the 150 mm thick bottom floor. They need to be anchored in haunches. The ducts have a diameter of 167 mm and will also not fit in the floor (Figure 3.19). A solution to this problem could be to apply the tendons externally.

To minimize the amount of prestressing that is required, the concrete cross-section must be reduced, for example by decreasing the deck thickness. However, one should pay attention to the possibility of punching shear failure due to axle loads. Tendons containing fewer strands may be a possibility if they can be installed in couples to satisfy the anchor spacing condition.

Tendon Type		Sheating	
0.5"	0.6"/0.62"	I.D. mm	O.D. mm
5901	6801	25	30
5902	6802	40	45
5904	6803	45	50
5905	6804	50	55
5907	6805	55	60
5909	6807	60	65
5912	6809	70	75
5915	6812	80	85
5920	6815	85	90
5927	6819	95	100
5932	6822	100	105
5937	6827	110	117
–	6831	120	127
–	6837	130	137
–	6843	140	147
–	6849	150	157
–	6855	160	167

Figure 3.19: dimensions of corrugated duct (Dywidag-Systems International, 2015)

Ø15.2/15.7 mm, Ultimate Load 261/279 kN						
Type 0.62"	Distances of the anchorages		Additional Reinforcement Helix[2)]			
f_{pk}1860 N/mm²	Center Distance mm	Edge Distance[1)] mm	Ø da mm	mln l* mm	n*	ds mm
6805	235	140	185	225	4	12
6807	280	160	220	260	4	14
6809	305	175	250	310	5	14
6812	350	195	265	410	7	14
6815	390	215	310	465	8	14
6819	435	240	375	470	8	16
6822	470	255	370	500	8.5	16
6827	520	280	430	525	9	16
6831	640	340	560	615	9	20
6837	700	370	620	615	9	20
6843[3)]	640	340	530	675	10	20
6849[3)]	680	360	550	675	10	20
6855[3)]	710	375	580	700	11	20

Figure 3.20: details of the anchorage zone (Dywidag-Systems International, 2015)

3.7 Rectangular unreinforced UHPFRC beam

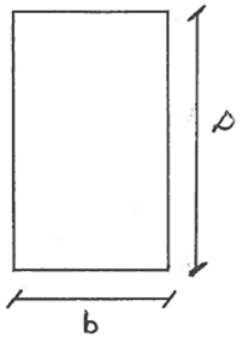

Figure 3.21: rectangular unreinforced UHPFRC beam

For NSC, the ultimate bending moment resistance is reached when the concrete compressive strain $\varepsilon_c = \varepsilon_{cu3}$ at the end of the moment-strain diagram, as can be seen in Figure 3.9. For unreinforced UHPFRC, the ultimate bending moment resistance is reached just after $\varepsilon_b = \varepsilon_{t,p}$, which is not at the end of the graph. Figure 3.6 & Figure 3.22 illustrate, that the beam can undergo further deformation until $\varepsilon_b = \varepsilon_{t,u}$.

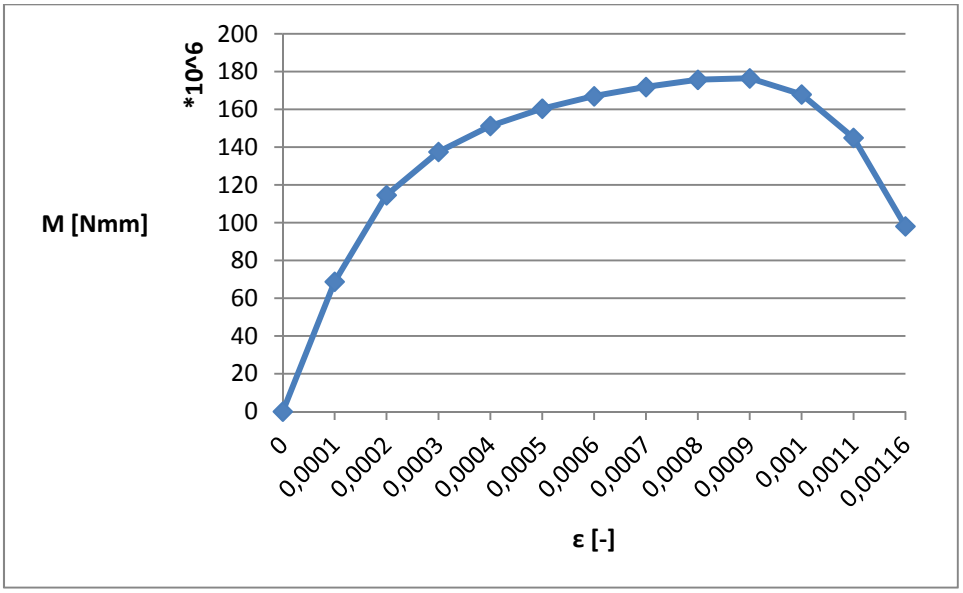

Figure 3.22: moment-strain diagram for a rectangular unreinforced UHPFRC beam

Unreinforced UHPC, which is loaded in pure bending, is not used efficiently. Appendix 11.11 shows that only a slight amount of concrete $(1.65 \cdot 10^5 / 2.00 \cdot 10^5 = 0.825 \rightarrow 17.5\%)$ can be saved to reach a moment capacity similar to the reinforced NSC beam from paragraph 3.1.

The cross-sectional analysis in Appendix 11.11 also shows that an unreinforced UHPC beam, loaded in pure bending, fails in tension ($\varepsilon_b = \varepsilon_{t,u}$) long before the maximum compressive strain at the top of the beam is reached ($\varepsilon_0 = \varepsilon_{c,p}$). To make use of the strength of the material UHPC, which is the high compressive strength, a large compressive force should be introduced onto the cross-section.

3.8 Rectangular prestressed UHPFRC beam

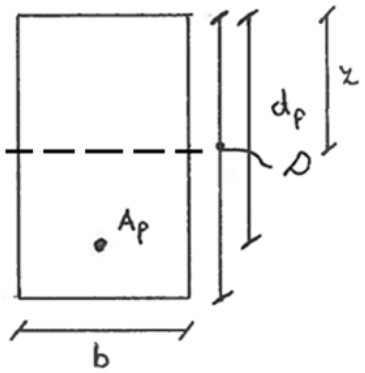

Figure 3.23: rectangular prestressed UHPFRC beam

The cross-sectional analysis of the rectangular prestressed UHPFRC beam from Figure 3.23 can be found in Appendix 11.12. Figure 3.24 shows that for a small amount of prestressing steel the top of the moment-strain diagram can be found just after $\varepsilon_b = \varepsilon_{t,p}$. Then the curve descends until the prestressing steel reaches its maximal strain, when $\varepsilon_p = \varepsilon_{ud}$ and fails. The concrete has a lot of capacity left ($\varepsilon_0 \ll \varepsilon_{c,p}$) and is not used efficiently.

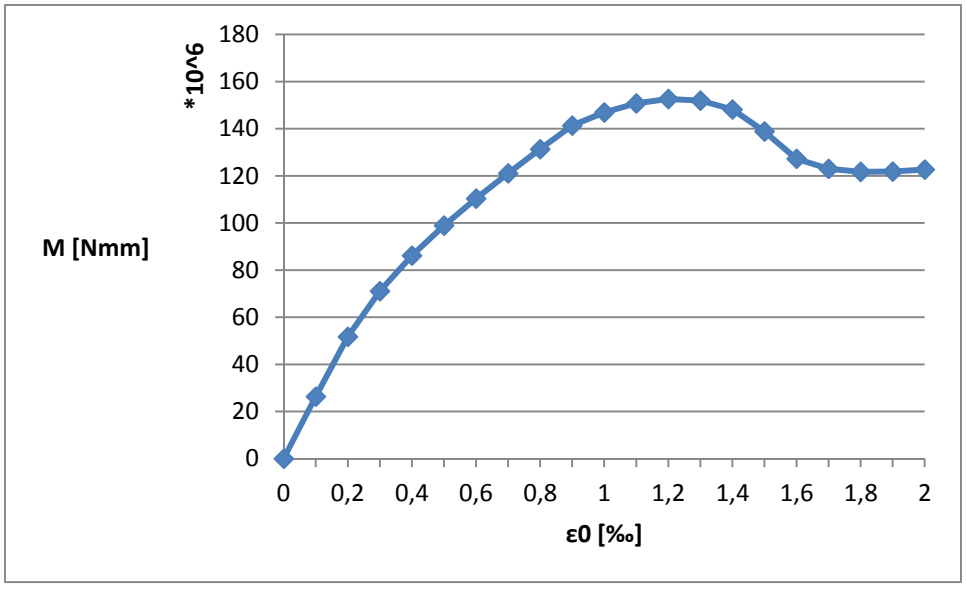

Figure 3.24: moment-strain diagram for a rectangular UHPFRC beam with little prestressing

In order to use the full capacity of the concrete a huge amount of prestressing steel is required. Appendix 11.13 presents the cross-sectional analysis of a heavily prestressed UHPFRC beam. As opposed to the moment-strain diagram from Figure 3.24, Figure 3.25 shows that after a small bump in the curve just after $\varepsilon_b = \varepsilon_{t,p}$, the curve continues to rise until $\varepsilon_p = \varepsilon_{ud}$.

The analysis also shows that eight strands are required to use the full capacity of the concrete. However, these eight strands will not fit next to each other in the cross-section and need to be bundled to fulfill the strand spacing criterion.

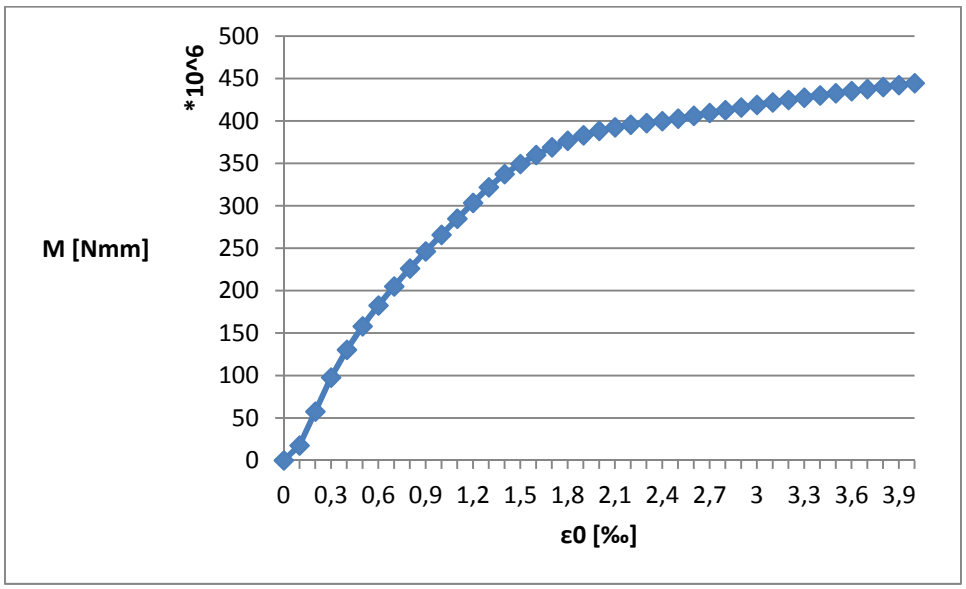

Figure 3.25: moment-strain diagram for a rectangular heavily prestressed UHPFRC beam

For UHPFRC the shear capacity V_u consists of three parts. Just like for conventional concrete there is the contribution of the concrete V_{Rb} and the shear reinforcement V_s. Additionally, there is the participation of the fibers V_f. The contribution of all three components to the total shear capacity is presented in Appendix 11.12. It can be seen, that the fibers have a substantial contribution to the total shear capacity: $(4.20 \cdot 10^5 / 8.63 \cdot 10^5) \cdot 100 = 49\%$.

3.9 Unreinforced UHPFRC box girder

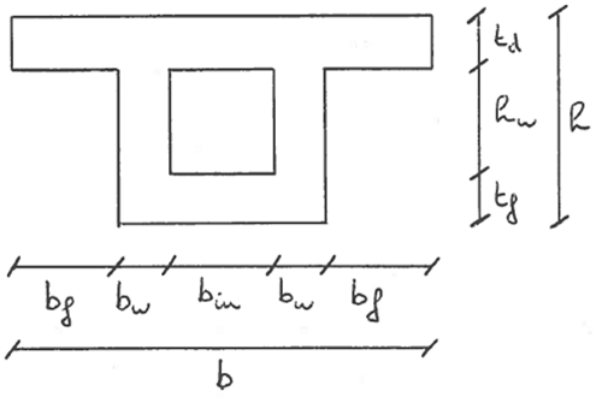

Figure 3.26: unreinforced UHPFRC single cell box girder

Based on dimensions from (van der Meulen, 1991) and (van der Veen, 2014), an unreinforced UHPFRC single cell box girder (Figure 3.26) has been designed with dimensions and properties that can be found in Appendix 11.14.

Figure 3.27 shows the moment-strain diagram of the unreinforced UHPFRC box girder. The maximum can be found just after: $\varepsilon_b = \varepsilon_{t,p} \rightarrow \varepsilon_0 = 0.000125$ (Appendix 11.14). The box girder fails in tension $\varepsilon_b = \varepsilon_{t,u} \rightarrow \varepsilon_0 = 0.000209$ long before the concrete reaches the plastic phase, when $\varepsilon_0 = \varepsilon_{cmax} = 0.00255$ or even fails at $\varepsilon_0 = \varepsilon_{c,p} = 0.004$. This confirms the fact, that UHPFRC must be prestressed heavily in order to have an efficient use.

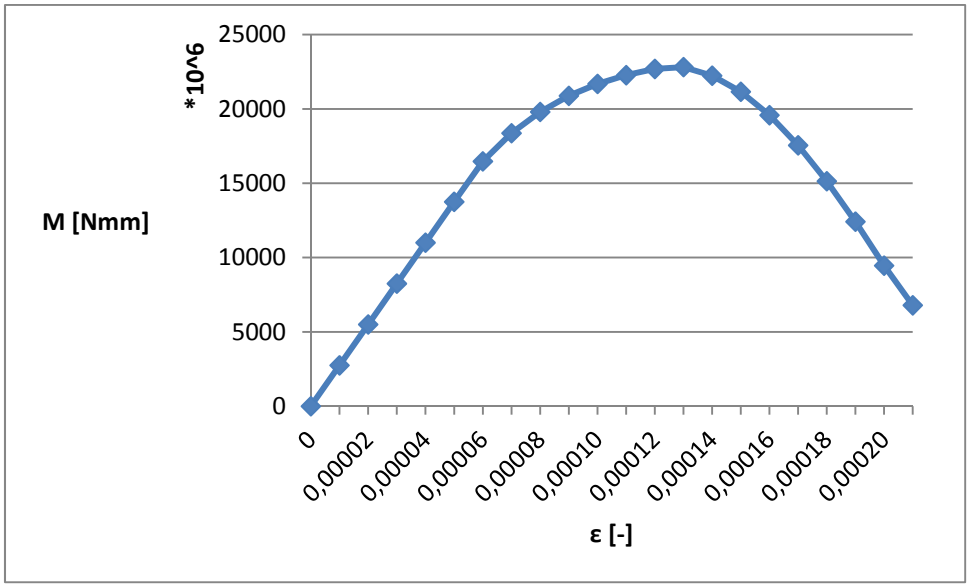

Figure 3.27: moment-strain diagram for an unreinforced UHPFRC single cell box girder

3.10 Prestressed UHPFRC box girder

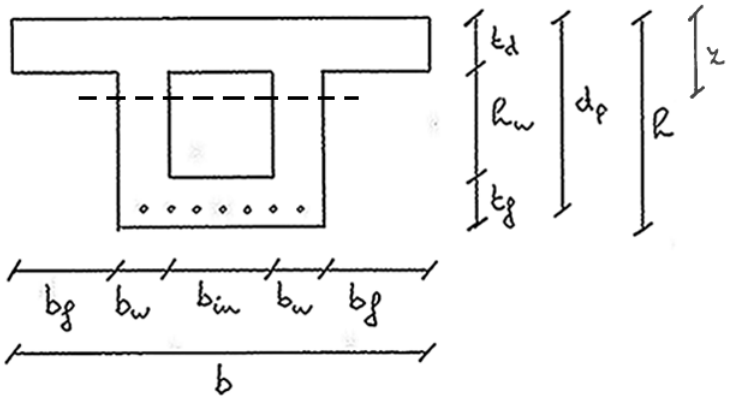

Figure 3.28: prestressed UHPFRC single cell box girder

Based on dimensions from (van der Meulen, 1991) and (van der Veen, 2014), a prestressed UHPFRC single cell box girder (Figure 3.28) has been designed with dimensions and properties that can be found in Appendix 11.15.

Figure 3.29 shows the moment-strain diagram for a UHPFRC box girder with little prestressing. The top of the graph is reached just after $\varepsilon_b = \varepsilon_{t,p}$ Appendix 11.15. After this point, the graph descends and again rises until the prestressing steel reaches its maximal strain, when $\varepsilon_p = \varepsilon_{ud}$ and fails. The shape of the moment-strain diagram shows similarities to the moment-strain diagram of a rectangular prestressed UHPFRC beam (Figure 3.24).

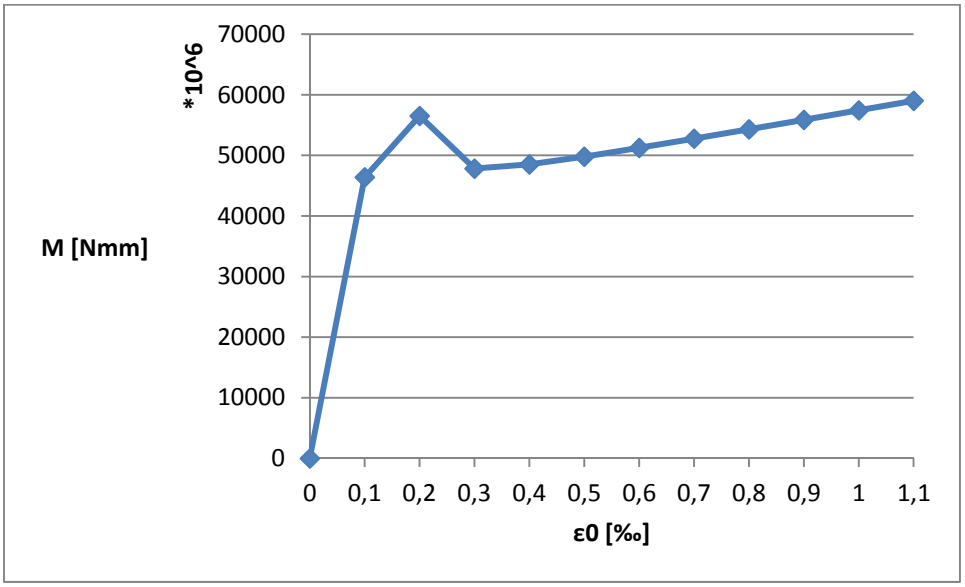

Figure 3.29: moment-strain diagram for a UHPFRC box girder with little prestressing

When the cross-section is subject to much more prestressing (Appendix 11.16), the moment-strain behavior (Figure 3.30) changes and shows parallelism to (Figure 3.25) where the first extreme just after $\varepsilon_b = \varepsilon_{t,p}$ disappears and the top is found at the end of the graph, when $\varepsilon_p = \varepsilon_{ud}$.

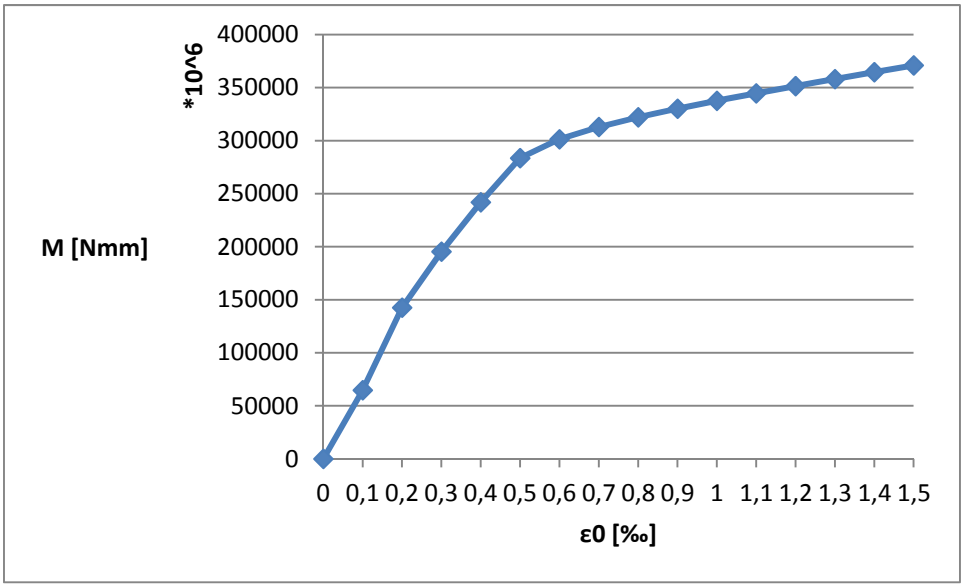

Figure 3.30: moment-strain diagram for a heavily prestressed UHPFRC box girder

In the literature review (Oostra, 2014), it was found that the moment of resistance above the neutral axis needed to be twice the moment of resistance below the neutral axis for a favorable box girder cross-section for incremental bridge launching. As a first step in optimization of the cross-section, the influence of varying the cross-sectional dimensions on the bending moment capacity, shear capacity and the ratio of moment of resistance above and below the neutral axis will be studied. As a start, we take the dimensions from Appendix 11.15.

3.10.1 Varying the deck depth

By reducing the box girder deck depth, huge savings in the amount of concrete can be made – the steepest line in Figure 3.31 represents the effect of changing the deck depth – and the W0/Wb-ratio decreases fast (Figure 3.32). The effect on the ultimate bending moment capacity is small compared to changing the box girder height (Figure 3.33) and the effect on the shear capacity is negligible (Figure 3.34).

3.10.2 Varying the web width

By reducing the box girder web width, substantial savings in the amount of concrete can be made (Figure 3.31) and the W0/Wb-ratio has a moderate increase (Figure 3.32). The effect on the ultimate bending moment capacity is small (Figure 3.33), but the effect on the shear capacity is huge (Figure 3.34).

3.10.3 Varying the floor depth

Reducing the box girder floor depth has the smallest effect on the concrete cross-sectional area (Figure 3.31) and the W0/Wb-ratio increases fast (Figure 3.32). The effect on the ultimate bending moment capacity is small (Figure 3.33) and the effect on the shear capacity is negligible (Figure 3.34).

3.10.4 Varying the box girder height

By reducing the box girder height, substantial savings in the amount of concrete can be made (Figure 3.31) and the W0/Wb-ratio has a moderate increase (Figure 3.32). The effect on the ultimate bending moment capacity is huge (Figure 3.33), so is the effect on the shear capacity (Figure 3.34).

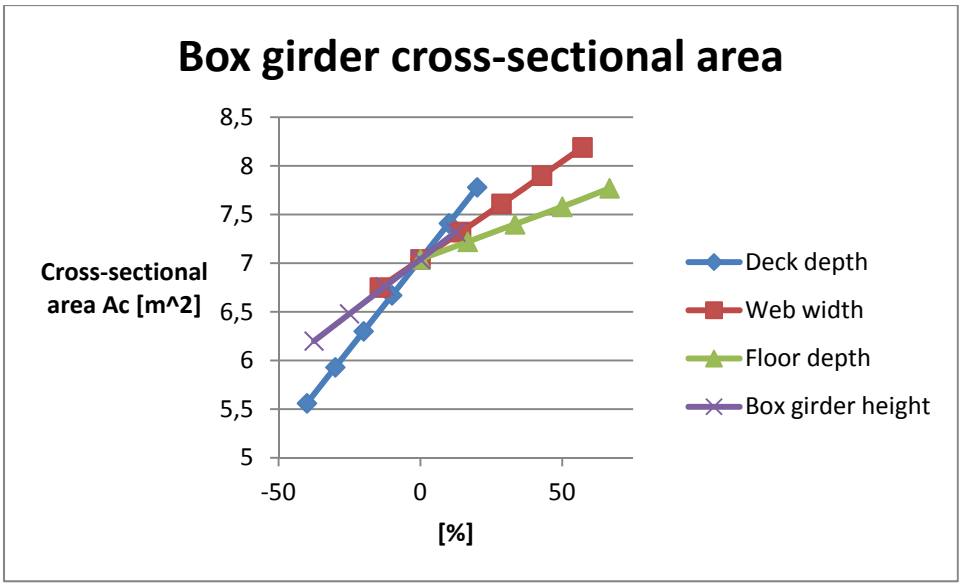

Figure 3.31: size of box girder components vs. cross-sectional area

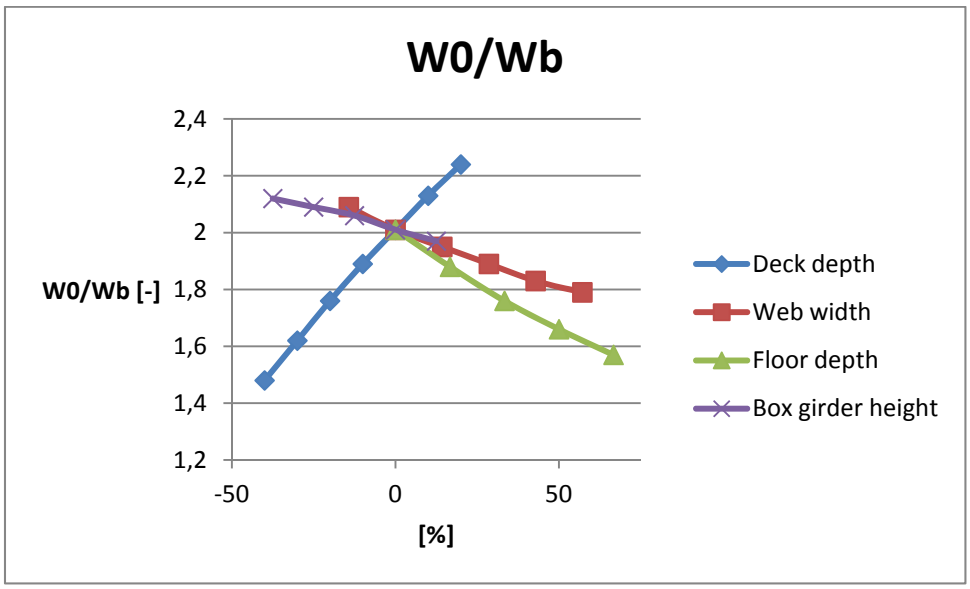

Figure 3.32: size of box girder components vs. moment of resistance ratio

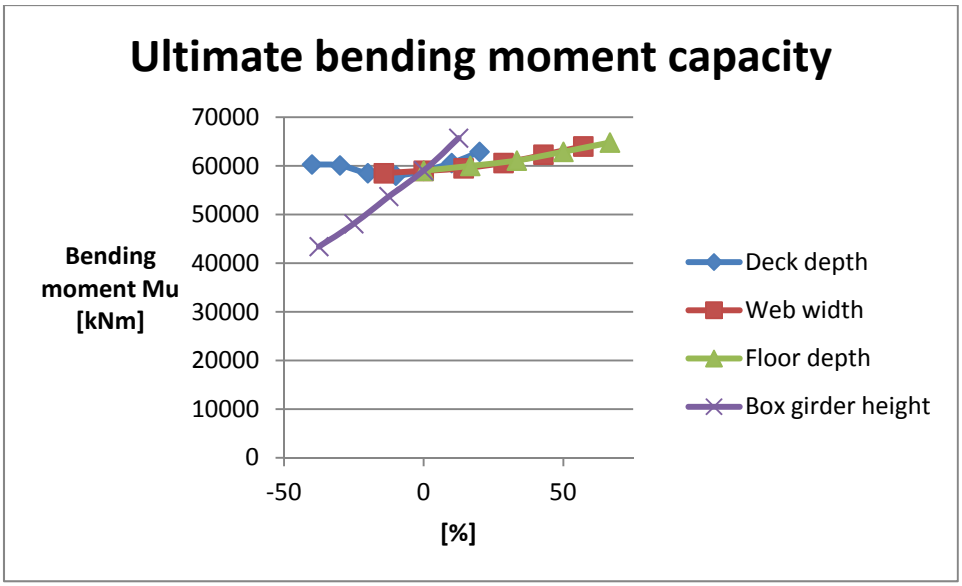

Figure 3.33: size of box girder components vs. ultimate bending moment capacity

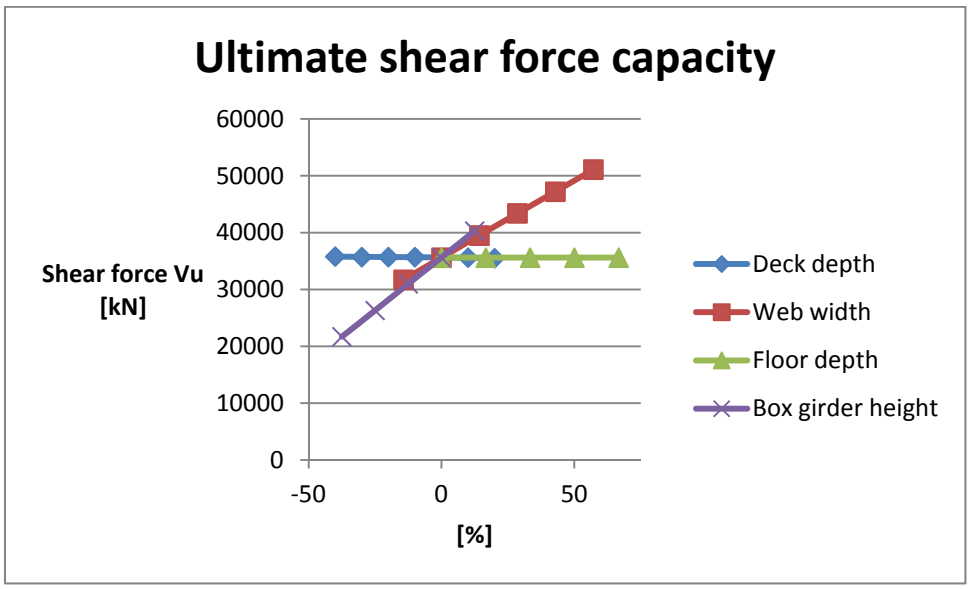

Figure 3.34: size of box girder components vs. ultimate shear force capacity

3.10.5 Increasing the concrete compressive strength f_{ck} from 150 MPa to 200 MPa

The bending moment capacity will not change, as the concrete has such high strength that it will never reach its maximum compressive strain before the prestressing steel fails. For this to happen, too much prestressing steel would be required, which could never fit in the cross-section.

There is a small increase in shear capacity, which is caused by the contribution of the concrete part.

3.10.6 Increasing the design tensile strength σ_{ctmax} from 5 MPa to 6 MPa

The bending moment capacity will have a slight increase. The shear capacity will not change. The bending moment in serviceability limit state that is allowed for the box girder to remain uncracked will have an increased value.

3.10.7 Increasing the modulus of elasticity E_c from 50000 MPa to 60000 MPa

The bending moment capacity will have a slight increase. The shear capacity will not change.

3.10.8 UHPFRC without fibers

When the concrete mixture does not contain any fibers or when the fiber orientation appears to be unfavorable due to some kind of error in the production process, the bending moment and shear capacity will decrease. Appendix 11.17 shows the bending moment and shear capacity that have been obtained for the box girder with no fibers in the concrete.

The bending moment capacity decreases with: $5.33 \cdot 10^{10} / 5.90 \cdot 10^{10} = 0.90 = 10\%$. The shear capacity decreases with: $1.23 \cdot 10^{7} / 3.56 \cdot 10^{7} = 0.35 = 65\%$. This shows, that the absence of the fibers in the concrete mixture has a detrimental effect on the shear capacity.

3.10.9 Using VHPFRC instead of UHPFRC

The very-high performance fiber-reinforced concrete being considered has mechanical properties, which have been obtained by decreasing the mechanical properties of UHPFRC with 20% . When the box girder is executed in very-high instead of ultra-high performance fiber-reinforced concrete, the bending moment and shear capacity will change (Appendix 11.18).

The bending moment capacity decreases with: $5.71 \cdot 10^{10} / 5.90 \cdot 10^{10} = 0.97 = 3\%$. The shear capacity decreases with: $3.52 \cdot 10^{7} / 3.56 \cdot 10^{7} = 0.99 = 1\%$.

4 The hardening process and quality of concrete

Incremental bridge launching requires quick hardening of the concrete, so demoulding and post-tensioning can happen at an early stage. The building speed directly depends on the hardening of the concrete. In (Reinhardt, 1985), the hardening of regular concrete is described. The next paragraph summarizes the most important findings. Paragraph 4.2 describes the hardening properties of UHPC.

4.1 Hardening of conventional concrete

Hardening of the concrete is the result of hydration (Figure 4.1). Immediately after cement and water are mixed, solvation and crystallization processes begin. At first, a small amount of C_3A dissolves, which reacts with calcium sulfate (gypsum) to form tricalcium sulfate (ettringite). This reaction already stops after a few minutes, because the cement grains are being covered by a thin layer of trisulfate crystals. However, during this dormant period, the crystals are still small and do not bridge the space between the cement grains; the cement paste remains workable. As soon as the larger crystals start to grow, chemical bond begins and the cement paste starts to harden. At a later stage the trisulfate will react with calcium hydroxide and aluminate to form monosulfate.

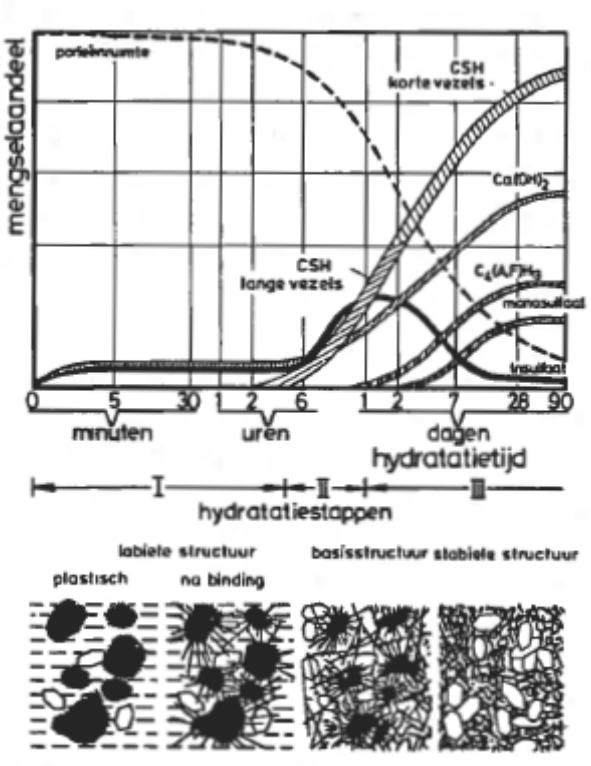

Figure 4.1: diagram of the hydration process (Locher, et al., 1976)

In the first minutes calcium hydroxide is formed as well. Without gypsum, the cement and water mixture would stiffen instantly. The reason is the formation of tetracalcium aluminate hydrate, which connects the cement grains and prevents them from being mobile. The right composition of C_3A and gypsum defines the bonding properties and workability of the cement.

Concrete hardening starts when C_3S dissolves and forms calcium silicate hydrate. C_2S forms calcium silicate hydrate as well, but at a later stage and in a more fine distribution. Calcium silicate hydrate is responsible for the concrete strength.

The amount and composition of cement are responsible for the speed of hardening. The amount of cement in a concrete mixture can be defined by the water-cement ratio. Higher strength concretes have a lower water-cement ratio than normal strength concretes and will thus harden more quickly. Cement contains the following four important clinker compounds:

1. Tricalcium silicate (C_3S);
2. Dicalcium silicate (C_2S);
3. Tricalcium aluminate (C_3A);
4. Tetracalcium aluminate ferrite (C_4AF).

The clinker has hydraulic properties. Being hydraulic means, the matter can react with water, has the ability to harden under water and does not dissolve in water after it has hardened. The compressive strength development of the individual clinker compounds has been plotted in Figure 4.2. The quick chemical reaction of C_3S: $2(3CaO.SiO_2)$ with the corresponding strength development and the much slower strength development of C_2S: $2(2CaO.SiO_2)$ can clearly be seen. A high C_3S content practically means quick hardening of the concrete.

The speed of reaction depends on the reachability of the water. A surface reaction happens at a fast rate. However, as soon as the water needs to penetrate through the thin layer of ettringite, deeper into the cement grains, the reaction will slow down. Such movement is called diffusion.

The speed of reaction is positively influenced when the particle size of the cement is reduced, as the surface – the first reaction in the hydration process is a surface reaction – is increased.

Hydration rate increases for higher temperatures, so concrete in a warm environment will develop its strength more quickly than concrete in a cold environment.

High pressures during hydration will increase the hydration rate. A high pressure will squeeze the water molecules into the cement gel and the unhydrated cement and will therefore favor diffusion and hydration.

Finally, accelerators can be added to the concrete mixture to speed up the hydration process. The most frequently used accelerator is calcium chloride, which accelerates the chemical bond and hardening process. However, the chloride will only be partly chemically bonded. The remaining chloride may contribute to corrosion of reinforcing or prestressing steel.

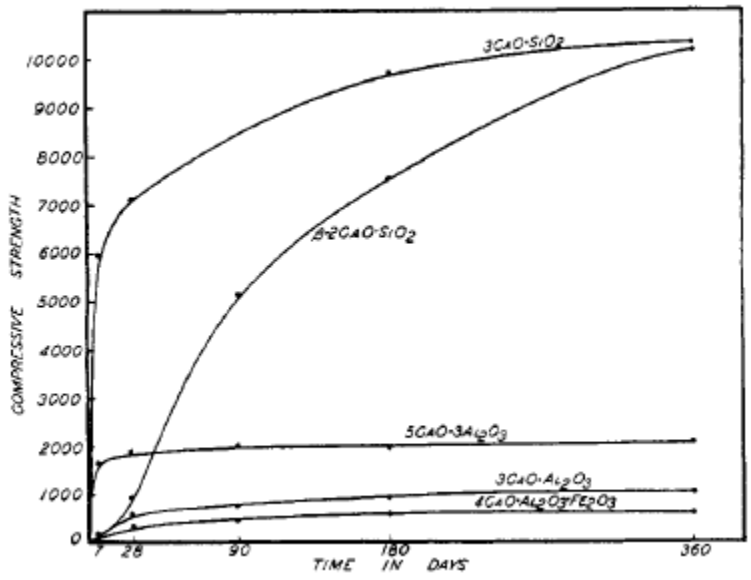

Figure 4.2: comparison of compressive strengths of cement compounds (in pounds per square inch)(Bogue & Lerch, 1934)

The final strength for concrete that undergoes quick hardening is lower, because the composition of the concrete is less structured and more porous when the hydration rate is high.

A slow hydration rate benefits the concrete quality, because the corresponding heat development is reduced and the concrete can cool down without cracking. Cooling, shrinkage and the ability of the young concrete to deform under tension, together determine the concrete cracking.

4.2 Hardening of ultra-high performance concrete

Ultra-high performance concrete has a very low water-cement ratio and degree of hydration. The degree of hydration is a measure for the amount of cement that has hydrated during the hardening process. This means, that a lot of cement stays unhydrated. The unhydrated cement will act as filler for the capillary pores, which appear during the hardening of the concrete, to improve the packing density and microstructure of the concrete.

Besides the unhydrated cement that acts as filler, silica fume can be added to the concrete mixture. Silica fume are ultra-fine particles that improve the tightness and strength of the concrete. They react with calcium hydroxide to form additional calcium silicate hydrates.

In (Burge, 1982), it was demonstrated that silica fume contributes to an early strength development. Just after one day, it is possible to reach a concrete compressive strength over 100 MPa (Figure 4.3).

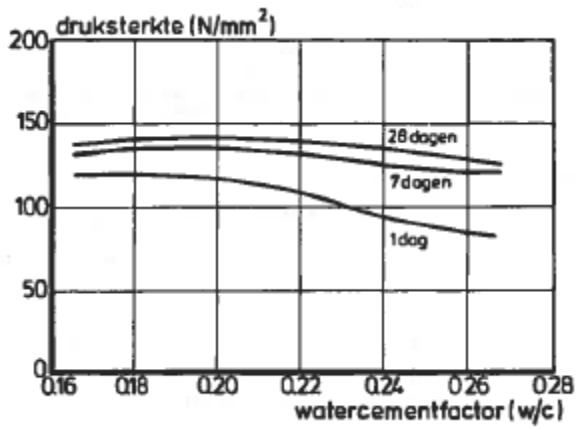

Figure 4.3: compressive strength plotted against water-cement factor for concrete with silica fume (Burge, 1982)

In (Association Francaise de Génie Civil, 2013), the effects of heat treatment are explained. Two types of heat treatment can be distinguished:

1. The first type must be carried out during the first couple of hours of the hydration process to speed up concrete hardening. A moderate temperature ($< 65℃$) is required to avoid any risk of delayed ettringite formation.
2. The second type can be carried out when the concrete has set. The goal is to further develop the concrete strength and to reduce any delayed time-dependent deformations. The temperature will be raised up to $90℃$.

The main effects of heat treatment are:

- an accelerated maturity;
- a total shrinkage equal to zero;
- significantly reduced creep: the creep coefficient is 0.2 instead of 0.8;
- an improved durability due to a reduced porosity.

It can be said, that the quick hardening of ultra-high performance concrete leads to a porous microstructure. However, due to the presence of a lot of unhydrated cement and additives like silica fume, a dense microstructure may be obtained. Heat treatment can be carried out to reduce time-dependent deformations and to improve durability.

5 Building with ultra-high performance fiber-reinforced concrete

This chapter presents two UHPC manufacturers that offer premix kits ready to be batched on-site, a typical mixture composition and the preconditions for on-site production and application of the material.

5.1 Ultra-high performance concrete manufacturers

Quantz is an ultra-high performance fiber-reinforced concrete technology that has been developed by G.tecz engineering. Material parameters can be adapted regarding the designers requirements (Figure 5.1). After development, the technology will be transferred to the consumer and production can immediately start. In (G.tecz Engineering, 2015), Quantz is claimed to be three to four times cheaper than regular ultra-high performance concretes.

	typical	*range*
- compressive strength	175	80 – 600 MPa
- tensile strength	7	3 – 20 MPa
- flexural strength (matrix)	15	3 – 27 MPa
- flexural strength (reinforced)	25	5 – 75 MPa
- fracture energy	55	50 - 90 kN/m
- possible unit thickness	> 2	> 2 mm
- carbonating	1.5	1.5 mm after 3 years
- chloride-diffusion	n.m.	not measurable
- water resistance	n.m.	not measurable
- frost-resistance	< 100	< 100 g/m²
- dispersion	80	up to 80 cm
- shrinkage	1	1 - 1.5 ‰
- crack width	<< 0.1	<< 0.1 mm
- weight	2.4	0.6 - 2.7 t/m³

Figure 5.1: mechanical properties of Quantz (G.tecz Engineering, 2015)

Ductal is an ultra-high performance fiber-reinforced concrete that has been developed by Lafarge and Bouygues. Ductal elements can be precast in a plant and shipped to the site location or, in some cases, may be poured on-site (Lafarge and Bouygues, 2015). When there is need to build with minimal interruption to the public, Ductal provides a solution for accelerated bridge construction. Ductal is sold as a kit including the premix powder, fibers and admixtures.

5.2 Mixture composition

The ultra-high performance fiber-reinforced concrete mixture differs from conventional concrete mixtures. Figure 5.2 illustrates a typical composition of Ductal. The meaning of the water-cement ratio and the function of silica fume and steel fibers have been addressed in chapter 4 and the literature review (Oostra, 2014).

Component Material	Quantity (kg/m^3)
Cement	705
Silica fume	230
Crushed quartz	210
Sand	1010
Superplasticizer	17
Steel fibres	190
Water	195

Figure 5.2: typical composition of Ductal (VSL Australia, 2000)

In ultra-high performance concrete, the aggregate forms the weakest link, as the cement paste has such high strength. Unlike conventional concrete, cracking will develop through the aggregate grains and not at the interface between cement paste and aggregate. High-strength aggregates, like crushed quartz, are required to prevent loss of concrete strength.

	regular concrete C38	HPC C100	UHPC	Quantz
Cement content	*low*	*middle*	*high*	middle
Silica fume content	-	*low*	*high*	low
Fines	-	*low*	*middle*	high
Coarse Aggregates	*high*	*middle*	*low*	low - high [1]
Water Cement Ratio	*0.5*	*0.33*	*0.24*	0.19 - 0.40 [1]
Workability	*high*	*middle*	*low*	earth-moist - fluid [1]
Compr. Strength after 28d	*45*	*100*	*145*	80 -300 [1]
Compr. Strength after 56d	*45*	*110*	*160*	100 - 300 [1]
Flex. Strength after 28d	*35*	*6*	*13*	6 - 25 [1]
Density	*2.36*	*2.48*	*2.45*	2.3 - 2.7 [1]
Porosity Vol.%	*15.0*	*8.3*	*6.0*	4.5 - n.m. [1]
Permeability	*high*	*middle*	*low*	n.m.
Water absorption coefficient	*high*	*middle*	*low*	n.m.
Fire resistance	*middle*	*middle*	*low*	high - very high
Freeze Thaw Resistance	*low*	*middle*	*high*	high - very high
Prize per m^3	*low*	*middle*	*high*	low - middel [1]

Figure 5.3: comparing Quantz to regular, high performance and ultra-high performance concrete (G.tecz Engineering, 2015)

Figure 5.3 shows some remarkable properties of Quantz. Unlike other ultra-high performance concretes, Quantz has medium cement content, contains little silica fume, has a moderate water-cement ratio and remains supremely workable.

5.3 Preconditions and equipment for on-site production and application of UHPC

In (Association Francaise de Génie Civil, 2013) an overall design approach for ultra-high performance concrete is presented. The concrete must satisfy this procedure's conditions to qualify for application in the incrementally launched bridge.

At the very beginning of the project design stage, the constitutive laws and characteristics of the required material must be known. Assuming the concrete mixture that has been batched in the factory has attained the characteristics required by the designer, it should pass full-scale tests in order to qualify for the proposed application. A mockup of the actual structure, under the same conditions of on-site placement, must be produced to validate constitutive laws and characteristics of the concrete. To determine the K-factor, which takes the disparity in fiber orientation into account, samples must be taken from the mockup along the directions of principal stresses.

Tolerances for premix need to be defined and checked with the manufacturer's quality sheet, which must come with each delivery. The contractually bound mix design is defined by the overall quantity of premix, admixtures, water and fibers. The batch plant must be sufficiently accurate to meet a tolerance of at least 2% for all mixture components. If the premix manufacturer can guarantee a tolerance of 1%, the batch plant must be able to have that accuracy as well.

A mobile concrete batch plant is required that can be installed on the construction site. The quantities of water as well as the regularities of the mixtures components that go into the batch plant must be carefully monitored. Routine checks must be performed on the mix design after production.

The time between batching of the ultra-high performance concrete and completion of placement must be consistent. It is strictly prohibited to add water or admixtures, after the concrete has been batched.

Drop heights exceeding half a meter should be avoided concerning segregation of fibers from the cement paste and formation of fiber clusters. Besides that, concrete should be poured without interruption to guarantee fiber continuity.

In cold weather, special arrangements should be made to guarantee the strength development of the concrete, such as heating of the aggregate and water, insulation and hardening accelerators. Three follow-up specimens must be taken during concrete pouring. Their maturity must be monitored. Demoulding cannot happen until the strength development is sufficient. When the outdoor temperature exceeds 35℃, the same precautions as for conventional concrete must be taken to prevent high temperatures inside thick elements.

Since ultra-high performance concrete has little or no bleeding, special attention should be paid to the curing. When evaporation occurs at a faster rate than bleeding, the concrete surface will dry and capillary stresses arise. The concrete wants to shrink, but is held in place by the mould, resulting in tensile stresses and cracking. Curing must be carried out carefully in order to prevent the concrete from drying out before it has set.

6 Case study: bridge over “Het Pannerdensch Kanaal”

The infrastructure in the Arnhem – Nijmegen region currently cannot handle the traffic intensity and the problem is likely to become worse in the future. To improve the regions traffic flow and the link between port of Rotterdam and Germany, highway A15 will be extended from the Valburg interchange to the Oud-Dijk interchange, on highway A12, with 2x2 driving lanes (Figure 6.1).

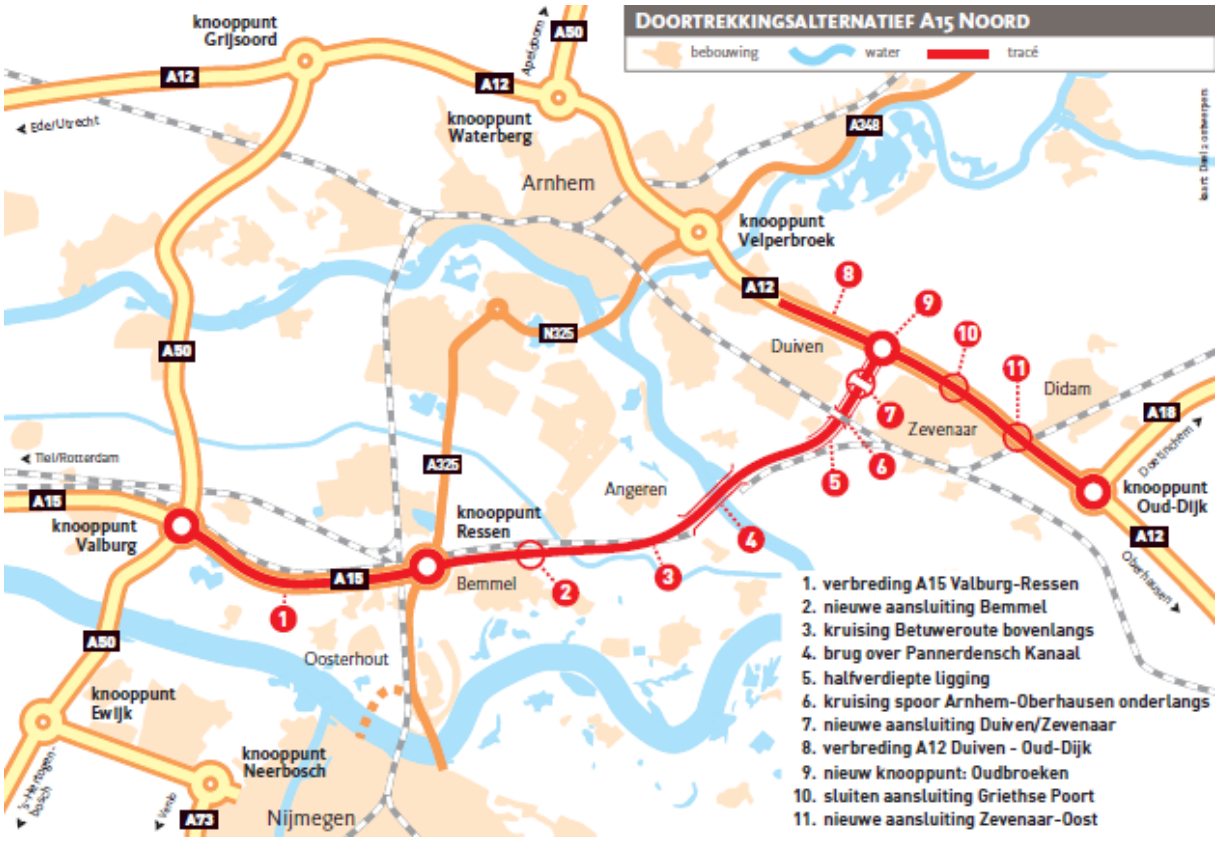

Figure 6.1: route of the highway A15 elongation (Projectbureau ViA15, 2015)

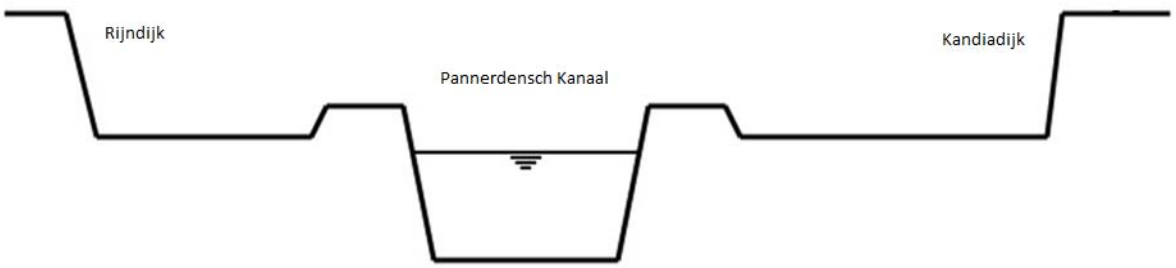

Figure 6.2: cross-section river, floodplains and levees

Part of the route is a bridge that crosses “het Pannerdensch Kanaal”. The channel is positioned between the Rijndijk in the west and the Kandiadijk in the east (Figure 6.2). The approach bridges span the channels floodplains and connect the main span with the infrastructure on the protected lowland. Because of the repetitive flooding of the floodplains and poor ground conditions, the approach bridges cannot be constructed on stationary or movable scaffolding on rollers, so that incremental bridge launching may be a good solution.

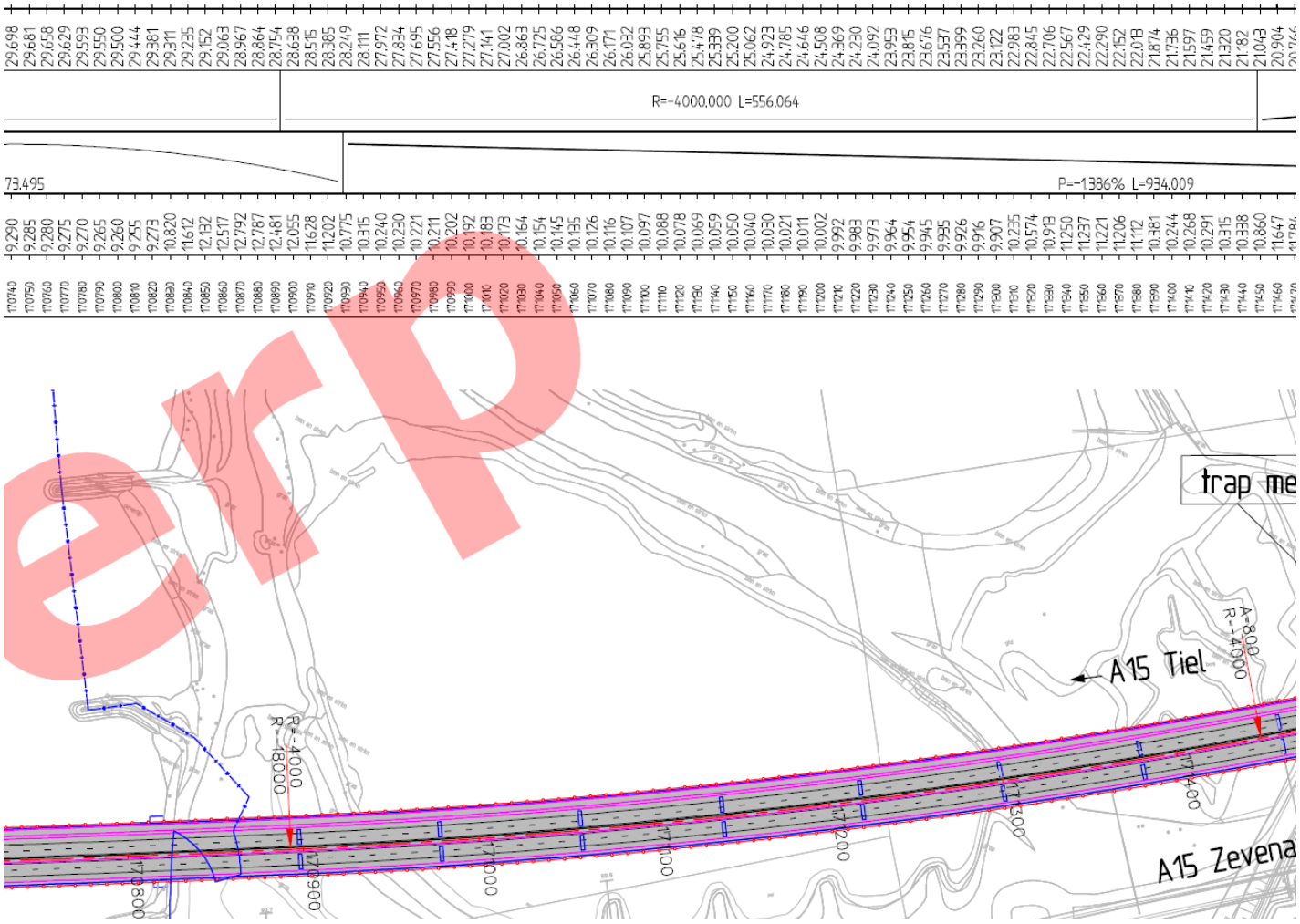

Figure 6.3: preliminary draft of the eastern approach bridge (Rijkswaterstaat, 2013)

Other optional construction techniques are the span-by-span casting method with an assembly truss and construction with precast beams. The assembly truss can be placed beneath the superstructure when the construction clearance provides enough space for the formwork. The bridge piers need to be adapted to be able to launch. The assembly truss can also be placed above the superstructure. However, a major disadvantage is that the formwork requires termporary suspension rods passing through the superstructure. The span-by-span casting method with an assembly truss requires a high

capital investment, which must often be recovered in one or only a couple of structures. Both span-by-span casting and construction with precast beams are limited by their maximal span length of around 60 meters. In general, incremental bridge launching enables longer spans and requires fewer bridge piers.

The preliminary draft of the eastern approach bridge seems to meet the preconditions for use of incremental bridge launching (Figure 6.3). Over a length of more than 550 meters the approach bridge has a constant horizontal and vertical curvature.

6.1 Functional requirements

- The approach bridge must be designed for a working life of 100 years.
- The approach bridge can be classified in consequence class CC3. In the launch phase, the approach bridge may temporarily be classified in consequence class CC1.
- The approach bridge is part of a highway and must therefore be able to carry Load Model 1.
- The approach bridge must accommodate 2x2 driving lanes, two hard shoulders, two hard strips, two verges, a central reserve, safety barriers, a side path designated for pedestrians and cyclists and parapets.
- The approach bridge must connect the main span with the new highway that begins at the eastern abutment near Zevenaar.

6.2 Geometrical requirements

- The approach bridge has a total length of 550 meters (Rijkswaterstaat, 2013).
- According to (Rijkswaterstaat, 2011) a high water clearance of 9.1 meters is required for “Het Pannerdensch Kanaal”.
- The traffic clearance at a levee (Kandiadijk) must be at least 4.2 meters.
- At the floodplains, the bottom of the box girder floor must always exceed high water level .
- The cross-section must be uniform.
- All intermediate spans must be equal in length. End spans must have 80% of that length.
- Joints cannot be positioned above a support or at mid-span.
- The approach bridge has a radius of curvature of 4,000 meters in its horizontal plane.
- The approach bridge has a constant elevation of 1.386% in its vertical alignment.
- The deck must be sufficiently thick to prevent punching shear failure caused by axle loads.
- The deck, webs and floor must provide enough space for reinforcement and ducts when internal prestressing will be used. Continuity prestressing is anchored in haunches.

- The floor must be sufficiently thick to prevent punching shear failure when the cross-section slides over a support.
- The maximum deflection with respect to the characteristic value of traffic loading: $u_{el} \leq L/300$ for $L > 10$ meters (Rijkswaterstaat, 2013).

6.3 Physical requirements

- The approach bridge must be built with reinforced or prestressed concrete.
- The volumetric mass density of reinforced or prestressed NSC/HSC is 25 kN/m^3
- The volumetric mass density of prestressed UHPFRC is 26 kN/m^3.

6.4 Boundary conditions

- The approach bridge will be launched from the eastern (lower) abutment near Zevenaar, which makes a braking system unnecessary. The abutment and embankment will not be considered in the design.
- The superstructure is supported by bridge piers that will not be considered in the design.
- The number of bridge piers is still to be determined. For the preliminary design, the bridge piers are positioned according to (Rijkswaterstaat, 2013).
- All segments should exactly fit into the span to achieve high repetition in lay-out of reinforcement and cable alignment.
- In relation with seep or piping, bridge piers are not permitted within four meters of a levee .
- The approach bridge should be constructed without auxiliary supports.
- Continuity prestressing must be anchored at zero bending moment points at approximately one fifth of the span length.

6.5 Design assumptions

- The approach bridge will be built up out of two single-cell concrete box girders that will operate independent of each other. Between both box girders, a one meter interspace will be present that will be bridged by grids.
- A single box girder will be considered in the design.
- All bridge piers will support both box girders. The bearings are positioned directly beneath the webs to avoid bending moments caused by eccentric reactions.
- The protected lowland provides sufficient space and load bearing capacity to erect a fabrication yard.

- Aesthetics will not be considered in the design.
- Cross-beams may be required above the supports to ensure (torsion) stability.
- The superstructure can be classified in structural class S4, assuming the concrete strength to be ≥ C45/55 and a special quality control that can be ensured by the factory-like conditions.
- The superstructure can be classified in exposure classes XC4, XD3 and XF4.
- Longitudinal and shear reinforcement will be fabricated from B500 steel.
- Y1860S7 prestressing strands will be used in the design.
- Only load model 1 will be considered in the design.
- Loads and load combinations will be determined with (NEN-EN 1991).
- Central prestressing can be re-used as continuity prestressing.
- The batch plant on-site is sufficiently accurate to guarantee the required quality for UHPC.

7 Box girder dimensions for preliminary design

Before we can start with the design and optimization process we need to define the box girder shape and dimensions.

7.1 The shape of the box girder

The shape of the box girder will be based on a study by (van der Meulen, 1991). He investigated the optimal box girder cross-section for different span lengths and execution methods.

7.1.1 Inclined webs versus straight webs

Inclined webs reduce the span of the box girder floor, so it may be designed more slender. Bridge piers may become less wide and inclined webs work aesthetically pleasing. The force distribution for a box girder with inclined webs differs from a box girder with straight webs. Self weight causes a compressive stress in the floor and a tensile stress in the deck (Figure 7.1). Prestressing cables in the webs that have a parabolic lay-out cause a tensile stress in the floor.

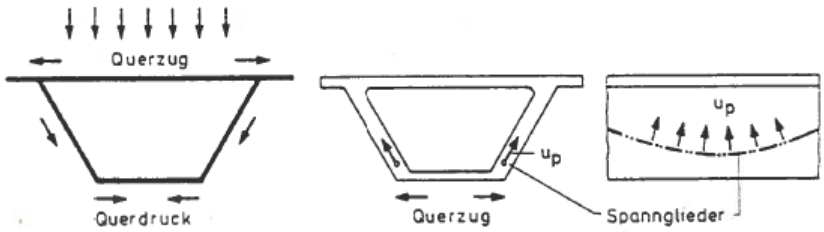

Figure 7.1: box girder with inclined webs (Leonhardt, 1979)

For conventional reinforced concrete box girders inclined webs may cause difficulties with respect to pouring and vibrating the concrete and installation of reinforcement. Straight webs may simplify execution. An ultra-high performance fiber-reinforced concrete box girder that does not have longitudinal reinforcement does not have these problems. However, the fiber orientation for inclined and straight webs may deviate, as fibers tend to align in the direction of flow and fibers close to formwork walls are naturally aligned to them.

The shear capacity of ultra-high performance fiber-reinforced concrete consists of a concrete part, a shear reinforcement part and a fiber part. Since the fiber orientation and the shear plane of the concrete differ for inclined and straight webs the shear capacity will differ as well.

Because the floor of a box girder with inclined webs has less concrete and thus a smaller compressive capacity, the internal lever arm must be increased to provide sufficient capacity. This means an increase in construction depth. In order to meet the clearance criterion for the bridge or viaduct, the embankment must be enhanced, which provides additional cost. Also, approach bridges often are connected to balanced cantilever bridges. Balanced cantilever box girder bridges with varying depth cannot have inclined webs, because they lead to a varying floor width and thus a complicated execution. Therefore almost all incrementally launched box girder bridges in The Netherlands have straight webs, except for Viaduct Ravensbosch that crosses a 25 meters deep valley (Thomaes, et al., 1974).

Since clearance is an important geometrical requirement at the approach bridge location, and to simplify calculations, the box girder will have straight webs and will have the shape from Figure 7.2.

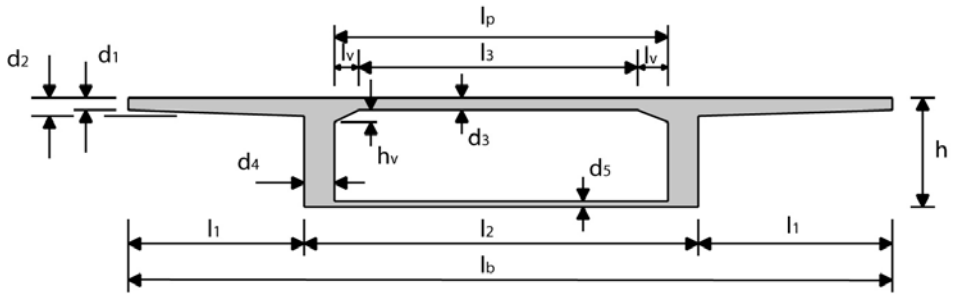

Figure 7.2: box girder dimensions (van der Veen, 2014)

7.2 The deck width

The deck width l_b will be based on dimensions from Figure 7.3 and (Rijkswaterstaat, 2013).

The single cell box girder must accommodate:

- two driving lanes + centre line: 2x3.50m + 0.15m.
- a hard shoulder + side line: 3.15m + 0.15m.
- a verge + safety barrier + footpath: 0.50m + 1.41m.
- a hard strip + side line: 1.50m + 0.15m.
- a safety barrier + footpath: 1.41m.
- total: 15.42m.

For purpose of execution the deck width will be set to: $l_b = 15.50\ m$.

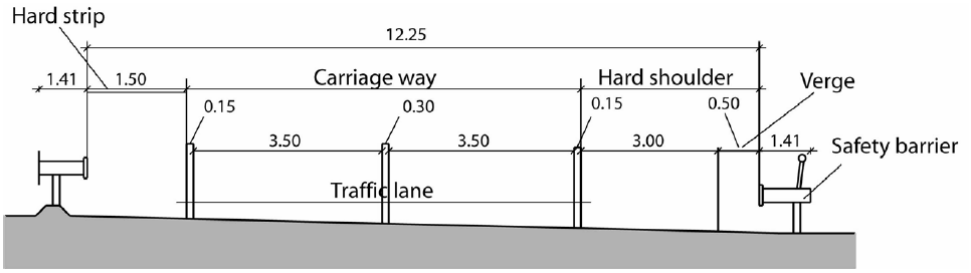

Figure 7.3: dimensions on a bridge deck (van der Veen, 2014)

7.3 Remaining box girder dimensions

The remaining box girder dimensions will be determined with rules of thumb from (van der Meulen, 1991) and (van der Veen, 2014).

For an incrementally launched conventional concrete box girder without auxiliary supports the span to depth ratio is: $l/h \approx 18$. When temporary bridge piers are used, a slenderness of: $l/h \approx 25$ can be reached.

The approach bridge has a constant curvature in its horizontal and vertical alignment for a length of 550 meters. The span length for incrementally launched conventional concrete box girder bridges is 35 to 75 meters. End spans must have a length of about 80% of the intermediate span length. As a start, the span length will be set to 57.3 meters. End spans will be 45.8 meters long.

The box girder depth: $h = l/18 = 57.3/18 = 3.2\ m.$

The cantilever length: $l_1 = 2 - 3.5\ m.$

The box girder width: $l_2 = 5 - 7\ m.$

$$\frac{l_1}{l_2} \approx 0.45$$

$$2l_1 + l_2 = 15.5\ m \rightarrow l_1 = 3.75\ m\ \&\ l_2 = 8\ m.$$

The width of the upper haunch: l_v.

The deck width in between webs: l_p.

$$l_p = l_2 - 2d_4 = 8 - 2 \cdot 0.35 = 7.3\ m.$$

$$\frac{l_v}{l_p} \leq 0.2 \rightarrow l_v < 0.2 \cdot 7.3 = 1.4\ m$$

The thickness at the cantilever's end: d_1.

The thickness of the cantilever at the web: d_2.

For a conventional concrete box girder the thickness of the cantilever will be governed by the bending moment and shear forces in transverse direction.

$$d_1 \geq 0.2\ m \rightarrow d_1 = 0.2\ m.$$

$$\frac{d_2}{d_1} \approx 2 \text{ à } 3 \rightarrow d_2 = 0.4\ m$$

The thickness of the deck: d_3.

The web thickness: d_4.

The floor thickness: d_5.

For an incrementally launched conventional concrete box girder the web thickness will be governed by the shear forces in longitudinal direction. The floor thickness will be governed by the bending moment at the support.

$$d_3 > \frac{l_p}{30} > 0.2\ m \rightarrow d_3 > \frac{7.3}{30} > 0.2\ m \rightarrow d_3 = 0.25\ m$$

$$d_4 \geq 0.35\ m \rightarrow d_4 = 0.35\ m.$$

$$d_5 \geq 0.15\ m \rightarrow d_5 = 0.15\ m.$$

The height of the upper haunch: h_v.

$$h_v = d_3 = 0.25\ m.$$

8 Design of the superstructure

This chapter describes the special procedure for box girder design and provides an analysis of the force distribution and capacity in transverse direction to optimize the dimensions that were adopted for the preliminary design.

When the slenderness $l/h \geq 4$, the span length $l \geq 1.5l_b$ and the box girder is loaded symmetrically in the transverse direction, the box girder may be designed longitudinally as a beam and transversely as a frame, independent of each other. When the loads are positioned asymmetrically in transverse direction, the box girder may not be designed separate and independent in longitudinal and transverse direction (Schlaich & Scheef, 1982).

8.1 Design procedure

The design of the box girder cross-section takes the following procedure:

1. Determination of governing load cases in longitudinal and transverse direction.
2. Beam analysis with a rigid cross-section in longitudinal direction, yielding M_X, V_X, M_T & σ_X.
3. Splitting up the loading into a symmetrical and an asymmetrical part (Figure 8.1).
4. Frame analysis in transverse direction for symmetrical loading, yielding $(m, n, v)_{sym}$.
5. Frame analysis in transverse direction for asymmetrical loading, yielding $(m, n, v)_{asym}$ & S.
6. Superposition of the sectional forces in transverse direction, yielding m, n & v.
7. Determination of longitudinal stresses σ_F and transverse bending moments m_F, which are a result of the diagonal force S caused by the combination of longitudinal and transverse bending (Figure 8.1d).
8. Superposition of σ_F with σ_X and m_F with m, yielding the actual longitudinal and transverse stresses.

8.2 The loads

8.2.1 Self weight

The volumetric mass density of UHPFRC: $\gamma = 26\ kN/m^3$. The self-weight is permanently present in both the launch phase and the use phase.

8.2.2 Super imposed dead load

The super imposed dead load consists of the weight of non-structural elements, such as asphalt and safety barriers. The super imposed dead load is a permanent load and is only present in the use phase. (Rijkswaterstaat, 2013) demands an asphalt layer thickness of $50 + a + 70\ mm$, with:

$$a = 20 + \frac{l - 30}{4} \leq 50\ mm$$

Assume: $l = 50\ m \rightarrow a = 25\ mm$.

The volumetric mass density of dense asphalt concrete (DAB): $\gamma = 23\ kN/m^3$.

The volumetric mass density of ZOAB: $\gamma = 21.5\ kN/m^3$.

Estimated dead load from asphalt: $0.145 \cdot 23 = 3.3 \rightarrow 3.5\ kN/m^2$.

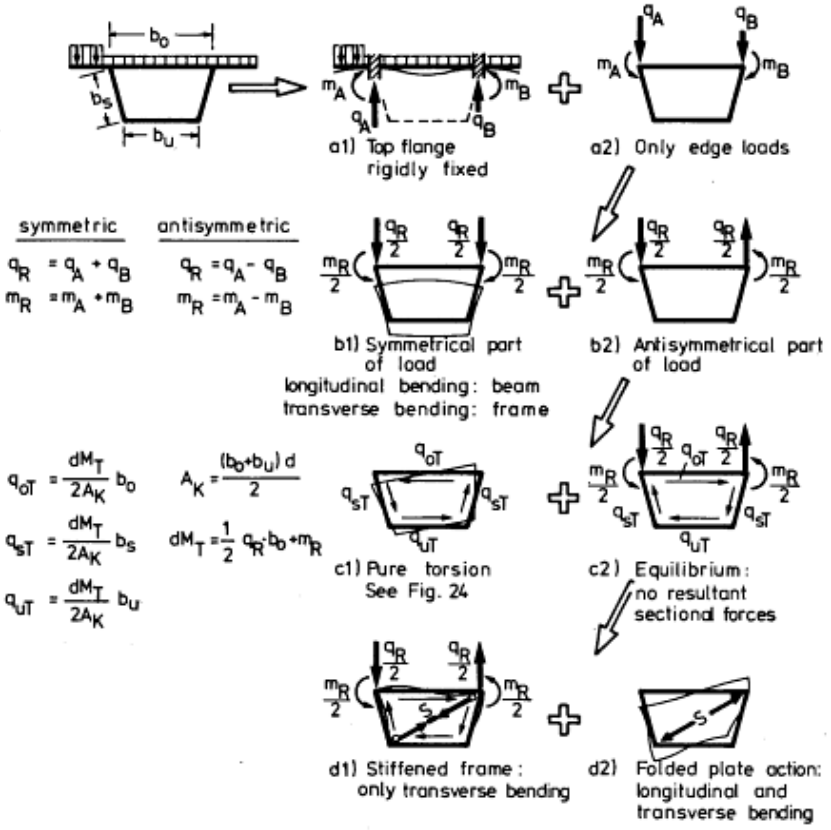

Fig. 16 Splitting up of the structural system and the loading of a box girder. All arrows drawn represent external loads. The cantilevers are partially omitted for greater clarity.

Figure 8.1: splitting up of the structural system and the loading of a box girder (Schlaich & Scheef, 1982)

The weight of the safety barrier: $1\ kN/m$.

The weight of the footpath (Figure 8.2): $A_c \cdot \gamma = (0.15 \cdot (0.4 + 0.6) + 0.3 \cdot 0.4) \cdot 25 = 6.75\ kN/m$.

The weight of the parapet: $0.75\ kN/m$.

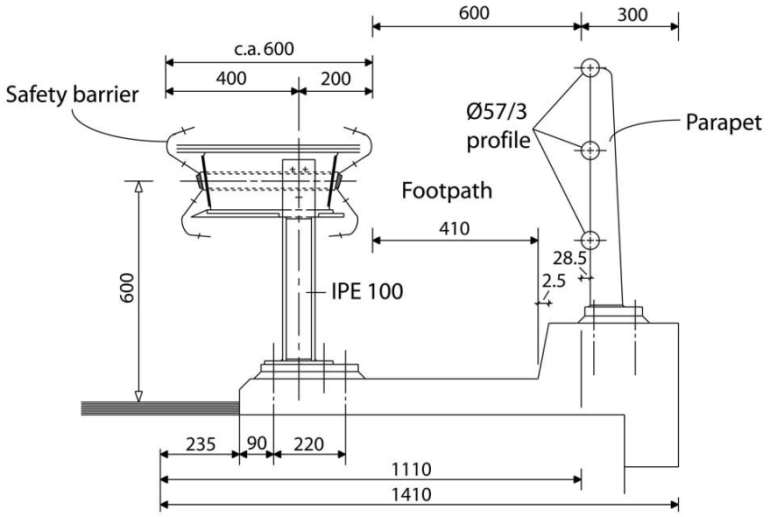

Figure 8.2: safety barrier, footpath and parapet

8.2.3 Traffic loading

Traffic loading is a live load that is active in the use phase. Only load model 1 will be considered in the design. Load model 1 consists of two partial systems: a uniformly distributed load (UDL) and a tandem system (TS).

The UDL has the following weight per square meter of notional lane: $\alpha_q q_k$, with α_q from NEN-EN 1991-2 NB 4.3.2 and q_k from NEN-EN 1991-2 Table 4.2.

The tandem system consists of double-axle concentrated loads, each axle having following weight: $\alpha_Q Q_k$, with α_Q from NEN-EN 1991-2 Table NB1 and Q_k from NEN-EN 1991-2 Table 4.2.

8.2.4 Temperature loading

Due to daily variations, the bridge deck its upper surface will heat up and cool down. These temperature differences may cause bending moments in the box girder when the bridge deck cannot freely deform. The bridge deck can be classified into type 3 in accordance with NEN-EN 1991-1-5 6.3.2. The effect of vertical temperature differences can be considered by using equivalent linear temperature difference components $\Delta T_{M,heat}$ and $\Delta T_{M,cool}$ combined with a factor k_{sur} conform NEN-EN 1991-1-5 Table 6.1 & Table 6.2.

8.3 Load combinations

8.3.1 Ultimate limit state

The ULS combinations consist of:

- ULS – EQU: loss of equilibrium of the structure, e.g. buckling.
- ULS – STR: failure by excessive deformation or transformation of the structure into a mechanism.
- ULS – GEO: failure or excessive deformation of the ground.
- ULS – FAT: failure caused by fatigue or other time-dependent effects.

For ULS – STR, the less favorable of the two following fundamental combinations applies (NEN-EN 1990: equations 6.10a & 6.10b):

$$\sum_{j\geq 1} \gamma_{G,j} G_{k,j} + \gamma_P P + \gamma_{Q,1}\psi_{0,1} Q_{k,1} + \sum_{i\geq 1} \gamma_{Q,i}\psi_{0,i} Q_{k,i}$$

$$\sum_{j\geq 1} \zeta_j \gamma_{G,j} G_{k,j} + \gamma_P P + \gamma_{Q,1} Q_{k,1} + \sum_{i\geq 1} \gamma_{Q,i}\psi_{0,i} Q_{k,i}$$

The partial factors γ follow from NEN-EN 1990: Table NB.13 – A2.4(B). The ψ factors must be derived from NEN-EN 1990: NB.9 – A2.1.

8.3.2 Serviceability limit state

The SLS combinations consist of:

- a characteristic combination;
- a frequent combination;
- a quasi-permanent combination.

For the frequent combination the following expression applies (NEN-EN 1990: equation 6.15b):

$$\sum_{j\geq 1} G_{k,j} + P + \psi_{1,1} Q_{k,1} + \sum_{i\geq 1} \psi_{2,i} Q_{k,i}$$

For the quasi-permanent combination the following expression applies (NEN-EN 1990: equation 6.16b):

$$\sum_{j\geq 1} G_{k,j} + P + \sum_{i\geq 1} \psi_{2,i} Q_{k,i}$$

In SLS all partial factors γ are set to zero (NEN-EN 1990: A2.4.1).

8.4 Transverse direction and mobile loads

(van der Meulen, 1991) found, that the mobile loads are decisive for the bending moment in the top flange. It is therefore to necessary to determine the governing positions for the mobile loads.

The governing load cases for box girder dimensions have been determined with Figure 8.3. The concentrated vehicle loads will not just spread in the direction perpendicular to the box girder cross-section and need to be adapted before they can be put into a framework model to obtain realistic results.

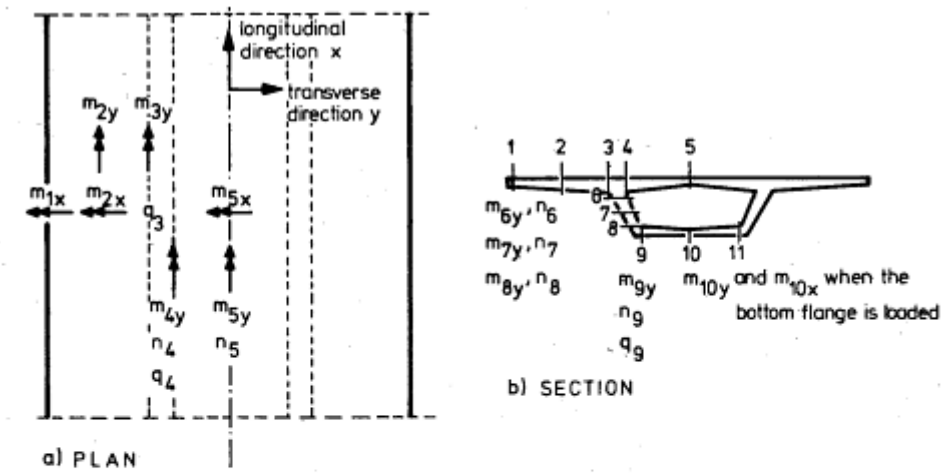

Fig. 13 Sectional forces required for the dimensioning of the flanges

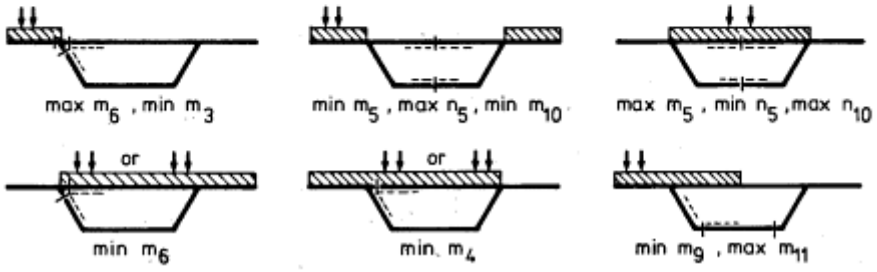

Fig. 14 Critical loadings, in general

Figure 8.3: critical loading for box girder dimensions (Schlaich & Scheef, 1982)

As the load distribution in transverse direction only governs the dimensions of the deck, just the first four load cases will be considered in the design.

For load case 1, the UDL and TS are applied on one of the flanges (Figure 8.3 top left). It will provide the extreme:

- cantilever bending moment
- bending moment at the top of the web

For load case 2, the UDL and TS are applied at both flanges (Figure 8.3 top middle). It will provide the extreme:

- negative bending moment at the centre of the deck
- normal force (tension) in the deck
- negative bending moment at the centre of the floor

For load case 3, the UDL + TS are applied on the deck between the webs (Figure 8.3 top right). It will provide the extreme:

- positive bending moment at the centre of the deck
- normal force (compression) in the deck
- normal force (tension) in the floor

For load case 4, the UDL is applied on the deck between the webs and on one of the flanges. The TS is applied close to the web (Figure 8.3 bottom left). It will provide the extreme bending moment at the web-deck connection.

A single cell box girder will now be considered with dimensions from Table 8.1.

h	3200	mm
lb	15500	mm
l1	3925	mm
l2	7650	mm
d1, d2, d3	250	mm
d4	350	mm
d5	150	mm

Table 8.1: single cell box girder dimensions

8.4.1 Load case 1

Figure 8.4 illustrates the spreading of the axle loads under an angle of $45°$. The tandem system is applied at the most unfavorable position on the cantilever; as close to the edge as possible. Only the uniformly distributed load $q_{1k} = 9\ kN/m^2$ and the tandem system $Q_{1k} = 300\ kN$ of lane number 1 (the slow lane) will be applied in load case 1.

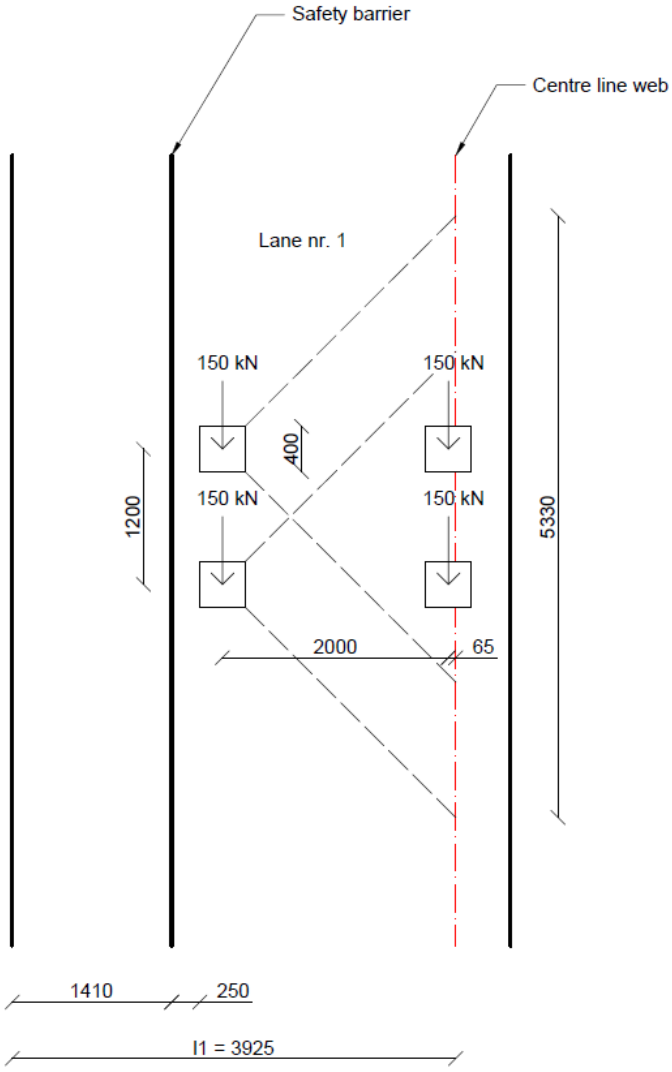

Figure 8.4: spreading of axle loads from load case 1

The cantilever bending moment due to the tandem system:

$$M_{TS} = -\frac{2 \cdot 150 \cdot 2.065}{1.2 + 2 \cdot 2.065} = -116\ kNm/m$$

The distribution of the concentrated vehicle loading can also be evaluated by an influence surface for a cantilever slab with a thickness ratio 1:2 (Figure 8.5).

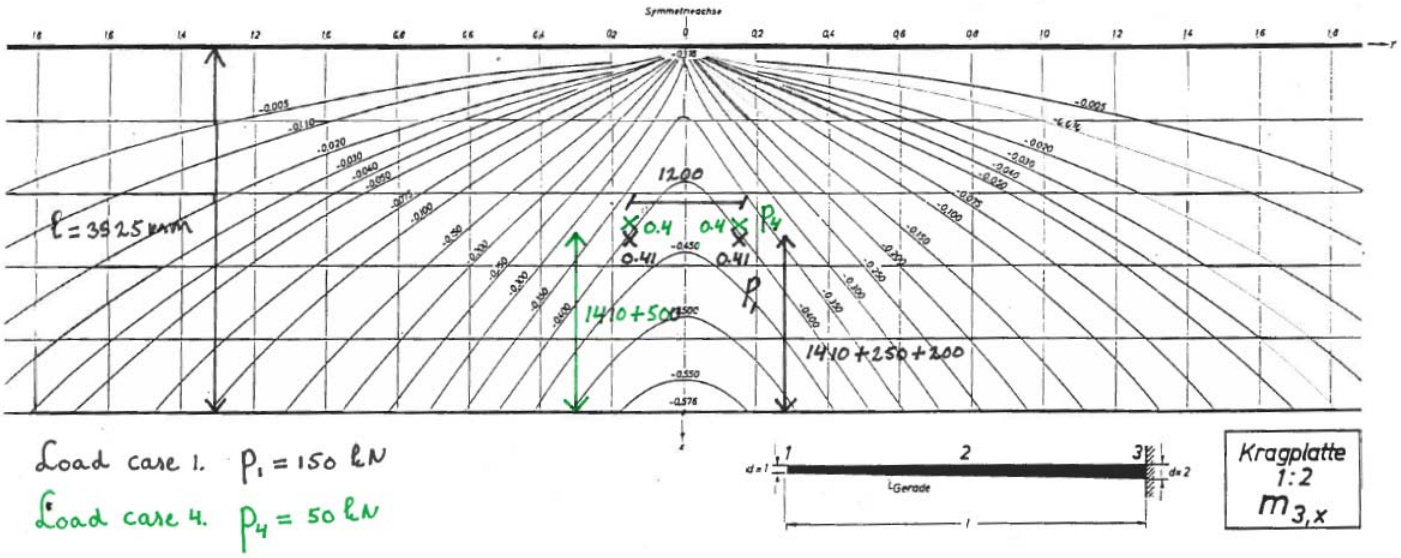

Figure 8.5: influence surface for a cantilever slab(Homberg & Ropers, 1965)

The cantilever bending moment due to the tandem system:

$$M_{TS} = -(0.41 + 0.41) \cdot 150 = -123\ kNm/m$$

In order to obtain a similar bending moment value in the framework model, a point load of 59 kN needs to be applied on the flange:

$$M_{TS} = -59 \cdot 2.065 = -122\ kNm/m$$

The cantilever bending moment due to the uniformly distributed load:

$$M_{UDL} = -\frac{1}{2} \cdot 10.35 \cdot (3.925 - 1.41)^2 = -33\ kNm/m$$

Load case 1 gives (Appendix 12):

$$M_{cantilever} = 155\ kNm/m$$

$$V_{cantilever} = 85\ kN/m$$

$$M_{web\ top} = 130\ kNm/m$$

$$V_{web} = 44\ kN/m$$

8.4.2 Load case 2

For load case 2 the influence surface of Figure 8.5 can be evaluated again. The left flange is subject to the same loading as for load case 1, i.e. the UDL = 9 kN/m^2 and the heaviest tandem system of 300 kN. The right flange will be subjected to the UDL = 2.5 kN/m^2 and the second heaviest tandem system of 200 kN (Figure 8.6).

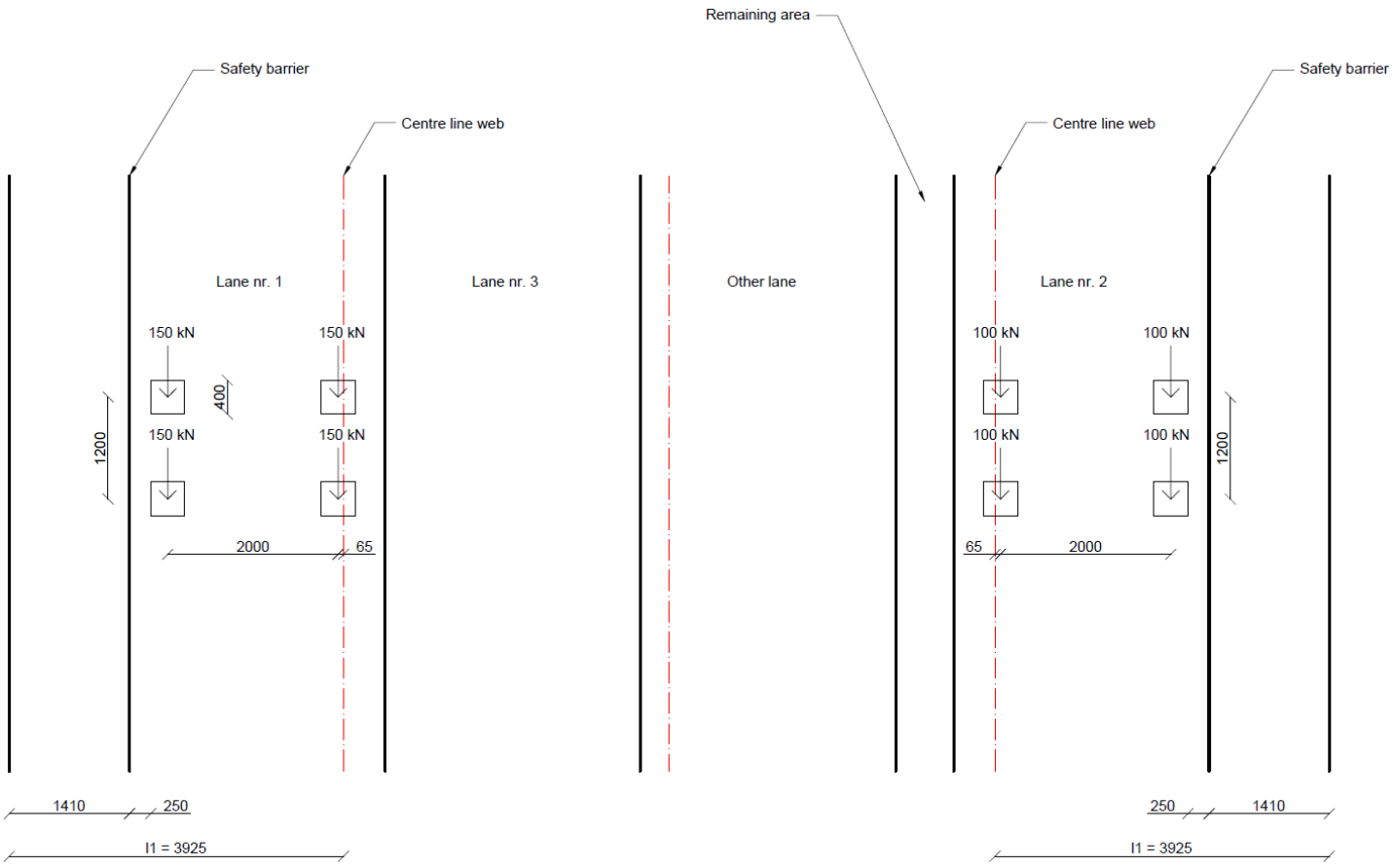

Figure 8.6: tandem system position for load case 2

The cantilever bending moment due to the tandem system from lane number two:

$$M_{TS} = -(0.41 + 0.41) \cdot 100 = -82\ kNm/m$$

In order to obtain a similar bending moment value in the framework model, a point load of 40 kN needs to be applied on the flange:

$$M_{TS} = -40 \cdot 2.065 = -83\ kNm/m$$

The cantilever bending moment due to the uniformly distributed load from lane number two:

$$M_{UDL} = -\frac{1}{2} \cdot 3.5 \cdot (3.925 - 1.41)^2 = -11\ kNm/m$$

Load case 2 gives (Appendix 12):

$M_{deck\ span} = -11\ kNm/m.$

$N_{deck} = -30\ kN/m$ (tension).

$M_{floor\ span} = 1\ kNm/m.$

8.4.3 Load case 3

Figure 8.7 illustrates the most unfavorable position of the tandem system for load case 3; as close to the centre of the deck as possible.

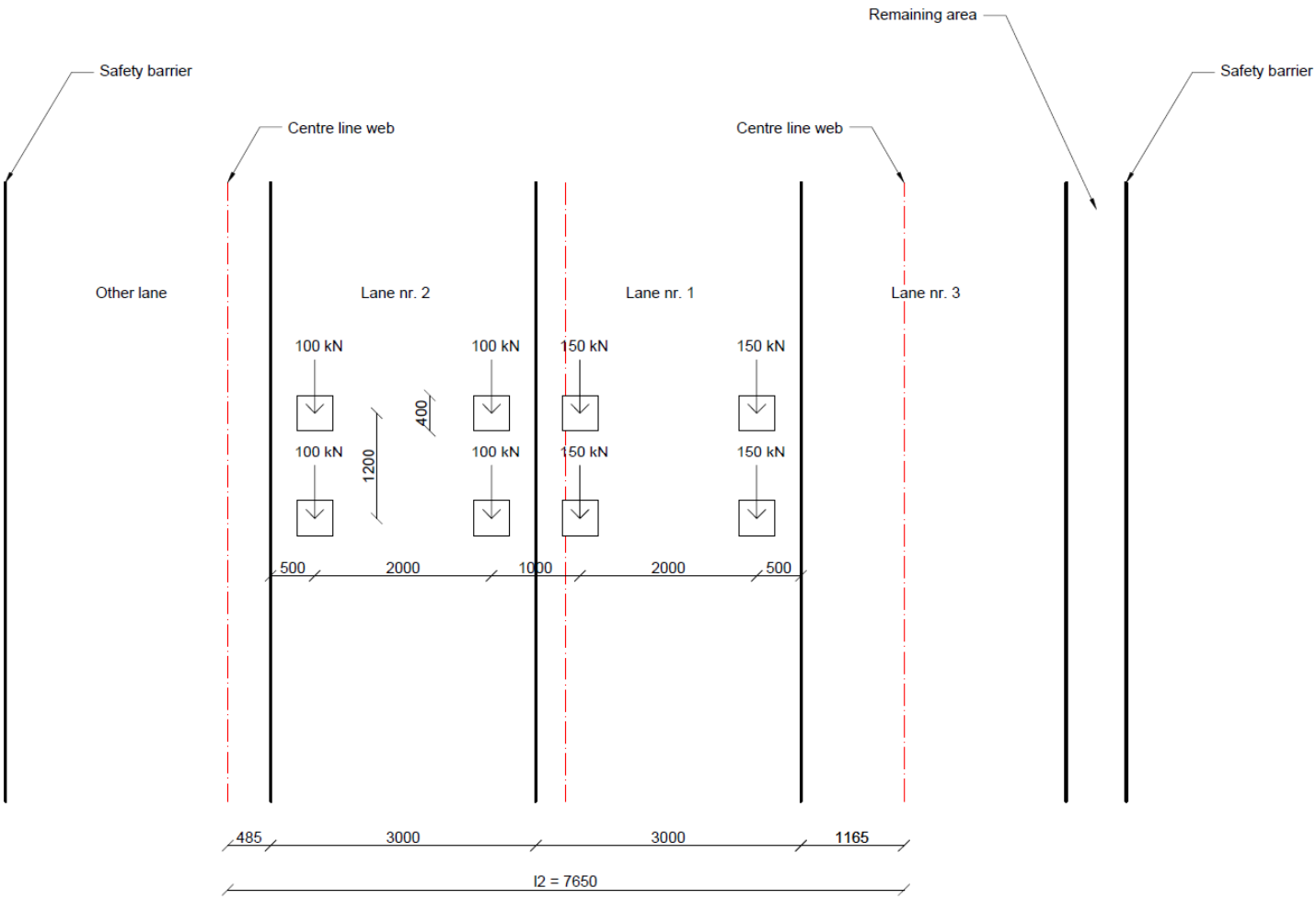

Figure 8.7: most unfavorable tandem system position for load case 3

The distribution of the concentrated vehicle loading can be determined with the influence surface from Figure 8.8.

The bending moment at mid span due to the tandem system from load case 3 (Figure 8.8):

$$M_{TS,LC3,span} = (2 \cdot 0.15 + 2 \cdot 0.01) \cdot 150 + (2 \cdot 0.07 + 2 \cdot 0.003) \cdot 100 = 63\ kNm/m.$$

The bending moment at the support due to the tandem system from load case 3 (Figure 8.10):

$$M_{TS,LC3,support} = -\big((2 \cdot 0.21 + 2 \cdot 0.04) \cdot 150 + (2 \cdot 0.26 + 2 \cdot 0.31) \cdot 100\big) = -189\ kNm/m$$

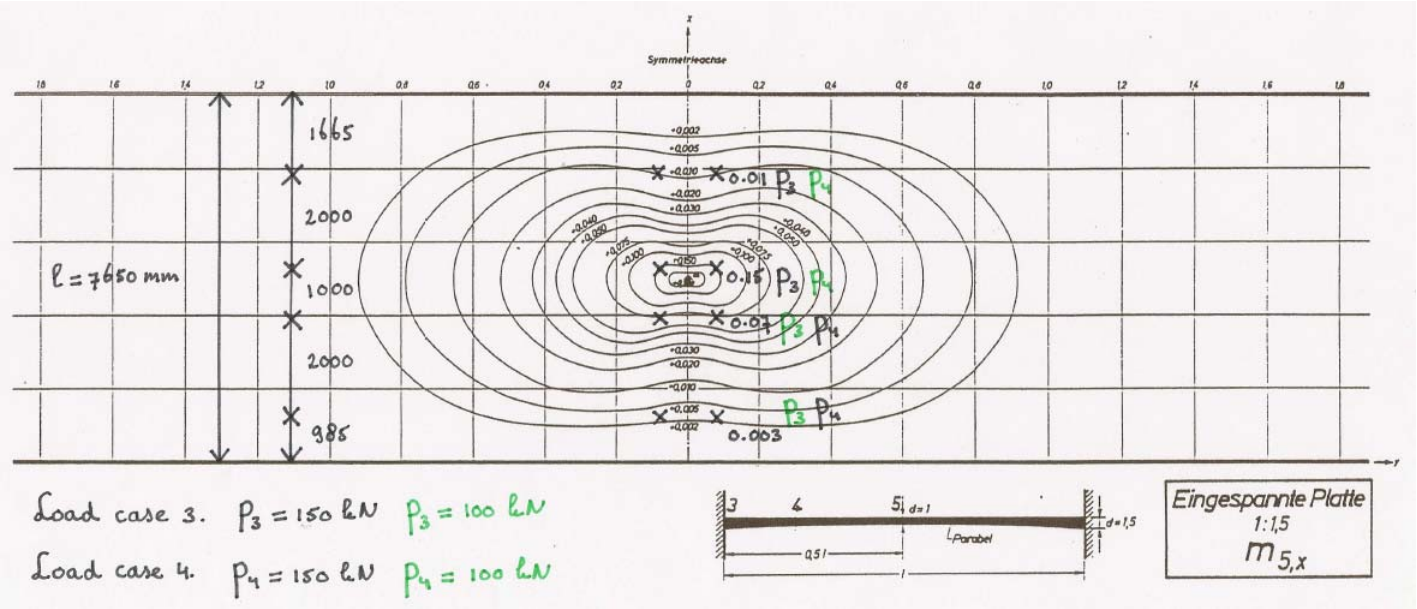

Figure 8.8: influence surface for the moment at mid span for a double clamped slab

In order to obtain a similar bending moment value in the framework model, the magnitude of the point loads that need to be applied in the framework program can be determined with the fourth order Euler-Bernoulli bending beam differential equation.

The bending moment at mid span due to a point load F at a distance from the left support a can be expressed by:

$$a < \frac{1}{2}l \rightarrow M_{span} = EI\left(\frac{1}{2}\frac{Fa^2(2a-3l)}{l^2EI} - \frac{Fa^2(a-2l)}{l^2EI}\right)$$

$$a > \frac{1}{2}l \rightarrow M_{span} = EI\left(\frac{1}{2}\frac{F(2a^3-3a^2l+l^3)}{l^2EI} - \frac{Fa(a^2-2al+l^2)}{l^2EI}\right)$$

The contribution of all axle loads to the bending moment at mid span:

$2 \cdot 0.003 \cdot 100 = 1\ kNm/m.$

$2 \cdot 0.07 \cdot 100 = 14\ kNm/m.$

$2 \cdot 0.15 \cdot 150 = 45\ kNm/m.$

$2 \cdot 0.01 \cdot 150 = 3\ kNm/m.$

With a, l, EI and M being known, the point load F can be determined.

Resulting in:

$0.0634F_1 = 1 \rightarrow F_1 = 16\ kN.$

$0.582F_2 = 14 \rightarrow F_2 = 24\ kN.$

$0.878F_3 = 45 \rightarrow F_3 = 51\ kN.$

$0.181F_4 = 3 \rightarrow F_4 = 17\ kN.$

Appendix 13 shows how to determine the contribution of axle load 1 to the bending moment at mid span. The same procedure can be followed for the other axle loads.

All point loads can now be put into the framework program.

SCIA Engineer gives:

$M_{TS,span} = 71\ kNm/m.$

The deviation can be explained by the fact that web-deck connection is not a 100% fixed support. The web-deck connection has certain rotational stiffness, which depends on the geometry of the webs and the deck. For thick webs and a slender deck, the connection shifts to a fixed support. For thin webs and a heavy deck, the connection shifts to a hinge. Using the influence surface for a double clamped slab to determine the bending moment diagram for the deck of the box girder due to concentrated vehicle loading will underestimate the bending moment at mid span and overestimate the bending moment at the support.

Load case 3 gives (Appendix 12):

$M_{deck\ span} = 92\ kNm/m$

$N_{deck} = -38\ kN/m$ (compression).

$N_{floor} = 37\ kN/m$ (tension).

8.4.4 Load case 4

Figure 8.9 illustrates the most unfavorable position of the tandem system for load case 4.

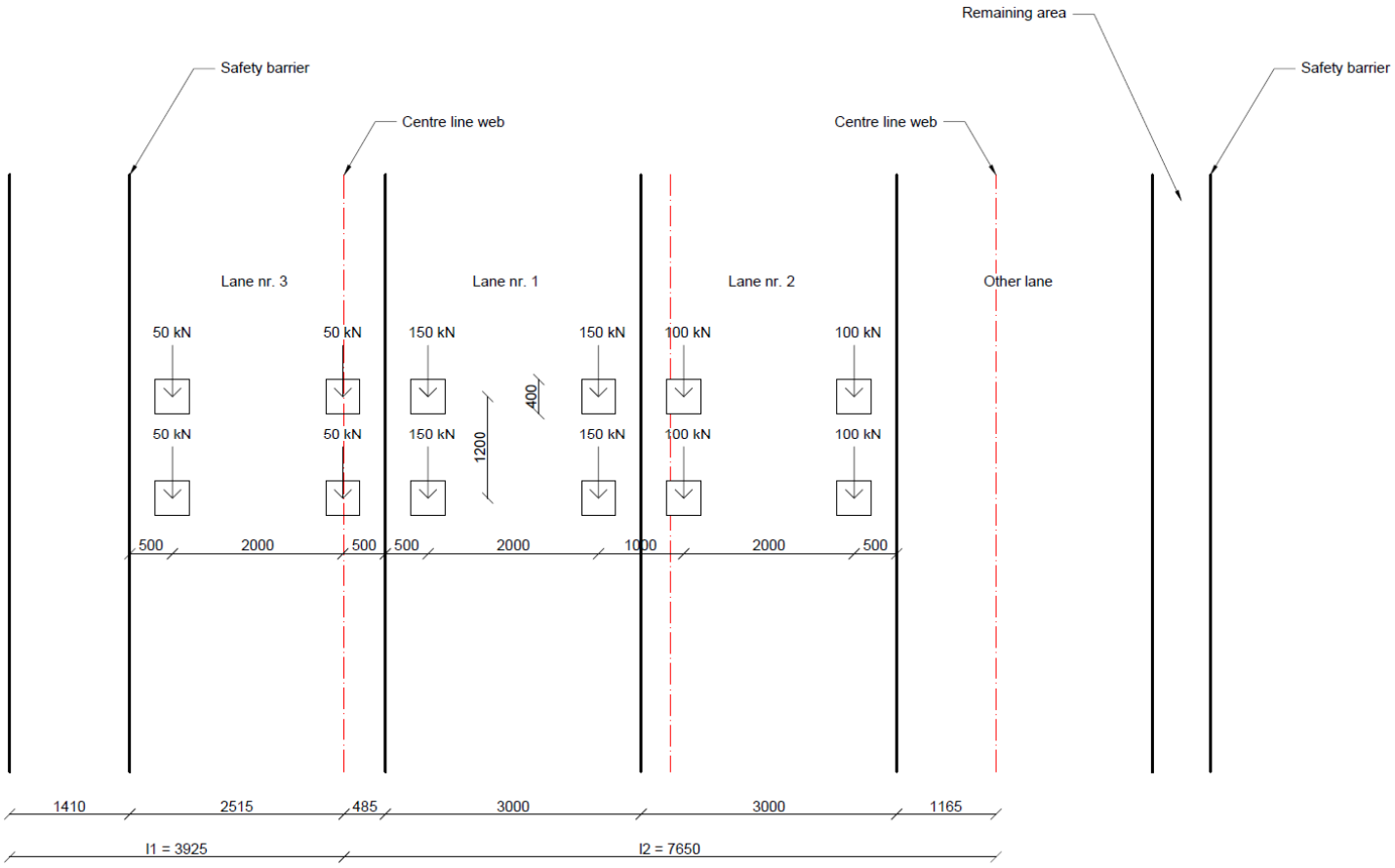

Figure 8.9: most unfavorable tandem system position for load case 4

The distribution of the concentrated vehicle loading can be determined with the influence surface from Figure 8.5 and Figure 8.10.

The bending moment at mid span due to the tandem system from load case 4 (Figure 8.8):

$$M_{TS,LC4,span} = (2 \cdot 0.15 + 2 \cdot 0.01) \cdot 100 + (2 \cdot 0.07 + 2 \cdot 0.003) \cdot 150 = 54\ kNm/m$$

The bending moment at the support due to the tandem system from load case 4 (Figure 8.10):

$$M_{TS,LC4,support} = -\big((2 \cdot 0.21 + 2 \cdot 0.04) \cdot 100 + (2 \cdot 0.26 + 2 \cdot 0.31) \cdot 150\big) = -221\ kNm/m$$

The bending moment at the support due to the tandem system from load case 4 (Figure 8.5):

$$M_{TS,LC4,support} = -(0.41 + 0.41) \cdot 50 = -41\ kNm/m.$$

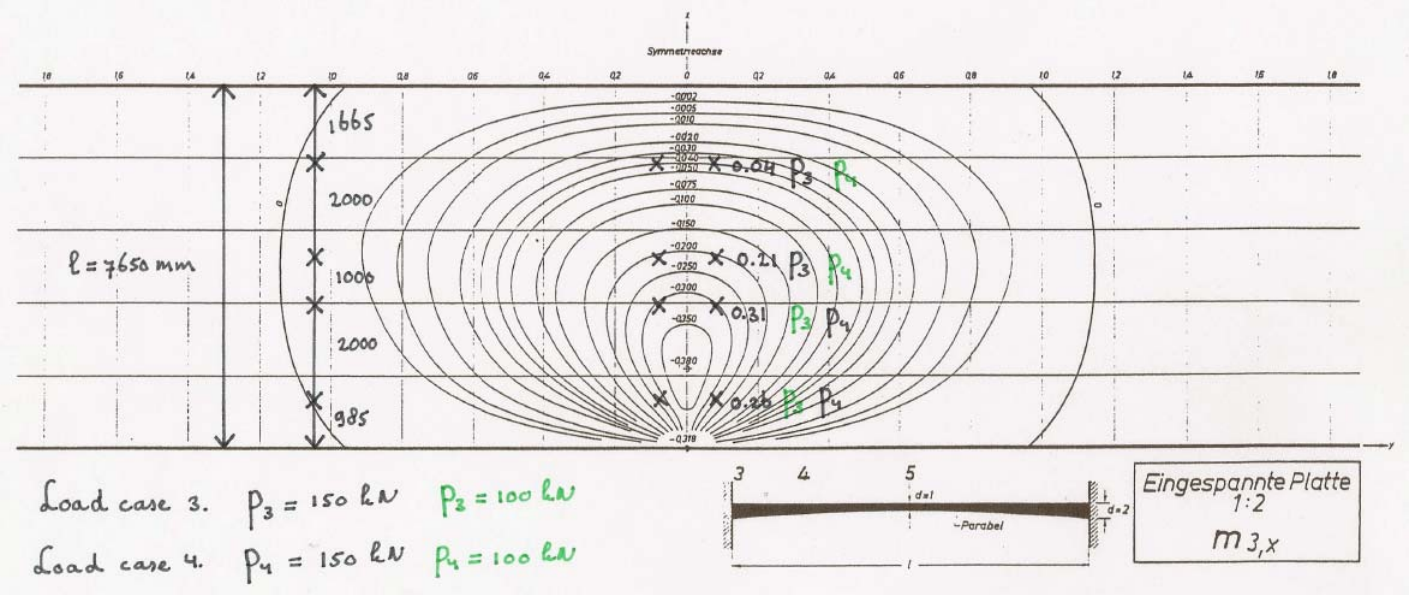

Figure 8.10: influence surface for the support moment for a double clamped slab

In order to obtain a similar bending moment value in the framework program, the magnitude of the point loads that need to be applied in the framework program can be determined with the fourth order Euler-Bernoulli bending beam differential equation.

The bending moment at the support due to a point load F at a distance from the left support a can be expressed by:

$$M_{support} = -\frac{Fa(a^2 - 2al + l^2)}{l^2}$$

The contribution of all axle loads to the bending moment at the support:

$$2 \cdot 0.26 \cdot 150 = 78\ kNm/m.$$

$$2 \cdot 0.31 \cdot 150 = 93\ kNm/m.$$

$$2 \cdot 0.21 \cdot 100 = 42\ kNm/m.$$

$$2 \cdot 0.04 \cdot 100 = 8\ kNm/m.$$

With a, l, EI and M being known, the point load F can be determined.

Resulting in:

$0.748F_1 = 78 \rightarrow F_1 = 104\ kN.$

$1.11F_2 = 93 \rightarrow F_2 = 84\ kN.$

$0.915F_3 = 42 \rightarrow F_3 = 46\ kN.$

$0.284F_4 = 8 \rightarrow F_4 = 28\ kN.$

Appendix 14 shows how to determine the contribution of axle load 1 to the bending moment at the support. The same procedure can be followed for the other axle loads.

All point loads can now be put into the framework program.

SCIA Engineer gives:

$M_{TS,support} = -203\ kNm/m.$

Load case 4 gives (Appendix 12):

$M_{deck\ support} = -237\ kNm/m$

The mobile loading on the cantilever and the deck causes extreme bending moments at the top of the box girder. The bending moment diagrams from load case 1 to 4 show, that the bending moments are directly transmitted to the webs. The bending moments in the floor and at the bottom of the web, due to the mobile loading on the top flange, are negligible.

8.5 Flange design

Load case 1 provides the extreme cantilever bending moment and shear force. The capacity of cross-section A (Figure 8.11) must be sufficient to transmit the load through the webs to the supports.

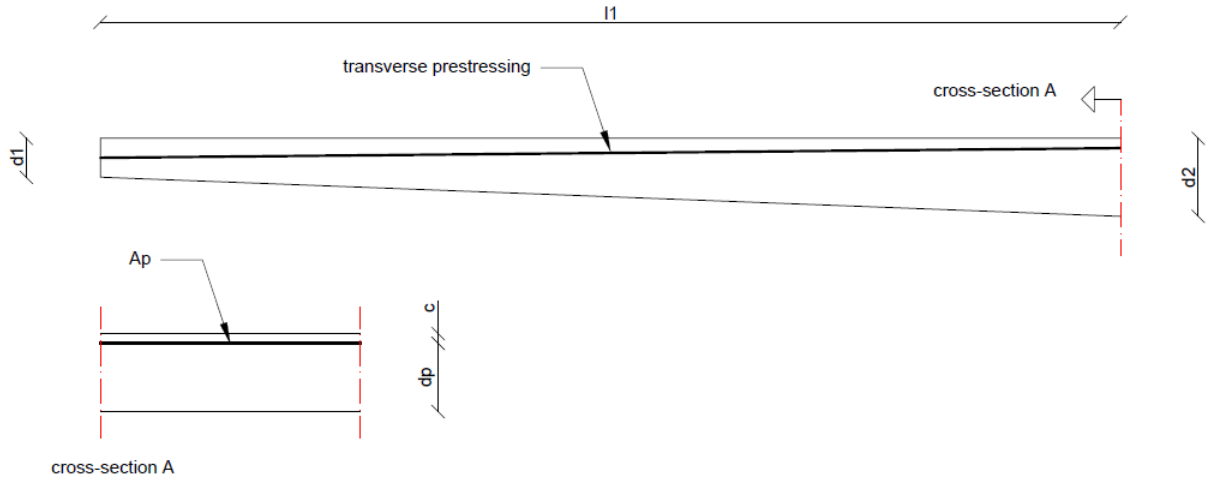

Figure 8.11: transverse prestressing in the cantilever

8.5.1 Self-weight

The bending moment and shear force due to the self-weight of the cantilever (Figure 8.12 & Figure 8.13):

$$M_{G,SW} = -\frac{1}{2}\gamma\left(d_1 + \frac{1}{3}(d_2 - d_1)\right)l_1^2 = -\frac{1}{2}\cdot 26\cdot\left(0.15 + \frac{1}{3}(0.3 - 0.15)\right)\cdot 3.925^2$$

$$= -40\ kNm/m$$

$$V_{G,SW} = \frac{1}{2}\gamma(d_1 + d_2)l_1 = \frac{1}{2}\cdot 26\cdot(0.15 + 0.3)\cdot 3.925 = 23\ kN/m$$

8.5.2 Asphalt layer

The asphalt layer causes a uniformly distributed load up to 1.41 m from the cantilever's edge, giving a bending moment and shear force of:

$$M_{G,A} = -\frac{1}{2}q_{G,A}(l_1 - 1.41)^2 = -\frac{1}{2}\cdot 3.5\cdot(3.925 - 1.41)^2 = -11.1\ kNm/m$$

$$V_{G,A} = q_{G,A}l_1 = 3.5\cdot(3.925 - 1.41) = 8.8\ kN/m$$

8.5.3 Footpath and edge element

The footpath and edge element cause line loads p_F and p_E at 0.8 m and 0.15 m from the cantilever's edge, resulting in a bending moment and shear force of:

$$M_{G,FE} = -p_F(l_1 - 0.8) + -p_E(l_1 - 0.15)$$
$$= -\big(0.15 \cdot 26 \cdot (0.4 + 0.6)\big) \cdot (3.925 - 0.8) + -(0.4 \cdot 26 \cdot 0.3) \cdot (3.925 - 0.15) = -24\ kNm/m$$

$$V_{G,FE} = p_F + p_E = 0.15 \cdot 26 \cdot (0.4 + 0.6) + 0.4 \cdot 26 \cdot 0.3 = 7\ kN/m$$

8.5.4 Parapet

The parapet causes a line load p_P at 0.15 m from the cantilever's edge, resulting in the following bending moment and shear force:

$$M_{G,P} = -p_P(l_1 - 0.15) = -0.75 \cdot (3.925 - 0.15) = -2.8\ kNm/m$$

$$V_{G,P} = p_P = 0.75\ kN/m$$

8.5.5 Safety barrier

The safety barrier causes a line load p_{SB} at 1.41 m from the cantilever's edge, resulting in the following bending moment and shear force:

$$M_{G,SB} = -p_{SB}(l_1 - 1.41) = -1 \cdot (3.925 - 1.41) = -2.5\ kNm/m$$

$$V_{G,SB} = p_{SB} = 1\ kN/m$$

The contribution from the asphalt layer, the footpath and edge element, the parapet and the safety barrier to the bending moment and shear force is combined to the super imposed dead load curve in Figure 8.12 & Figure 8.13.

8.5.6 All permanent loads

The characteristic value of the bending moment and shear force due to all permanent loads:

$$M_{Gk} = M_{G,SW} + M_{G,A} + M_{G,FE} + M_{G,P} + M_{G,SB} = -(40 + 11.1 + 24 + 2.8 + 2.5) = -80\ kNm/m$$

$$V_{Gk} = V_{G,SW} + V_{G,A} + V_{G,FE} + V_{G,P} + V_{G,SB} = 23 + 8.8 + 7 + 0.75 + 1 = 41\ kN/m$$

8.5.7 UDL

The UDL from the slow lane works up to 1.41 m from the cantilever's edge, resulting in the following characteristic values for bending moment and shear force (Figure 8.12 & Figure 8.13):

$$M_{Qk,UDL} = -\frac{1}{2} \cdot \alpha_{q1} q_{1k} \cdot (l_1 - 1.41)^2 = -\frac{1}{2} \cdot 10.35 \cdot (3.925 - 1.41)^2 = -33\ kNm/m$$

$$V_{Qk,UDL} = \alpha_{q1} q_{1k} \cdot (l_1 - 1.41) = 10.35 \cdot (3.925 - 1.41) = 26\ kN/m$$

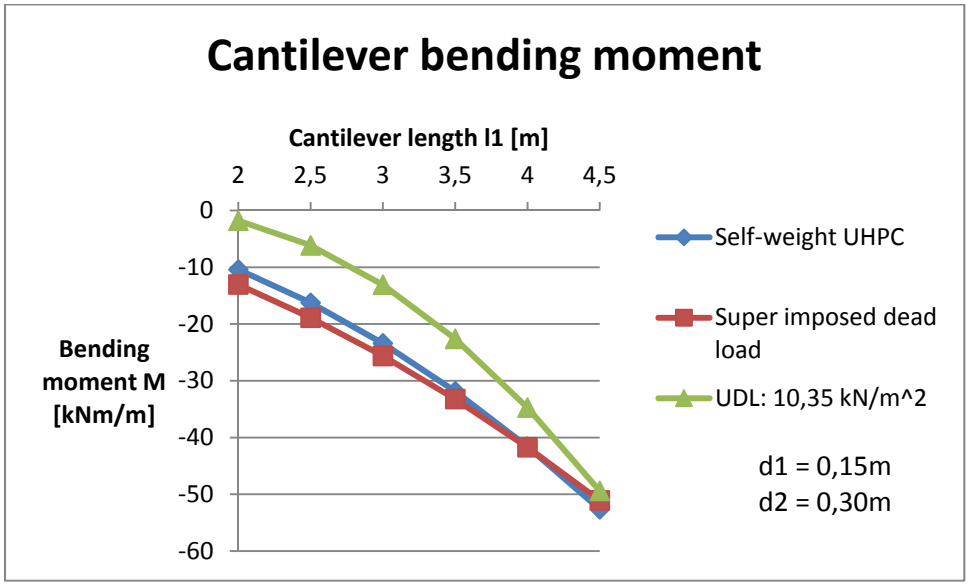

Figure 8.12: cantilever bending moment due to self-weight, super imposed dead load and UDL

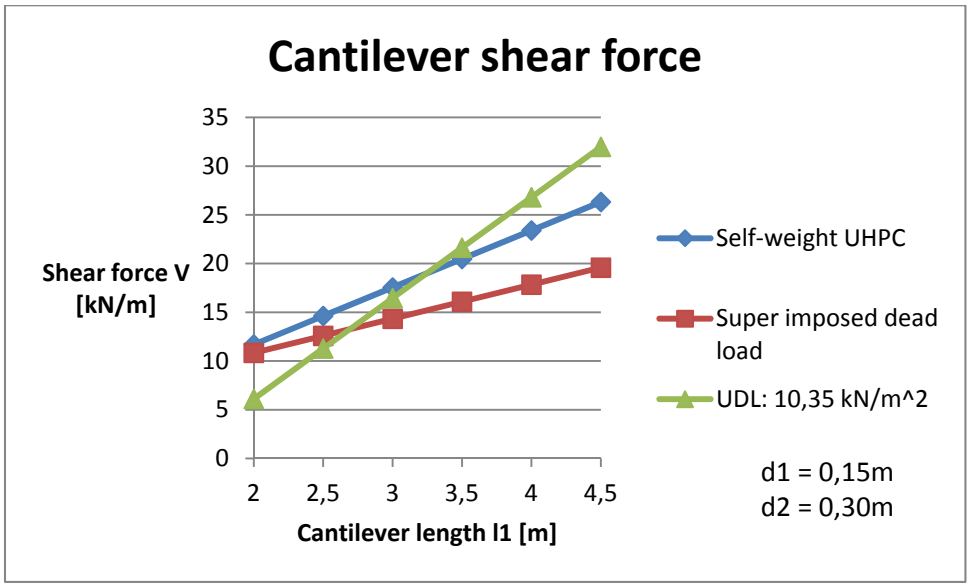

Figure 8.13: cantilever shear force due to self-weight, super imposed dead load and UDL

8.5.8 Tandem system

The bending moment due to the tandem system can be determined with the influence surface for a cantilever slab with a thickness ratio 1:2. Figure 8.14 illustrates the set of bending moment values that have been obtained for a cantilever length of 2, 2.5, 3, 3.5, 4, and 4.5 meters. If the cantilever is shorter than 4 meters, there is not enough space to accommodate the complete tandem system and only axle 1 will contribute to the cantilever bending moment.

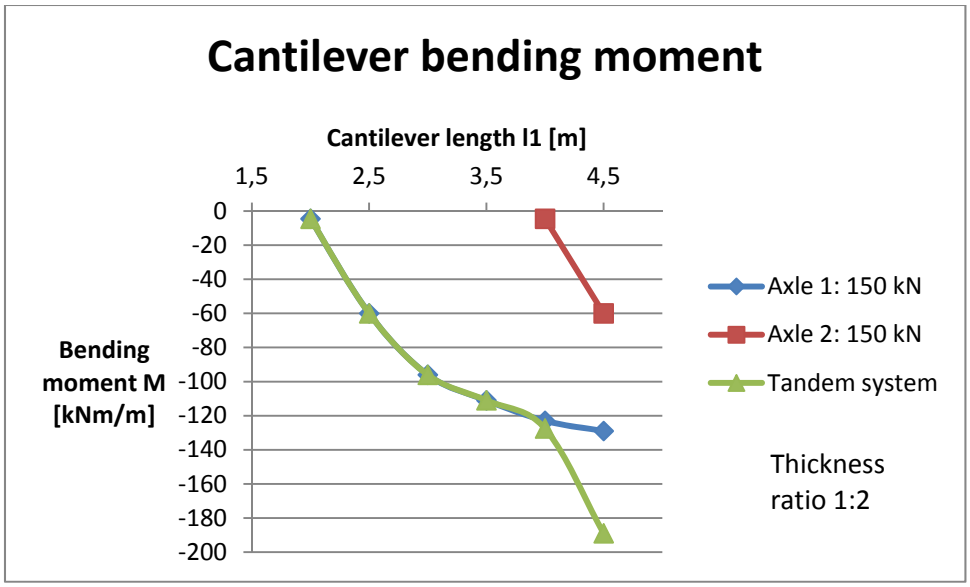

Figure 8.14: cantilever bending moment due to the tandem system

The contribution of axle 1 to the cantilever bending moment can be approximated by the curve: $M_{Qk,A1} = -96(l_1 - 2)^{0.36}$.

The contribution of axle 2 to the cantilever bending moment can be approximated by the curve: $M_{Qk,A2} = -96(l_1 - 4)^{0.36}$.

The cantilever bending moment due to the tandem system:

$l_1 < 4 \rightarrow M_{Qk,TS} = M_{Qk,A1}$

$l_1 \geq 4 \rightarrow M_{Qk,TS} = M_{Qk,A1} + M_{Qk,A2}$

$M_{Qk,TS} = -96(l_1 - 2)^{0.36} = -96(3.925 - 2)^{0.36} = -122\ kNm/m$

Figure 8.15 illustrates the set of shear force values that have been obtained with the influence surface for a cantilever slab with a thickness ratio 1:1. The influence surface for a cantilever slab with a thickness ratio 1:2 is not available and therefore the shear force will be somewhat underestimated.

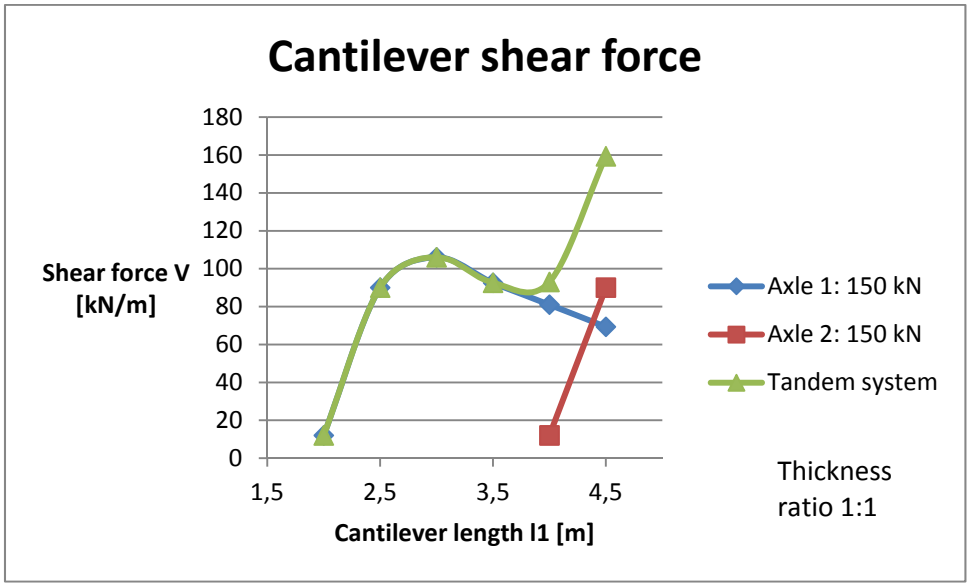

Figure 8.15: cantilever shear force due to the tandem system

The contribution of axle 1 to the cantilever shear force can be approximated by the equation:

$l_1 \leq 3 \rightarrow V_{Qk,A1} = 106(l_1 - 1.99)^{0.4}$

$l_1 > 3 \rightarrow V_{Qk,A1} = -25(l_1 - 3) + 106$

The contribution of axle 2 to the cantilever shear force can be approximated by the equation:

$V_{Qk,A2} = 106(l_1 - 3.99)^{0.4}$

The cantilever shear force due to the tandem system:

$l_1 < 4 \rightarrow V_{Qk,TS} = V_{Qk,A1}$

$l_1 \geq 4 \rightarrow V_{Qk,TS} = V_{Qk,A1} + V_{Qk,A2}$

$V_{Qk,TS} = -25(l_1 - 3) + 106 = -25(3.925 - 3) + 106 = 83\ kN/m$

8.5.9 ULS design

Design value of the bending moment and shear force at cross-section A, according to NEN-EN 1990: equations 6.10a & 6.10b:

$$M_{Ed,ULS} = max\begin{cases}\gamma_G M_{Gk} + \gamma_Q \psi_0 M_{Qk,TS} + \gamma_Q \psi_0 M_{Qk,UDL} \\ \zeta \gamma_G M_{Gk} + \gamma_Q M_{Qk,TS} + \gamma_Q M_{Qk,UDL}\end{cases} \rightarrow$$

$$M_{Ed,ULS} = max\begin{cases}-1.4 \cdot 80 - 1.5 \cdot 0.8 \cdot 122 - 1.5 \cdot 0.8 \cdot 33 = -298\ kNm/m \\ -1.25 \cdot 80 - 1.5 \cdot 122 - 1.5 \cdot 33 = -333\ kNm/m\end{cases}$$

$$V_{Ed,ULS} = max\begin{cases}\gamma_G V_{Gk} + \gamma_Q \psi_0 V_{Qk,TS} + \gamma_Q \psi_0 V_{Qk,UDL} \\ \zeta \gamma_G V_{Gk} + \gamma_Q V_{Qk,TS} + \gamma_Q V_{Qk,UDL}\end{cases} \rightarrow$$

$$V_{Ed,ULS} = max\begin{cases}1.4 \cdot 41 + 1.5 \cdot 0.8 \cdot 83 + 1.5 \cdot 0.8 \cdot 26 = 188\ kN/m \\ 1.25 \cdot 41 + 1.5 \cdot 83 + 1.5 \cdot 26 = 215\ kN/m\end{cases}$$

Appendix 15 shows that five Ø16 mm strands are required to provide sufficient bending moment and shear force capacity for cross-section A.

Unity check ultimate bending moment: $M_{Ed,ULS}/M_{Rd} = 333/352 = 0.95$

Unity check ultimate shear force: $V_{Ed,ULS}/V_{Rd} = 215/2080 = 0.10$

8.5.10 SLS design

As the cantilever is not restrained to deform in transverse direction due to temperature differences, no additional bending moments have to be taken into account.

Design value of the bending moment at cross-section A, according to NEN-EN 1990: equation 6.15b:

$$M_{Ed,SLS} = M_{Gk} + \psi_1 M_{Qk,TS} + \psi_1 M_{Qk,UDL} = -80 - 0.8 \cdot 122 - 0.8 \cdot 33 = -204\ kNm/m$$

Requirement: the flange remains uncracked in the serviceability state.

$t = 0 \rightarrow$ check top fiber:

$$-\frac{P_{m0}}{A_c} - \frac{P_{m0} \cdot e}{W_{top}} + \frac{M}{W_{top}} \leq f'_{ct} \rightarrow \frac{M}{W_{top}} \leq \frac{P_{m0}}{A_c} + \frac{P_{m0} \cdot e}{W_{top}} + f'_{ct} \rightarrow$$

$$M \leq \frac{P_{m0}}{A_c} W_{top} + P_{m0} \cdot e + f'_{ct} W_{top} \rightarrow M \leq 289\ kNm/m$$

$t = 0 \rightarrow$ check bottom fiber:

$$-\frac{P_{m0}}{A_c} + \frac{P_{m0} \cdot e}{W_{bot}} - \frac{M}{W_{bot}} \leq f'_{ct} \rightarrow \frac{M}{W_{bot}} \geq -\frac{P_{m0}}{A_c} + \frac{P_{m0} \cdot e}{W_{bot}} - f'_{ct} \rightarrow$$

$$M \geq -\frac{P_{m0}}{A_c} W_{bot} + P_{m0} \cdot e - f'_{ct} W_{bot} \rightarrow M \geq -55\ kNm/m$$

$t = \infty \rightarrow$ check top fiber:

$$-\frac{P_{m\infty}}{A_c} - \frac{P_{m\infty} \cdot e}{W_{top}} + \frac{M}{W_{top}} \leq f'_{ct} \rightarrow \frac{M}{W_{top}} \leq \frac{P_{m\infty}}{A_c} + \frac{P_{m\infty} \cdot e}{W_{top}} + f'_{ct} \rightarrow$$

$$M \leq \frac{P_{m\infty}}{A_c} W_{top} + P_{m\infty} \cdot e + f'_{ct} W_{top} \rightarrow M \leq 247\ kNm/m$$

$t = \infty \rightarrow$ check bottom fiber:

$$-\frac{P_{m\infty}}{A_c} + \frac{P_{m\infty} \cdot e}{W_{bot}} - \frac{M}{W_{bot}} \leq f'_{ct} \rightarrow \frac{M}{W_{bot}} \geq -\frac{P_{m\infty}}{A_c} + \frac{P_{m\infty} \cdot e}{W_{bot}} - f'_{ct} \rightarrow$$

$$M \geq -\frac{P_{m\infty}}{A_c} W_{bot} + P_{m\infty} \cdot e - f'_{ct} W_{bot} \rightarrow M \geq -71\ kNm/m$$

Unity check serviceability limit state bending moment: $M_{Ed,SLS}/M_{Rd} = 205/247 = 0.83$

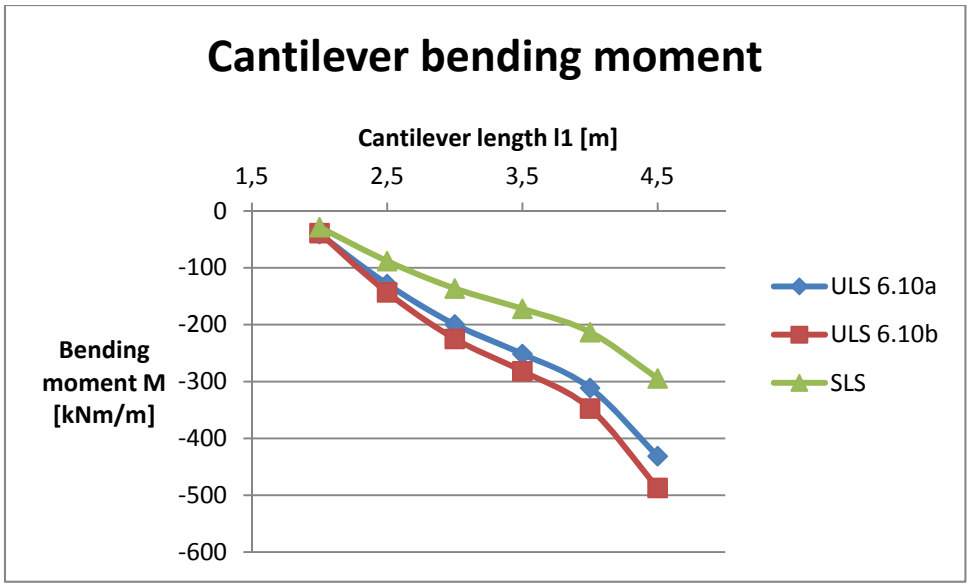

Figure 8.16: cantilever bending moment in ULS and SLS

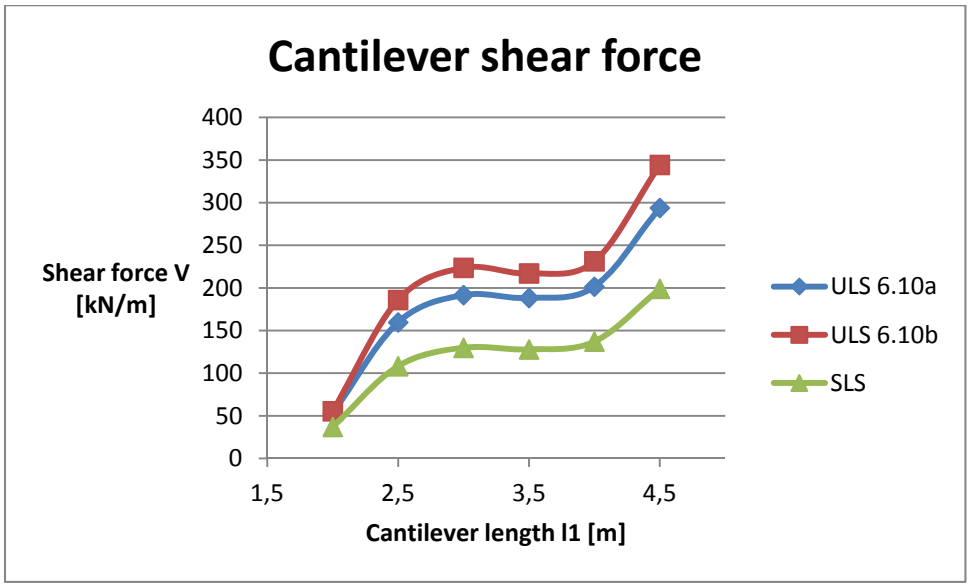

Figure 8.17: cantilever shear force in ULS and SLS

8.6 Deck support

Load case 4 provides the extreme bending moment and shear force in the deck at the support. The capacity of cross-section B (Figure 8.18) must be sufficient to transmit the load through the webs to the supports.

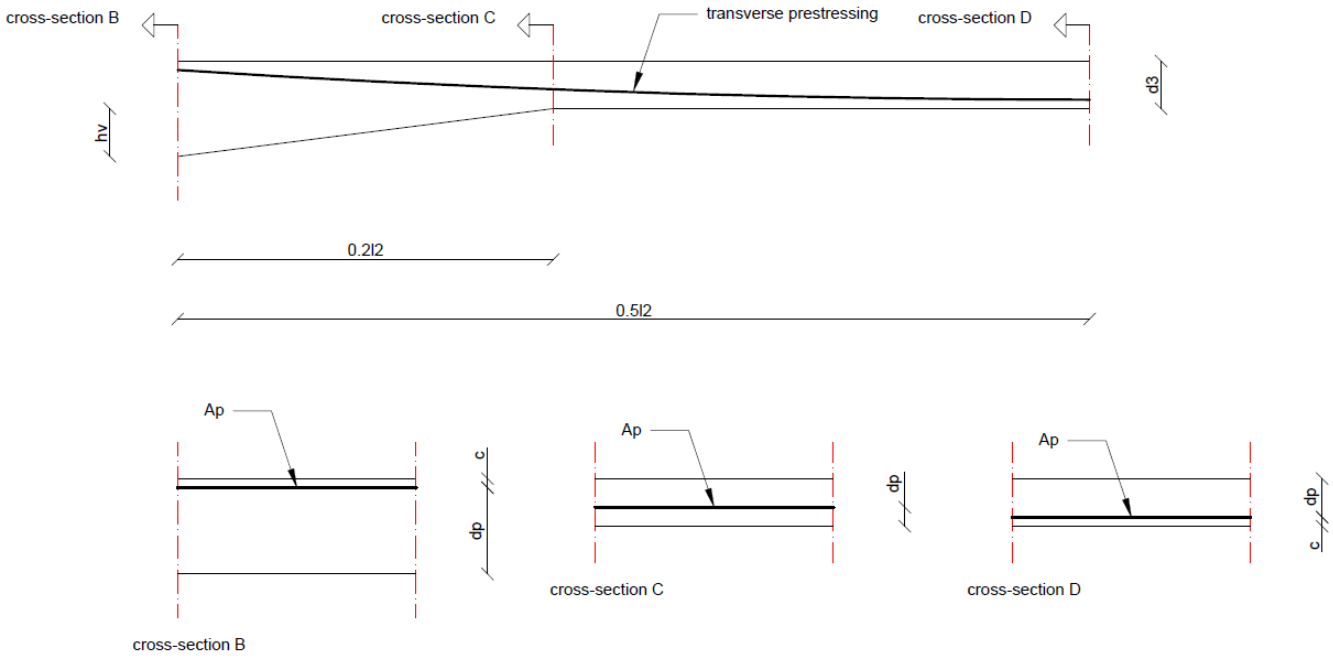

Figure 8.18: transverse prestressing in the deck

The maximum bending moment in the deck at the support, due to the tandem system, can be determined with influence surfaces. (van der Meulen, 1992) demonstrated, that for the deck between the webs, including haunches, the support moment is best approximated with the influence surface for a double clamped slab with a parabolic bottom edge and a thickness ratio 1:2.

8.6.1 Self-weight

The bending moment and shear force at the support, due to the self-weight of a double clamped slab with a parabolic bottom edge and a thickness ratio 1:2, are equal to (Figure 8.19 & Figure 8.20):

$$M_{G,SW} = -0.1216 g l_2^2 = -0.1216 \cdot 26 \cdot 0.2 \cdot 7.65^2 = -37\ kNm/m$$

$$V_{G,SW} = 0.5832 g l_2 = 0.5832 \cdot 26 \cdot 0.2 \cdot 7.65 = 23\ kN/m$$

8.6.2 Asphalt

The bending moment and shear force at the support, due to a uniformly distributed load q on a double clamped slab with a parabolic bottom edge and thickness ratio 1:2 (Figure 8.19 & Figure 8.20):

$$M_{G,A} = -0.1025 q_{G,A} l_2^2 = -0.1025 \cdot 3.5 \cdot 7.65^2 = -21\ kNm/m$$

$$V_{G,A} = \frac{1}{2} q_{G,A} l_2 = \frac{1}{2} \cdot 3.5 \cdot 7.65 = 13\ kN/m$$

8.6.3 Permanent loads

Characteristic value of the bending moment and shear force due to the permanent loads:

$$M_{Gk} = M_{G,SW} + M_{G,A} = -37 - 21 = -58\ kNm/m$$

$$V_{Gk} = V_{G,SW} + V_{G,A} = 23 + 13 = 36\ kN/m$$

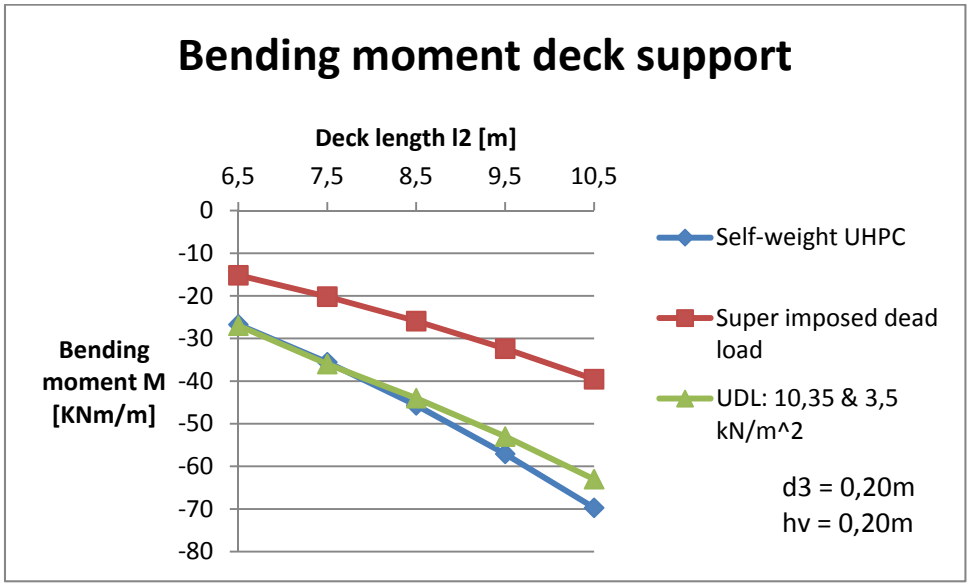

Figure 8.19: bending moment in the deck at the support due to self-weight, super imposed dead load and UDL

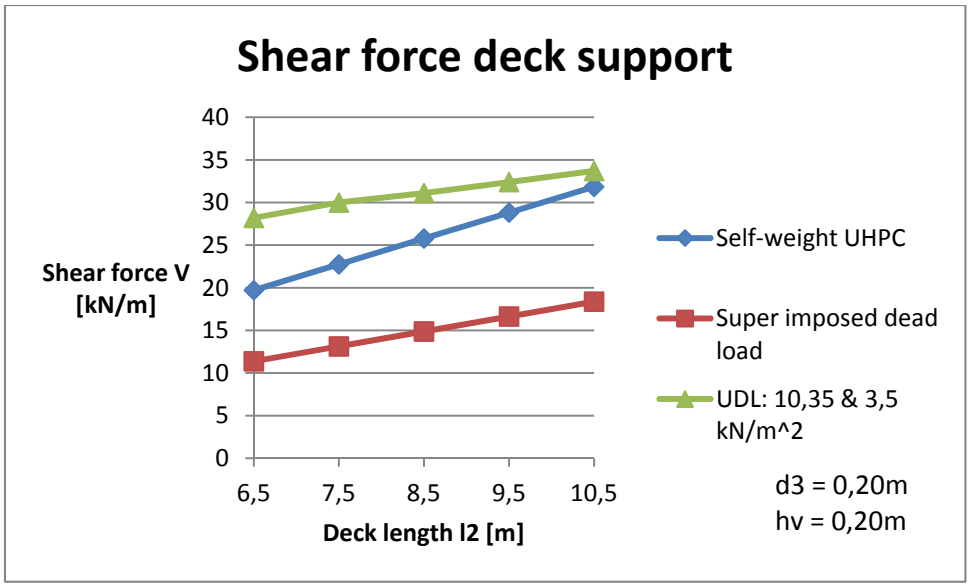

Figure 8.20: shear force in the deck at the support due to self-weight, super imposed dead load and UDL

8.6.4 UDL

The bending moment and shear force due to the UDL can be determined with the Euler-Bernoulli bending beam differential equation. The bending stiffness of the deck is assumed to be constant over the whole length. Bending moment and shear force values have been found for a deck length of 6.5, 7.5, 8.5, 9.5 and 10 meters (Figure 8.19 & Figure 8.20). From these values, a trend line can be derived. The characteristic value of the bending moment and shear force due to the UDL can be approximated by the following equations:

$$M_{Qk,UDL} = -9(l_2 - 3.5) = -9 \cdot (7.65 - 3.5) = -37\ kNm/m$$

$$V_{Qk,UDL} = 1.5(l_2 + 12) = 1.5 \cdot (7.65 + 12) = 29\ kN/m$$

Appendix 19 shows how to determine the bending moment and shear force at the support due to the UDL for a deck length of 7.5 meters. The same procedure can be followed for the other deck lengths.

8.6.5 Tandem system

The bending moment due to the tandem system can be determined with the influence surface for a double clamped slab with a parabolic bottom edge and a thickness ratio 1:2. Bending moment values have been found for a deck length of 6.5, 7.5, 8.5, 9.5 and 10 meters (Figure 8.21). The same procedure can be followed to determine the shear forces (Figure 8.22). However, since the influence surface for a cantilever slab with a thickness ratio 1:2 is not available, shear forces will be determined with a thickness ratio 1:1 and will therefore be somewhat underestimated.

From these values, a trend line can be derived. The characteristic value of the bending moment and shear force due to the tandem system can be approximated by the following equations:

$$M_{Qk,TS} = -45(l_2 - 6.5)^{0.74} - 170 = -45(7.65 - 6.5)^{0.74} - 170 = -220\ kNm/m$$

$$V_{Qk,TS} = -13(l_2 - 22) = -13(7.65 - 22) = 187\ kN/m$$

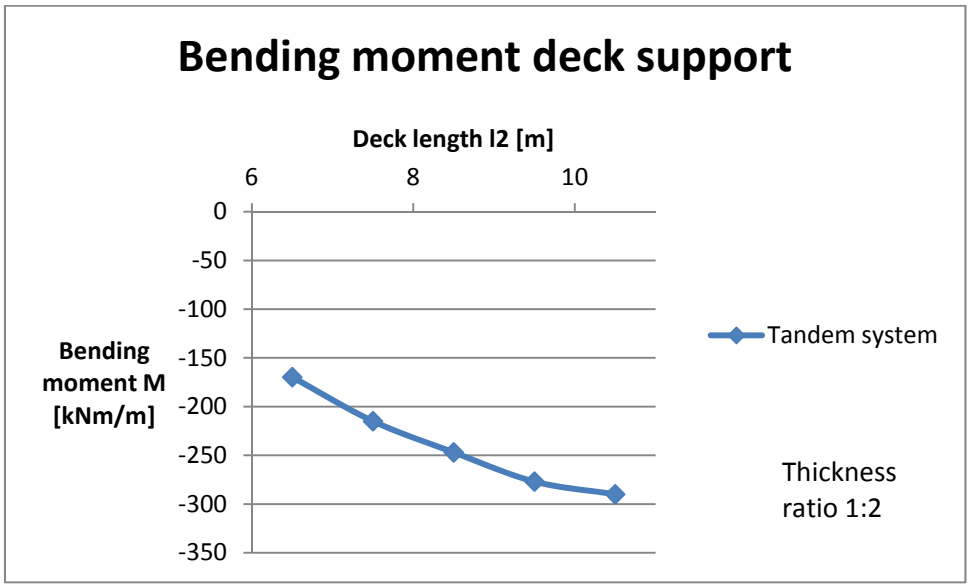

Figure 8.21: bending moment in the deck at the support due to the tandem system

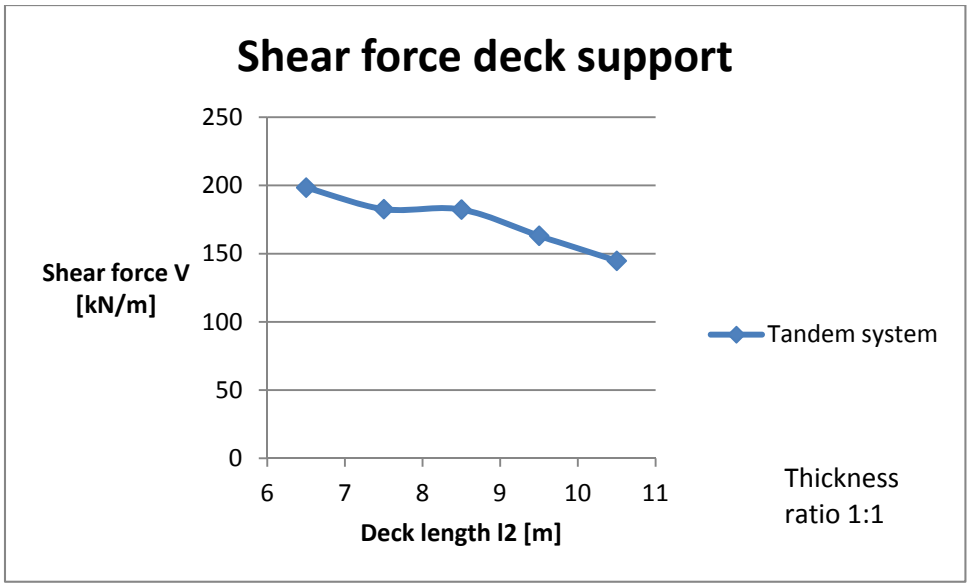

Figure 8.22: shear force in the deck at the support due to the tandem system

8.6.6 ULS design

The design value of the bending moment and shear force at cross-section B according to NEN-EN 1990: equations 6.10a & 6.10b:

$$M_{Ed,ULS} = max\begin{cases}\gamma_G M_{Gk} + \gamma_Q \psi_0 M_{Qk,TS} + \gamma_Q \psi_0 M_{Qk,UDL} \\ \zeta \gamma_G M_{Gk} + \gamma_Q M_{Qk,TS} + \gamma_Q M_{Qk,UDL}\end{cases} \rightarrow$$

$$M_{Ed,ULS} = max\begin{cases}-1.4 \cdot 58 - 1.5 \cdot 0.8 \cdot (37 + 220) = -390\ kNm/m \\ -1.25 \cdot 58 - 1.5 \cdot (37 + 220) = -458\ kNm/m\end{cases}$$

$$V_{Ed,ULS} = max\begin{cases}\gamma_G V_{Gk} + \gamma_Q \psi_0 V_{Qk,TS} + \gamma_Q \psi_0 V_{Qk,UDL} \\ \zeta \gamma_G V_{Gk} + \gamma_Q V_{Qk,TS} + \gamma_Q V_{Qk,UDL}\end{cases} \rightarrow$$

$$V_{Ed,ULS} = max\begin{cases}1.4 \cdot 36 + 1.5 \cdot 0.8 \cdot (29 + 187) = 310\ kN/m \\ 1.25 \cdot 36 + 1.5 \cdot (29 + 187) = 369\ kN/m\end{cases}$$

Appendix 16 shows that five Ø16 mm strands are required to provide sufficient bending moment and shear force capacity for cross-section B.

Unity check ultimate bending moment: $M_{Ed,ULS}/M_{Rd} = 458/561 = 0.82$

Unity check ultimate shear force: $V_{Ed,ULS}/V_{Rd} = 369/2780 = 0.13$

8.6.7 SLS design

As the deck between the webs cannot freely deform due to temperature differences, a temperature induced bending moment will arise.

When a double clamped slab is exposed to a uniform temperature drop ΔT_m, it wants to shorten. This deformation is restrained and leads to a normal force in the slab:

$N_{Qk,Temp} = -EA\alpha_c \Delta T_m$, with:

EA: the axial stiffness
α_c: the coefficient of thermal dilation

When a double clamped slab is exposed to a temperature differential ΔT_b, it wants to bend. The rotations at the slab ends cannot occur since they are prevented by the fixed supports. This will lead to a bending moment in the slab:

$M_{Qk,Temp} = EI\kappa\Delta T_b$, with:

$$\kappa = \frac{\alpha_c \Delta T_b}{h}$$

EI: the bending stiffness
κ: the curvature

Due to limited time available the magnitude of this temperature induced bending moment is not determined.

Design value of the bending moment at cross-section B according to NEN-EN 1990: equation 6.15b:

$$M_{Ed,SLS} = M_{Gk} + \psi_1 M_{Qk,TS} + \psi_1 M_{Qk,UDL} = -58 - 0.8(37 + 220) = -264\ kNm/m$$

Requirement: the deck remains uncracked in the serviceability state.

$t = 0 \rightarrow$ check top fiber:

$$-\frac{P_{m0}}{A_c} - \frac{P_{m0} \cdot e}{W_{top}} + \frac{M}{W_{top}} \leq f'_{ct} \rightarrow \frac{M}{W_{top}} \leq \frac{P_{m0}}{A_c} + \frac{P_{m0} \cdot e}{W_{top}} + f'_{ct} \rightarrow$$

$$M \leq \frac{P_{m0}}{A_c} W_{top} + P_{m0} \cdot e + f'_{ct} W_{top} \rightarrow M \leq 453\ kNm/m$$

$t = 0 \rightarrow$ check bottom fiber:

$$-\frac{P_{m0}}{A_c} + \frac{P_{m0} \cdot e}{W_{bot}} - \frac{M}{W_{bot}} \leq f'_{ct} \rightarrow \frac{M}{W_{bot}} \geq -\frac{P_{m0}}{A_c} + \frac{P_{m0} \cdot e}{W_{bot}} - f'_{ct} \rightarrow$$

$$M \geq -\frac{P_{m0}}{A_c} W_{bot} + P_{m0} \cdot e - f'_{ct} W_{bot} \rightarrow M \geq -114\ kNm/m$$

$t = \infty \rightarrow$ check top fiber:

$$-\frac{P_{m\infty}}{A_c} - \frac{P_{m\infty} \cdot e}{W_{top}} + \frac{M}{W_{top}} \leq f'_{ct} \rightarrow \frac{M}{W_{top}} \leq \frac{P_{m\infty}}{A_c} + \frac{P_{m\infty} \cdot e}{W_{top}} + f'_{ct} \rightarrow$$

$$M \leq \frac{P_{m\infty}}{A_c} W_{top} + P_{m\infty} \cdot e + f'_{ct} W_{top} \rightarrow M \leq 393\ kNm/m$$

$t = \infty \rightarrow$ check bottom fiber:

$$-\frac{P_{m\infty}}{A_c} + \frac{P_{m\infty} \cdot e}{W_{bot}} - \frac{M}{W_{bot}} \leq f'_{ct} \rightarrow \frac{M}{W_{bot}} \geq -\frac{P_{m\infty}}{A_c} + \frac{P_{m\infty} \cdot e}{W_{bot}} - f'_{ct} \rightarrow$$

$$M \geq -\frac{P_{m\infty}}{A_c} W_{bot} + P_{m\infty} \cdot e - f'_{ct} W_{bot} \rightarrow M \geq -139\ kNm/m$$

Unity check serviceability limit state bending moment: $M_{Ed,SLS}/M_{Rd} = 264/393 = 0.67$

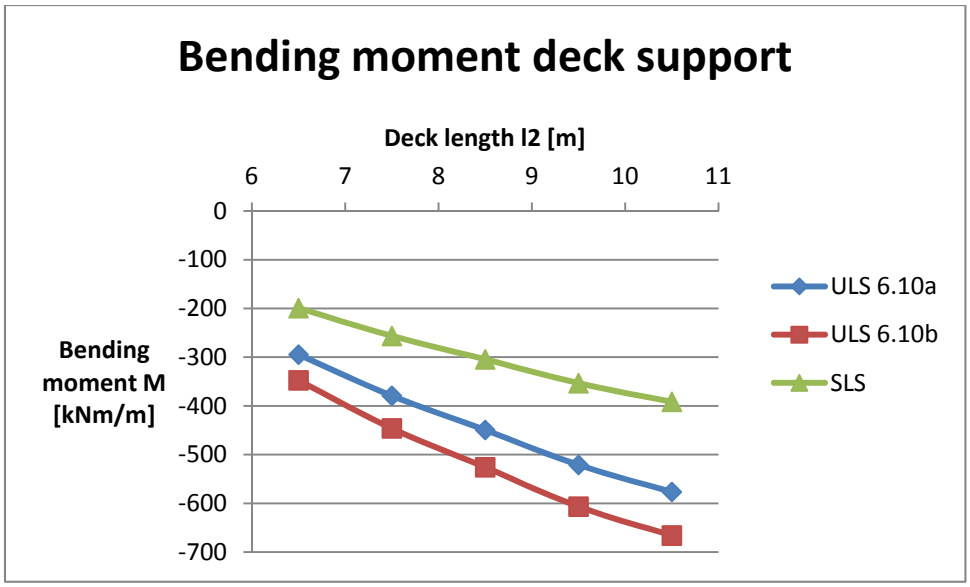

Figure 8.23: bending moment in the deck at the support in ULS and SLS

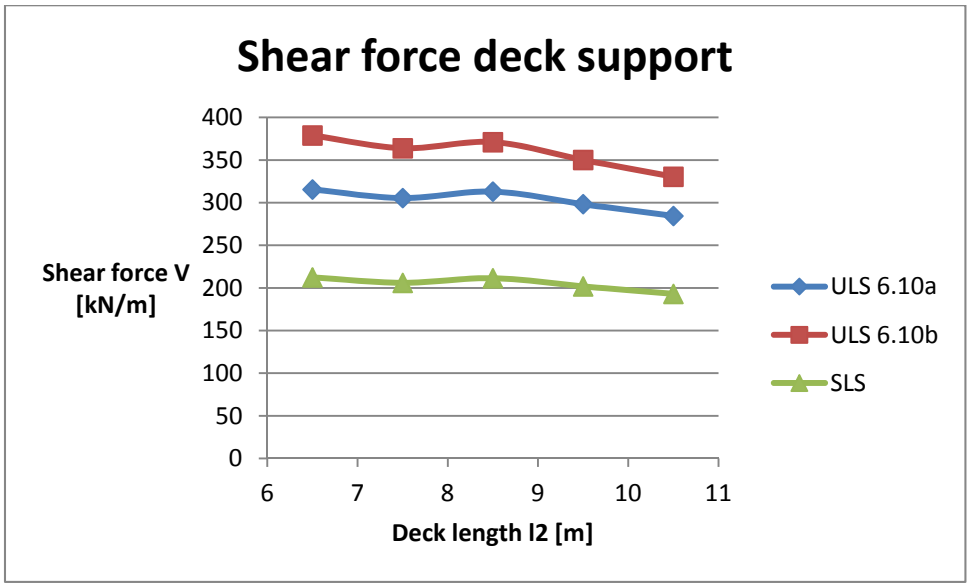

Figure 8.24: shear force in the deck at the support in ULS and SLS

8.7 Deck end haunch

Load case 4 provides the extreme bending moment and shear force in the deck at the haunch's end. The capacity of cross-section C (Figure 8.18) must be sufficient to transfer the load to the webs.

The maximum bending moment in the deck at the haunch's end, due to the tandem system, can be determined with influence surfaces. (van der Meulen, 1992) demonstrated, that for the deck between the webs, including haunches, the bending moment at the haunch's end is best approximated with the influence surface for a double clamped slab with a parabolic bottom edge and a thickness ratio 1:2.

8.7.1 Self-weight

The bending moment and shear force in the deck at the haunch's end, due to the self-weight of a double clamped slab with a parabolic bottom edge and a thickness ratio 1:2, are equal to (Figure 8.25 & Figure 8.26):

$$M_{G,SW} = -0.0235 g l_2^2 = -0.0235 \cdot 26 \cdot 0.2 \cdot 7.65^2 = -7\ kNm/m$$

$$V_{G,SW} = \frac{1}{2} g \cdot 0.6 l_2 = \frac{1}{2} \cdot 26 \cdot 0.2 \cdot 0.6 \cdot 7.65 = 12\ kN/m$$

8.7.2 Asphalt

The bending moment and shear force in the deck at the haunch's end, due to a uniformly distributed load q on a double clamped slab with a parabolic bottom edge and a thickness ratio 1:2, are equal to (Figure 8.25 & Figure 8.26):

$$M_{G,A} = -0.0225 q_{G,A} l_2^2 = -0.0225 \cdot 3.5 \cdot 7.65^2 = -5\ kNm/m$$

$$V_{G,A} = \frac{1}{2} q_{G,A} \cdot 0.6 l_2 = \frac{1}{2} \cdot 3.5 \cdot 0.6 \cdot 7.65 = 8\ kN/m$$

8.7.3 Permanent loads

The characteristic value of the bending moment and shear force due to the permanent loads:

$$M_{Gk} = M_{G,SW} + M_{G,A} = -7 - 5 = -12\ kNm/m$$

$$V_{Gk} = V_{G,SW} + V_{G,A} = 12 + 8 = 20\ kN/m$$

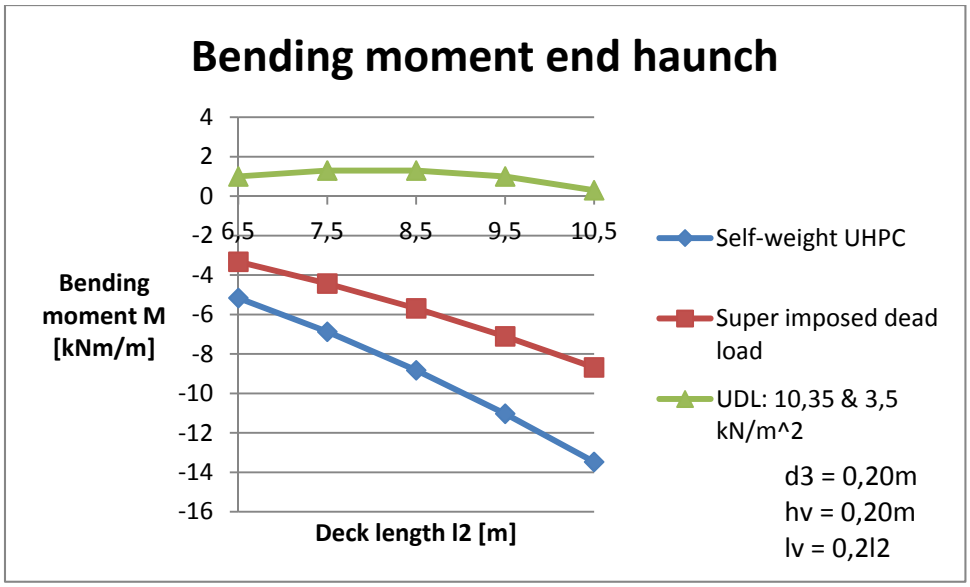

Figure 8.25: bending moment in the deck at the haunch's end due to self-weight, super imposed dead load and UDL

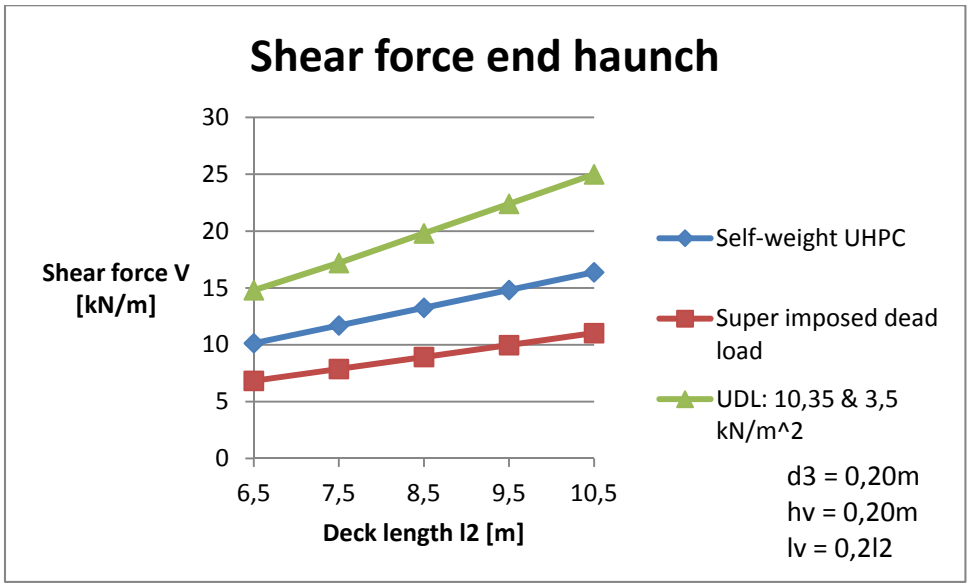

Figure 8.26: shear force in the deck at the haunch's end due to self-weight, super imposed dead load and UDL

8.7.4 UDL

The bending moment and shear force due to the UDL can be determined with the Euler-Bernoulli bending beam differential equation. The bending stiffness of the deck is assumed to be constant over the whole length. Bending moment and shear force values have been found for a deck length of 6.5, 7.5, 8.5, 9.5 and 10 meters (Figure 8.25 & Figure 8.26). From these values, a trend line can be derived. The characteristic value of the bending moment and shear force due to the UDL can be approximated by the following equations:

$$M_{Qk,UDL} = 1 = 1\ kNm/m$$

$$V_{Qk,UDL} = 2(l_2 + 1.5) = 2(7.65 + 1.5) = 18\ kN/m$$

Appendix 20 shows how to determine the bending moment and shear force at the haunch's end due to the UDL for a deck length of 8.5 meters. The same procedure can be followed for the other deck lengths.

8.7.5 Tandem system

The bending moment due to the tandem system can be determined with the influence surface for a double clamped slab with a parabolic bottom edge and a thickness ratio 1:2. Bending moment values have been found for a deck length of 6.5, 7.5, 8.5, 9.5 and 10 meters (Figure 8.27). The same procedure can be followed to determine the shear forces (Figure 8.28). However, since the influence surface for a cantilever slab with a thickness ratio 1:2 is not available, shear forces will be determined with a thickness ratio 1:1 and will therefore be somewhat underestimated. From the obtained values, a trend line can be derived. The characteristic value of the bending moment and shear force due to the tandem system can be approximated by the following equations:

$$l_2 \leq 7.5 \rightarrow M_{Qk,TS} = l_2 - 50.5$$

$$l_1 \geq 7.5 \rightarrow M_{Qk,TS} = -(4(l_2 - 9)^2) - 33$$

$$M_{Qk,TS} = -(4(l_2 - 9)^2) - 33 = -(4(7.65 - 9)^2) - 33 = -40\ kNm/m$$

$$V_{Qk,TS} = 2(l_2 - 9)^2 + 50 = 2(7.65 - 9)^2 + 50 = 54\ kN/m$$

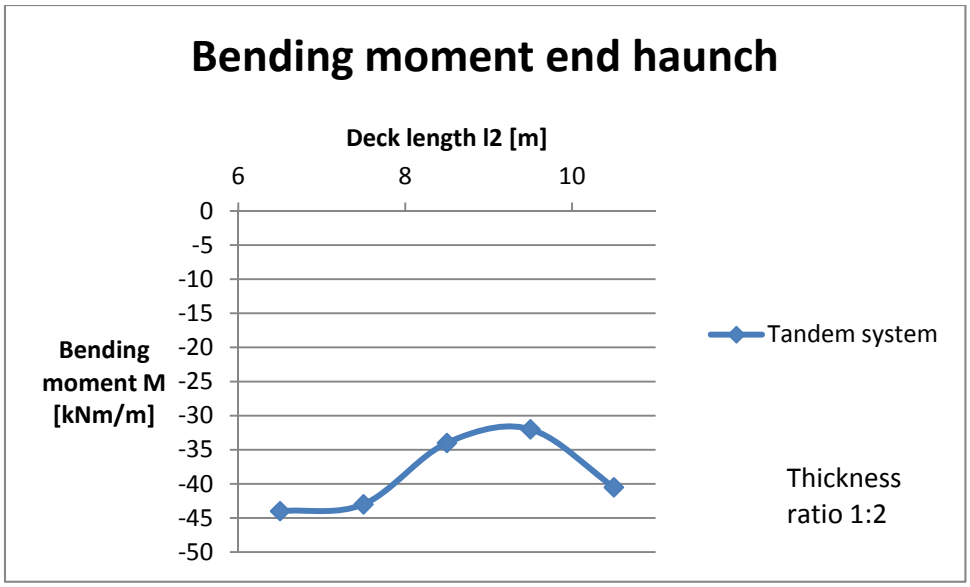

Figure 8.27: bending moment in the deck at the haunch's end due to the tandem system

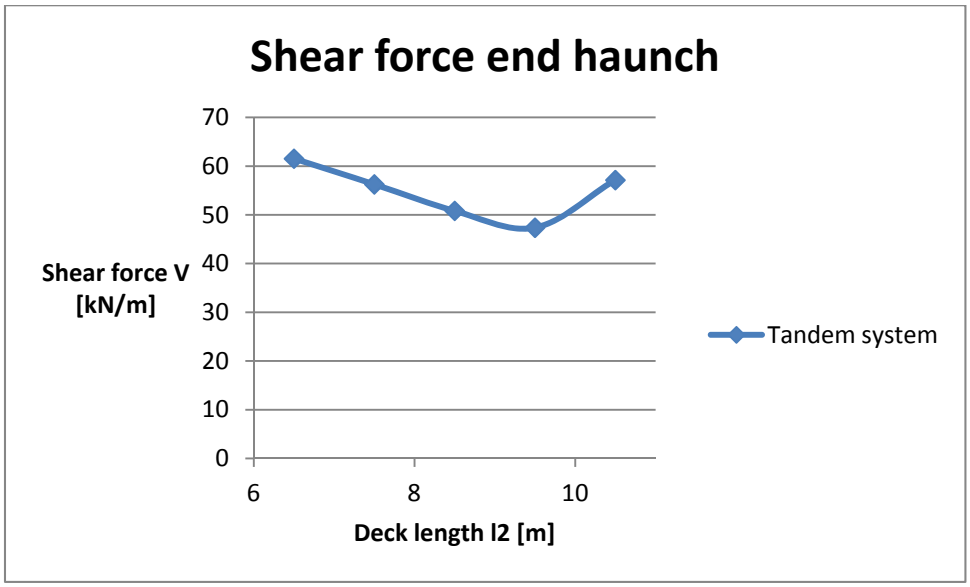

Figure 8.28: shear force in the deck at the haunch's end due to the tandem system

8.7.6 ULS design

Design value of the bending moment and shear force at cross-section C according to NEN-EN 1990: equations 6.10a & 6.10b:

$$M_{Ed,ULS} = max\begin{cases}\gamma_G M_{Gk} + \gamma_Q \psi_0 M_{Qk,TS} + \gamma_Q \psi_0 M_{Qk,UDL} \\ \zeta \gamma_G M_{Gk} + \gamma_Q M_{Qk,TS} + \gamma_Q M_{Qk,UDL}\end{cases} \rightarrow$$

$$M_{Ed,ULS} = max\begin{cases}-1.4 \cdot 12 - 1.5 \cdot 0.8 \cdot (40-1) = -64\ kNm/m \\ -1.25 \cdot 12 - 1.5 \cdot (40-1) = -74\ kNm/m\end{cases}$$

$$V_{Ed,ULS} = max\begin{cases}\gamma_G V_{Gk} + \gamma_Q \psi_0 V_{Qk,TS} + \gamma_Q \psi_0 V_{Qk,UDL} \\ \zeta \gamma_G V_{Gk} + \gamma_Q V_{Qk,TS} + \gamma_Q V_{Qk,UDL}\end{cases} \rightarrow$$

$$V_{Ed,ULS} = max\begin{cases}1.4 \cdot 20 + 1.5 \cdot 0.8 \cdot (18+54) = 114\ kN/m \\ 1.25 \cdot 20 + 1.5 \cdot (18+54) = 133\ kN/m\end{cases}$$

Appendix 17 shows that five Ø16 mm strands are required to provide sufficient bending moment and shear force capacity for cross-section C.

Unity check ultimate bending moment: $M_{Ed,ULS}/M_{Rd} = 74/145 = 0.51$

Unity check ultimate shear force: $V_{Ed,ULS}/V_{Rd} = 133/545 = 0.24$

8.7.7 SLS design

Design value of the bending moment at cross-section C according to NEN-EN 1990: equation 6.15b:

$$M_{Ed,SLS} = M_{Gk} + \psi_1 M_{Qk,TS} + \psi_1 M_{Qk,UDL} = -12 - 0.8(40 - 1) = -43\ kNm/m$$

Requirement: the deck remains uncracked in the serviceability state.

$t = 0 \rightarrow$ check top fiber:

$$-\frac{P_{m0}}{A_c} - \frac{P_{m0} \cdot e}{W_{top}} + \frac{M}{W_{top}} \leq f'_{ct} \rightarrow \frac{M}{W_{top}} \leq \frac{P_{m0}}{A_c} + \frac{P_{m0} \cdot e}{W_{top}} + f'_{ct} \rightarrow$$

$$M \leq \frac{P_{m0}}{A_c} W_{top} + P_{m0} \cdot e + f'_{ct} W_{top} \rightarrow M \leq 67\ kNm/m$$

$t = 0 \rightarrow$ check bottom fiber:

$$-\frac{P_{m0}}{A_c} + \frac{P_{m0} \cdot e}{W_{bot}} - \frac{M}{W_{bot}} \leq f'_{ct} \rightarrow \frac{M}{W_{bot}} \geq -\frac{P_{m0}}{A_c} + \frac{P_{m0} \cdot e}{W_{bot}} - f'_{ct} \rightarrow$$

$$M \geq -\frac{P_{m0}}{A_c} W_{bot} + P_{m0} \cdot e - f'_{ct} W_{bot} \rightarrow M \geq -109\ kNm/m$$

$t = \infty \rightarrow$ check top fiber:

$$-\frac{P_{m\infty}}{A_c} - \frac{P_{m\infty} \cdot e}{W_{top}} + \frac{M}{W_{top}} \leq f'_{ct} \rightarrow \frac{M}{W_{top}} \leq \frac{P_{m\infty}}{A_c} + \frac{P_{m\infty} \cdot e}{W_{top}} + f'_{ct} \rightarrow$$

$$M \leq \frac{P_{m\infty}}{A_c} W_{top} + P_{m\infty} \cdot e + f'_{ct} W_{top} \rightarrow M \leq 64\ kNm/m$$

$t = \infty \rightarrow$ check bottom fiber:

$$-\frac{P_{m\infty}}{A_c} + \frac{P_{m\infty} \cdot e}{W_{bot}} - \frac{M}{W_{bot}} \leq f'_{ct} \rightarrow \frac{M}{W_{bot}} \geq -\frac{P_{m\infty}}{A_c} + \frac{P_{m\infty} \cdot e}{W_{bot}} - f'_{ct} \rightarrow$$

$$M \geq -\frac{P_{m\infty}}{A_c} W_{bot} + P_{m\infty} \cdot e - f'_{ct} W_{bot} \rightarrow M \geq -95\ kNm/m$$

Unity check serviceability limit state bending moment: $M_{Ed,SLS}/M_{Rd} = 43/64 = 0.67$

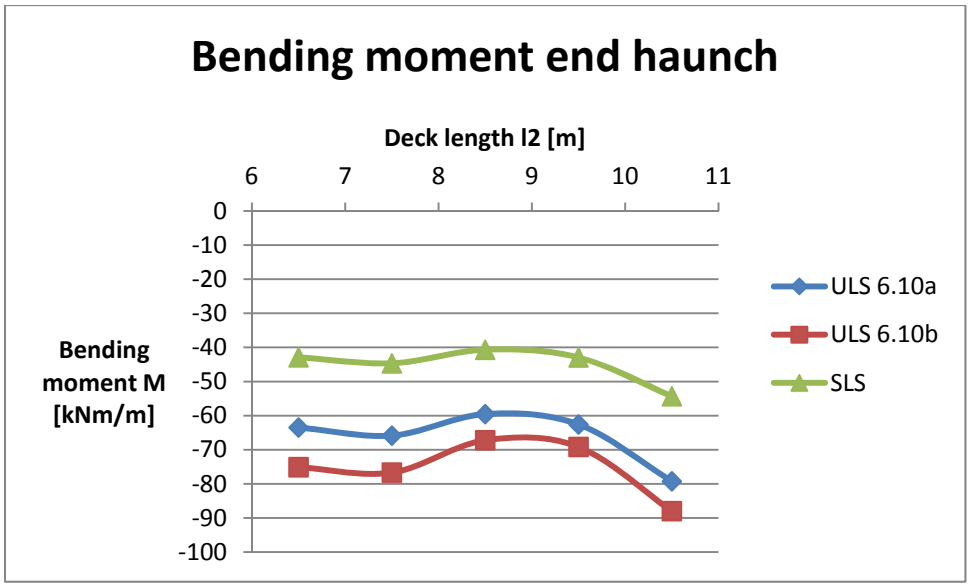

Figure 8.29: bending moment in the deck at the haunch's end in ULS and SLS

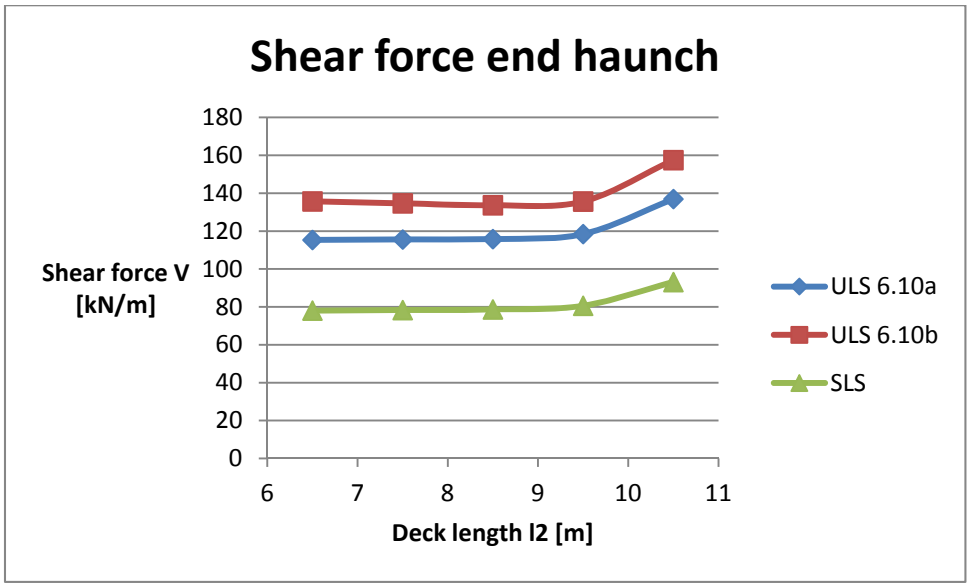

Figure 8.30: shear force in the deck at the haunch's end in ULS and SLS

8.8 Deck mid span

Load case 3 provides the extreme bending moment in the deck at mid span. The capacity of cross-section D (Figure 8.18) must be sufficient to transfer the load to the webs.

The maximum bending moment in the deck at mid span, due to the tandem system, can be determined with influence surfaces. (van der Meulen, 1992) demonstrated, that for the deck between the webs, including haunches, the bending moment at mid span is best approximated with the influence surface for a double clamped slab with a parabolic bottom edge and a thickness ratio 1:1.5.

8.8.1 Self-weight

The bending moment at mid span, due to the self-weight of a double clamped slab with a parabolic bottom edge and a thickness ratio 1:1.5, equals (Figure 8.31):

$$M_{G,SW} = 0.0307 g l_2^2 = 0.0307 \cdot 26 \cdot 0.2 \cdot 7.65^2 = 9\ kNm/m$$

8.8.2 Asphalt

The bending moment at mid span, due to a uniformly distributed load q on a double clamped slab with a parabolic bottom edge and a thickness ratio 1:1.5, equals (Figure 8.31):

$$M_{G,A} = 0.0295 q_{G,A} l_2^2 = 0.0295 \cdot 3.5 \cdot 7.65^2 = 6\ kNm/m$$

8.8.3 Permanent loads

The characteristic value of the bending moment due to the permanent loads:

$$M_{Gk} = M_{G,SW} + M_{G,A} = 9 + 6 = 15\ kNm/m$$

8.8.4 UDL

The bending moment due to the UDL can be determined with the Euler-Bernoulli bending beam differential equation. The bending stiffness of the deck is assumed to be constant over the whole length. Bending moment values have been found for a deck length of 6.5, 7.5, 8.5, 9.5 and 10 meters (Figure 8.31). From these values, a trend line can be derived. The characteristic value of the bending moment due to the UDL can be approximated by the equation:

$$M_{Qk,UDL} = 5(l_2 - 3.9) = 5(7.65 - 3.9) = 19\ kNm/m$$

Appendix 21 shows how to determine the bending moment and shear force at mid span due to the UDL for a deck length of 9.5 meters. The same procedure can be followed for the other deck lengths.

8.8.5 Tandem system

The bending moment due to the tandem system can be determined with the influence surface for a double clamped slab with a parabolic bottom edge and a thickness ratio 1:1.5. Bending moment values have been found for a deck length of 6.5, 7.5, 8.5, 9.5 and 10 meters (Figure 8.31). The characteristic value of the bending moment due to the tandem system can be approximated by the equation:

$$M_{Qk,TS} = 9(l_2 - 0.5) = 9(7.65 - 0.5) = 64\ kNm/m$$

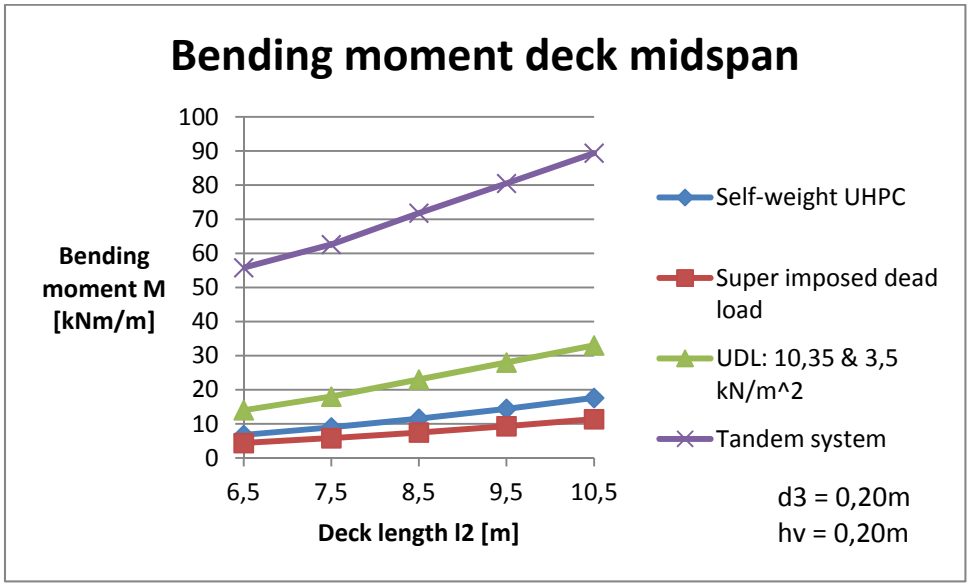

Figure 8.31: bending moment in the deck at mid span due to self-weight, super imposed dead load, UDL and tandem system

8.8.6 ULS design

Design value of the bending moment at cross-section D according to NEN-EN 1990: equations 6.10a & 6.10b:

$$M_{Ed,ULS} = max \begin{cases} \gamma_G M_{Gk} + \gamma_Q \psi_0 M_{Qk,TS} + \gamma_Q \psi_0 M_{Qk,UDL} \\ \zeta \gamma_G M_{Gk} + \gamma_Q M_{Qk,TS} + \gamma_Q M_{Qk,UDL} \end{cases} \rightarrow$$

$$M_{Ed,ULS} = max \begin{cases} 1.4 \cdot 15 + 1.5 \cdot 0.8 \cdot (19 + 64) = 121\ kNm/m \\ 1.25 \cdot 15 + 1.5 \cdot (19 + 64) = 143\ kNm/m \end{cases}$$

Appendix 18 shows that five Ø16 mm strands are required to provide sufficient bending moment capacity for cross-section D.

Unity check ultimate bending moment: $M_{Ed,ULS}/M_{Rd} = 143/186 = 0.77$

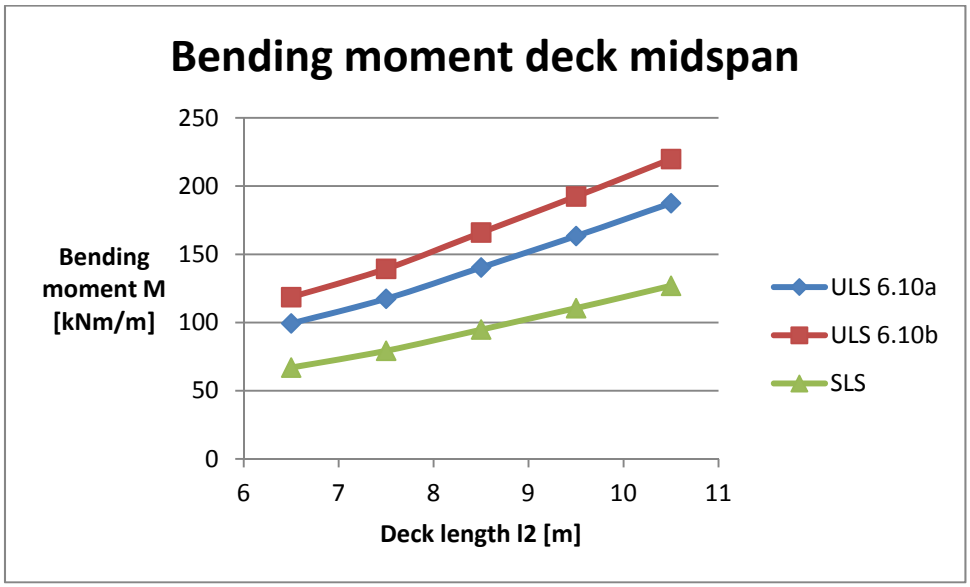

Figure 8.32: bending moment in the deck at mid span in ULS and SLS

8.8.7 SLS design

Design value of the bending moment at cross-section D according to NEN-EN 1990: equation 6.15b:

$$M_{Ed,SLS} = M_{Gk} + \psi_1 M_{Qk,TS} + \psi_1 M_{Qk,UDL} = 15 + 0.8 \cdot 83 = 81\ kNm/m$$

Requirement: the deck remains uncracked in the serviceability limit state.

$t = 0 \rightarrow$ check top fiber:

$$-\frac{P_{m0}}{A_c} + \frac{P_{m0} \cdot e}{W_{top}} - \frac{M}{W_{top}} \leq f'_{ct} \rightarrow \frac{M}{W_{top}} \geq -\frac{P_{m0}}{A_c} + \frac{P_{m0} \cdot e}{W_{top}} - f'_{ct} \rightarrow$$

$$M \geq -\frac{P_{m0}}{A_c} W_{top} + P_{m0} \cdot e - f'_{ct} W_{top} \rightarrow M \geq -23\ kNm/m$$

$t = 0 \rightarrow$ check bottom fiber:

$$-\frac{P_{m0}}{A_c} - \frac{P_{m0} \cdot e}{W_{bot}} + \frac{M}{W_{bot}} \leq f'_{ct} \rightarrow \frac{M}{W_{bot}} \leq \frac{P_{m0}}{A_c} + \frac{P_{m0} \cdot e}{W_{bot}} + f'_{ct} \rightarrow$$

$$M \leq \frac{P_{m0}}{A_c} W_{bot} + P_{m0} \cdot e + f'_{ct} W_{bot} \rightarrow M \leq 153\ kNm/m$$

$t = \infty \rightarrow$ check top fiber:

$$-\frac{P_{m\infty}}{A_c} + \frac{P_{m\infty} \cdot e}{W_{top}} - \frac{M}{W_{top}} \leq f'_{ct} \rightarrow \frac{M}{W_{top}} \geq -\frac{P_{m\infty}}{A_c} + \frac{P_{m\infty} \cdot e}{W_{top}} - f'_{ct} \rightarrow$$

$$M \geq -\frac{P_{m\infty}}{A_c} W_{top} + P_{m\infty} \cdot e - f'_{ct} W_{top} \rightarrow M \geq -31\ kNm/m$$

$t = \infty \rightarrow$ check bottom fiber:

$$-\frac{P_{m\infty}}{A_c} - \frac{P_{m\infty} \cdot e}{W_{bot}} + \frac{M}{W_{bot}} \leq f'_{ct} \rightarrow \frac{M}{W_{bot}} \leq \frac{P_{m\infty}}{A_c} + \frac{P_{m\infty} \cdot e}{W_{bot}} + f'_{ct} \rightarrow$$

$$M \leq \frac{P_{m\infty}}{A_c} W_{bot} + P_{m\infty} \cdot e + f'_{ct} W_{bot} \rightarrow M \leq 128\ kNm/m$$

Unity check serviceability limit state bending moment: $M_{Ed,SLS}/M_{Rd} = 81/128 = 0.63$

8.9 Force distribution in the webs

The webs are loaded by the resulting bending moment from the cantilever and the deck between the webs. The sum of the shear forces from the cantilever and the deck cause a centric normal force on the webs. This results in the following two load cases:

1. Maximum live load on cantilever (load case 1), deck between the webs loaded by self-weight and super imposed dead load.
2. Maximum live load on deck between the webs (load case 4), cantilever loaded by self-weight and super imposed dead load.

8.9.1 Mobile loading on cantilever (load case 1)

ULS

The design value of the bending moment and normal force on the web in ultimate limit state:

$$M_{Ed,ULS,web} = M_{Ed,ULS,cant} - M_{Ed,SW+SIDL,ULS,deck}$$

$$N_{Ed,ULS,web} = V_{Ed,ULS,cant} + V_{Ed,SW+SIDL,ULS,deck}$$

SLS

The design value of the bending moment and normal force on the web in serviceability limit state:

$$M_{Ed,SLS,web} = M_{Ed,SLS,cant} - M_{Ed,SW+SIDL,SLS,deck}$$

$$N_{Ed,SLS,web} = V_{Ed,SLS,cant} + V_{Ed,SW+SIDL,SLS,deck}$$

8.9.2 Mobile loading on deck between the webs (load case 4)

ULS

The design value of the bending moment and normal force on the web in ultimate limit state:

$$M_{Ed,ULS,web} = M_{Ed,SW+SIDL,ULS,cant} - M_{Ed,ULS,deck}$$

$$N_{Ed,ULS,web} = V_{Ed,SW+SIDL,ULS,cant} + V_{Ed,ULS,deck}$$

SLS

The design value of the bending moment and normal force on the web in serviceability limit state:

$$M_{Ed,SLS,web} = M_{Ed,SW+SIDL,SLS,cant} - M_{Ed,SLS,deck}$$

$$N_{Ed,SLS,web} = V_{Ed,SW+SIDL,SLS,cant} + V_{Ed,SLS,deck}$$

Figure 8.33 & Figure 8.34 show the resulting bending moment and normal force on the web for load cases 1 and 4. The cross-section at the top of the web should be able to withstand these bending moments in combination with the normal force.

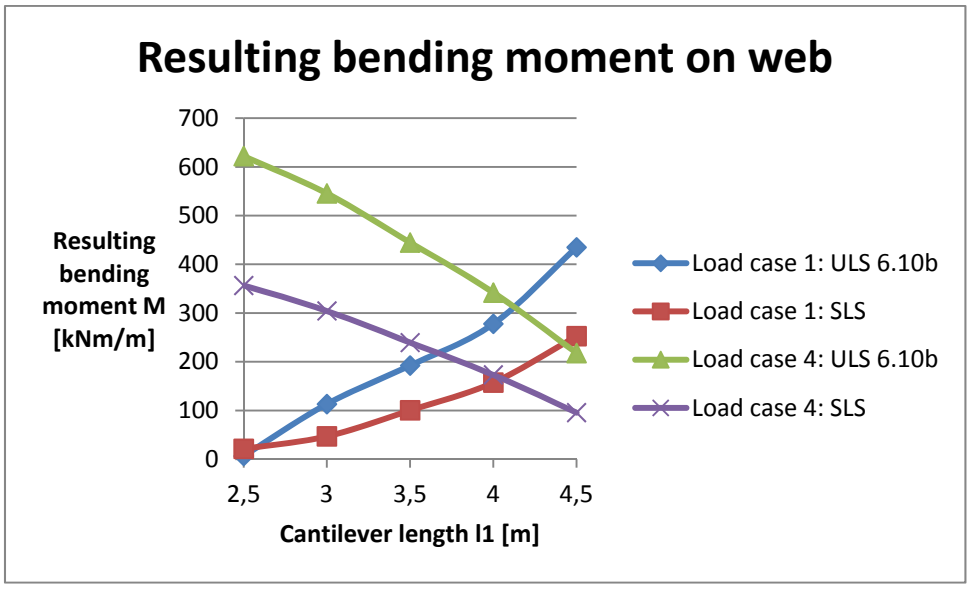

Figure 8.33: resulting bending moment on the web

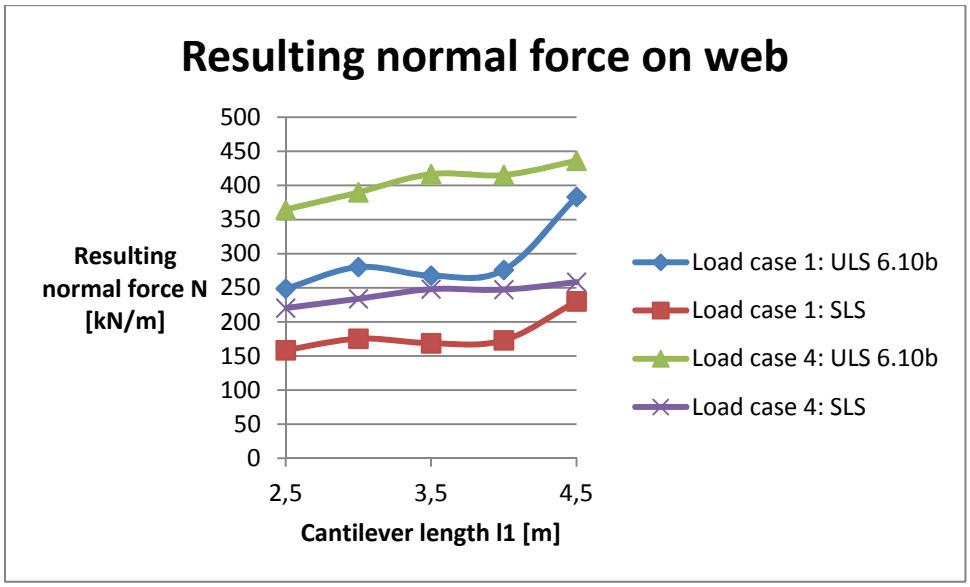

Figure 8.34: resulting normal force on the web

8.10 Force distribution in the floor

The bottom floor does not have any haunches, so the cross-section at the floor-web connection will be governing for the bending moment and shear force.

8.10.1 Self-weight

The bending moment and shear force at the floor-web connection, due to the self-weight of the bottom floor:

$$M_{G,SW} = -\frac{1}{12}\gamma d_5 l_2^2 = -\frac{1}{12}\cdot 26 \cdot 0.15 \cdot 7.65^2 = -19\ kNm/m$$

$$V_{G,SW} = \frac{1}{2}\gamma d_5 l_2 = \frac{1}{2}\cdot 25 \cdot 0.15 \cdot 7.65 = 14\ kN/m$$

8.10.2 Vehicle with hydraulic jack

The load due to the presence of a vehicle with a hydraulic jack in order to stress the tendons is assumed to be $3\ kN/m^2$. The bending moment and shear force at the floor-web connection will become:

$$M_{Q,vehicle} = -\frac{1}{12}\cdot 3 \cdot 7.65^2 = -15\ kNm/m$$

$$V_{Q,vehicle} = \frac{1}{2}\cdot 3 \cdot 7.65 = 12\ kNm/m$$

8.10.3 Tensile force in the floor due to mobile loading on deck

When the tandem system is positioned on the deck between the webs, it will cause a tensile force in the bottom floor, which has the following value:

$$N_{Ed,ULS,floor} = \frac{\left|M_{Ed,ULS,deck}\right| - \left|M_{Ed,SW+SIDL,cant}\right|}{h - \frac{1}{2}d_3 - \frac{1}{2}d_5} = \frac{|-449\cdot 10^6| - |-101\cdot 10^6|}{3200 - \frac{1}{2}\cdot 200 - \frac{1}{2}\cdot 150} = 115\ kN/m$$

$$N_{Ed,SLS,floor} = \frac{\left|M_{Ed,SLS,deck}\right| - \left|M_{Ed,SW+SIDL,cant}\right|}{h - \frac{1}{2}d_3 - \frac{1}{2}d_5} = \frac{|-259\cdot 10^6| - |-80\cdot 10^6|}{3200 - \frac{1}{2}\cdot 200 - \frac{1}{2}\cdot 150} = 59\ kN/m$$

8.10.4 ULS design

Design value of the bending moment and shear force at the floor-web connection, according to NEN-EN 1990: equations 6.10a & 6.10b:

$$M_{Ed,ULS} = max\begin{cases}\gamma_G M_{G,SW} + \gamma_Q \psi_0 M_{Q,vehicle} \\ \zeta\gamma_G M_{G,SW} + \gamma_Q M_{Q,vehicle}\end{cases} \rightarrow$$

$$M_{Ed,ULS} = max\begin{cases}-1.4 \cdot 19 - 1.65 \cdot 1.0 \cdot 15 = -51\ kNm/m \\ -1.25 \cdot 19 - 1.65 \cdot 15 = -49\ kNm/m\end{cases}$$

combined with the tensile force: $N_{Ed,ULS,floor}$.

$$V_{Ed,ULS} = max\begin{cases}\gamma_G V_{G,SW} + \gamma_Q \psi_0 V_{Q,vehicle} \\ \zeta\gamma_G V_{G,SW} + \gamma_Q V_{Q,vehicle}\end{cases} \rightarrow$$

$$V_{Ed,ULS} = max\begin{cases}1.4 \cdot 14 + 1.65 \cdot 1.0 \cdot 12 = 39\ kN/m \\ 1.25 \cdot 14 + 1.65 \cdot 12 = 37\ kN/m\end{cases}$$

Appendix 22 shows that one Ø16 mm strand is required to provide sufficient bending moment and shear force capacity for the bottom floor.

Unity check ultimate bending moment: $M_{Ed,ULS}/M_{Rd} = 51/63 = 0.81$

Unity check ultimate shear force: $V_{Ed,ULS}/V_{Rd} = 37/892 = 0.04$

8.10.5 SLS design

Design value of the bending moment at the floor-web connection according to NEN-EN 1990: equation 6.15b:

$M_{Ed,SLS} = M_{G,SW} + M_{Q,veh} = -34\ kNm/m$, combined with the tensile force: $N_{Ed,SLS,floor}$.

Requirement: the floor remains uncracked in the serviceability state.

$t = 0 \rightarrow$ check top fiber:

$$-\frac{P_{m0}}{A_c} - \frac{P_{m0} \cdot e}{W_{top}} + \frac{M}{W_{top}} + \frac{N_{Ed,SLS,floor}}{A_c} \leq f'_{ct} \rightarrow \frac{M}{W_{top}} \leq \frac{P_{m0}}{A_c} + \frac{P_{m0} \cdot e}{W_{top}} - \frac{N_{Ed,SLS,floor}}{A_c} + f'_{ct} \rightarrow$$
$$M \leq \frac{P_{m0}}{A_c} W_{top} + P_{m0} \cdot e - \frac{N_{Ed,SLS,floor}}{A_c} W_{top} + f'_{ct} W_{top} \rightarrow M \leq 43\ kNm/m$$

$t = 0 \rightarrow$ check bottom fiber:

$$-\frac{P_{m0}}{A_c} + \frac{P_{m0} \cdot e}{W_{bot}} - \frac{M}{W_{bot}} + \frac{N_{Ed,SLS,floor}}{A_c} \leq f'_{ct} \rightarrow \frac{M}{W_{bot}} \geq -\frac{P_{m0}}{A_c} + \frac{P_{m0} \cdot e}{W_{bot}} + \frac{N_{Ed,SLS,floor}}{A_c} - f'_{ct} \rightarrow$$
$$M \geq -\frac{P_{m0}}{A_c} W_{bot} + P_{m0} \cdot e + \frac{N_{Ed,SLS,floor}}{A_c} W_{bot} - f'_{ct} W_{bot} \rightarrow M \geq -28\ kNm/m$$

$t = \infty \rightarrow$ check top fiber:

$$-\frac{P_{m\infty}}{A_c} - \frac{P_{m\infty} \cdot e}{W_{top}} + \frac{M}{W_{top}} + \frac{N_{Ed,SLS,floor}}{A_c} \leq f'_{ct} \rightarrow \frac{M}{W_{top}} \leq \frac{P_{m\infty}}{A_c} + \frac{P_{m\infty} \cdot e}{W_{top}} - \frac{N_{Ed,SLS,floor}}{A_c} + f'_{ct} \rightarrow$$
$$M \leq \frac{P_{m\infty}}{A_c} W_{top} + P_{m\infty} \cdot e - \frac{N_{Ed,SLS,floor}}{A_c} W_{top} + f'_{ct} W_{top} \rightarrow M \leq 40\ kNm/m$$

$t = \infty \rightarrow$ check bottom fiber:

$$-\frac{P_{m\infty}}{A_c} + \frac{P_{m\infty} \cdot e}{W_{bot}} - \frac{M}{W_{bot}} + \frac{N_{Ed,SLS,floor}}{A_c} \leq f'_{ct} \rightarrow \frac{M}{W_{bot}} \geq -\frac{P_{m\infty}}{A_c} + \frac{P_{m\infty} \cdot e}{W_{bot}} + \frac{N_{Ed,SLS,floor}}{A_c} - f'_{ct} \rightarrow$$
$$M \geq -\frac{P_{m\infty}}{A_c} W_{bot} + P_{m\infty} \cdot e + \frac{N_{Ed,SLS,floor}}{A_c} W_{bot} - f'_{ct} W_{bot} \rightarrow M \geq -28\ kNm/m$$

Unity check serviceability limit state bending moment: $M_{Ed,SLS}/M_{Rd} = 34/40 = 0.85$

8.11 A different deflection at both webs

This paragraph is based on (Krebs & Lindlar, 1988) and (van der Meulen, 1992). When the tandem system is located near one of the webs, the deflection at that web will be larger than at the other web. The difference in deflection will cause bending moments in the box girder cross-section. This load case is illustrated in Figure 8.35, where the point load at the left web is split up into a symmetrical and asymmetrical part. The asymmetrical load is equivalent to the combination of pure torsion forces (Figure 8.35d) and distortion forces (Figure 8.35e).

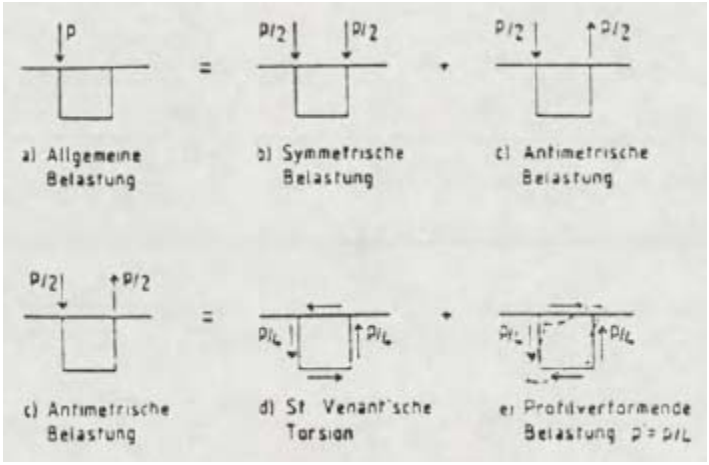

Figure 8.35: Splitting up the point load into a symmetrical and an asymmetrical part (Krebs & Lindlar, 1988).

The load caused by the box girder distortion is equal to:

$$p' = \frac{P_d}{4}$$

with P_d: the force difference between both webs.

In the design, the box girder cross-section will be replaced, in longitudinal direction, by a infinitely long beam on elastic foundation with moment of inertia: I_{ers}.

The frame stiffness of the box girder cross-section against distortion is equal to:

$$k_b = \frac{2}{\delta}$$

In longitudinal direction, the box girder cross-section will be modeled with hinged nodes. In transverse direction the box girder cross-section will be modeled with stiff nodes (Figure 8.36). The longitudinal and transverse direction will be coupled by equalizing the rotation between the deck and web ω for both models (Figure 8.37).

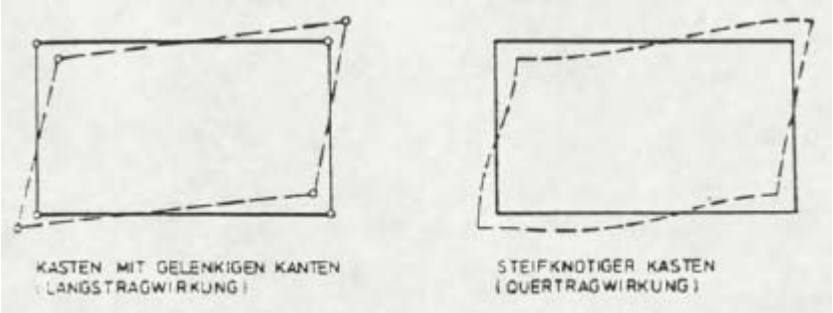

Figure 8.36: box girder cross-section model in longitudinal and transverse direction (Krebs & Lindlar, 1988).

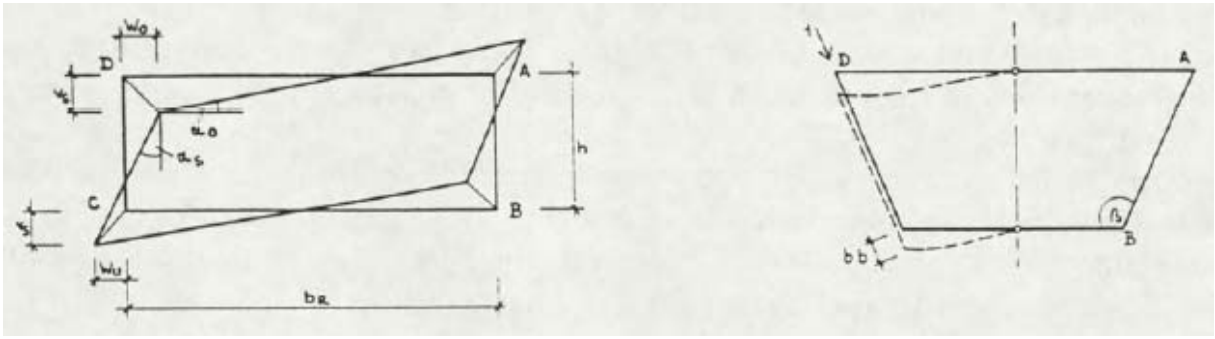

Figure 8.37: frame deformation for hinged nodes (left) and stiff nodes (right) (Krebs & Lindlar, 1988).

$$\omega_{ADC,hinged} = \alpha_0 + \alpha_s = 2\alpha_0 = \frac{4v_s}{b_r}$$

$$\omega_{ADC,stiff} = \frac{2\delta_b}{b_r}$$

$$\omega_{ADC,hinged} = \omega_{ADC,stiff} \rightarrow v_s = \frac{\delta_b}{2}$$

$$k_b = \frac{1}{v_s} = \frac{2}{\delta_b}$$

The frame stiffness k_b can be derived by considering half of the box girder cross-section and by determining the deflection δ_b at the web due to a unit load $F = 1\ kN$ (Figure 8.38). The cantilevers will not be considered. This unit deflection δ_b can be approximated by a simply supported slab with a length l_p and a point load $F = 2\ kN$ (Figure 8.39).

The deflection at mid span will be equal to the deflection at the web in the model with half of the box girder cross-section. The maximum bending moment at mid span is then equal to the sum of the support moments at the box girder deck and bottom floor. In this model, the webs are assumed to be infinitely stiff.

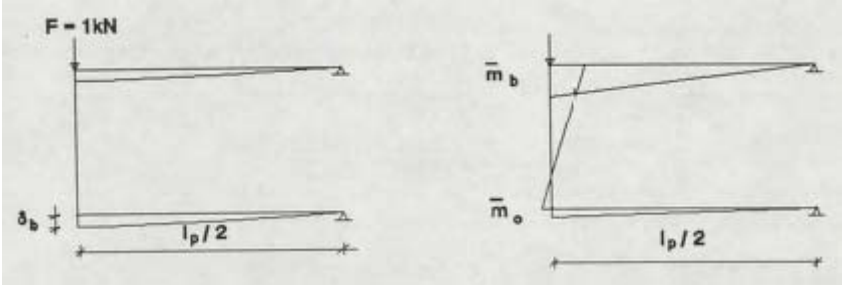

Figure 8.38: model of half the box girder cross-section (van der Meulen, 1992).

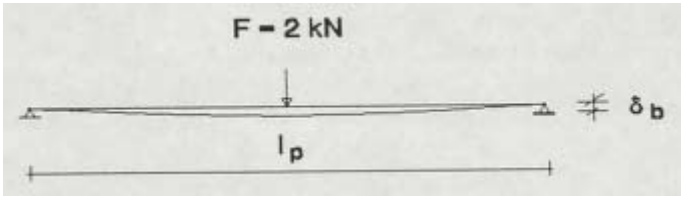

Figure 8.39: model simply supported slab (van der Meulen, 1992).

The maximum deflection and bending moment of a simply supported slab:

$$\delta_{max} = \frac{Fl^3}{48EI}$$

$$M = \frac{1}{4}Fl$$

$$F = 2\ kN$$

The moment of inertia of the deck and floor together, with $b = 1\ m$:

$$I = \frac{1}{12}\left(d^{*3} + d_5^3\right)$$

with d^*: the mean thickness of the deck.

The unit displacement and frame stiffness become:

$$\delta_b = \frac{2l_p^3}{48 \cdot E \cdot \frac{1}{12}\left(d^{*3} + d_5^3\right)} = \frac{l_p^3}{2E\left(d^{*3} + d_5^3\right)}$$

$$k_b = \frac{2}{\delta_b} = \frac{4E\left(d^{*3} + d_5^3\right)}{l_p^3}$$

The support moments in the deck and floor due to a unit load:

$$\overline{m}_d = \frac{d^{*3}}{d^{*3} + d_5^3} \cdot \frac{1}{4} \cdot 2 \cdot l_p = \frac{d^{*3} l_p}{2\left(d^{*3} + d_5^3\right)}$$

$$\overline{m}_f = \frac{d_5^3}{d^{*3} + d_5^3} \cdot \frac{1}{4} \cdot 2 \cdot l_p = \frac{d_5^3 l_p}{2\left(d^{*3} + d_5^3\right)}$$

The difference in deflection at both webs will reach a maximum at mid span in longitudinal direction. In longitudinal direction, the box girder cross-section will be replaced by a infinitely long beam on elastic foundation with moment of inertia I_{ers}. In transverse direction, the bending moments can be determined with:

$$m = \overline{m} \cdot v_{ers} \cdot k_b$$

with v_{ers}: the deflection of the elastically supported beam, under the point load, in longitudinal direction.

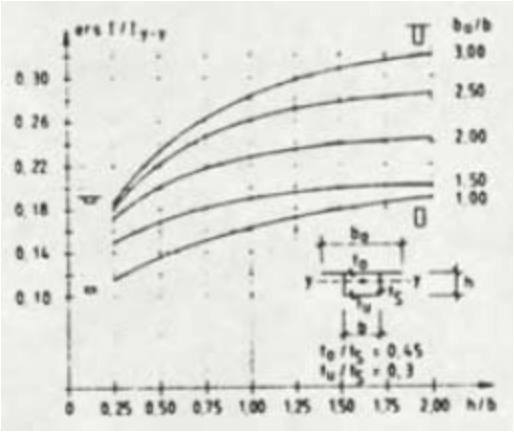

Figure 8.40: I_{ers} for rectangular box girder cross-sections (Krebs & Lindlar, 1988).

Figure 8.40 can be used to derive I_{ers}. However, this figure is valid for a box girder with the following properties:

$$\frac{d_3}{d_4} = 0.45$$

$$\frac{d_5}{d_4} = 0.30$$

For $d_3 = 0.2\ m$, $d_4 = 0.35\ m$ and $d_5 = 0.15\ m$, these ratio's become:

$$\frac{d_3}{d_4} = \frac{0.2}{0.35} = 0.57$$

$$\frac{d_5}{d_4} = 0.43$$

Since these values are substantially deviating from the values corresponding to Figure 8.40, I_{ers} will probably deviate as well. However, when Figure 8.40 is used, I_{ers} becomes:

$$\frac{l_b}{l_2} = \frac{15.5}{8} = 1.94$$

$$\frac{h}{l_b} = \frac{3.2}{15.5} = 0.21$$

$$\frac{I_{ers}}{I_{yy}} = 0.17 \rightarrow I_{ers} = 0.17 I_{yy}$$

The maximum deflection of the elastically supported beam, under the point load, in longitudinal direction:

$$v_{ers} = \frac{\beta p'}{2c_b}$$

$$\beta = \sqrt[4]{\frac{c_b}{4EI_{ers}}}$$

$$c_b = \frac{k_b}{b}$$

with:

β: a parameter in the differential equation for a beam on elastic foundation.

c_b: the foundation constant.

$$v_{ers} = \frac{\sqrt[4]{\frac{c_b}{4E \cdot 0.17 I_{yy}}} \cdot p'}{2c_b}$$

The support moments in the deck and floor due to the total point load become:

$$m_d = \bar{m}_d \cdot v_{ers} \cdot k_b = \frac{d^{*3} l_p}{4\left(d^{*3} + d_5^3\right)} \cdot \sqrt[4]{\frac{d^{*3} + d_5^3}{0.17 I_{yy} l_p^3}} \cdot p'$$

$$m_f = \bar{m}_f \cdot v_{ers} \cdot k_b = \frac{d_5^3 l_p}{4\left(d^{*3} + d_5^3\right)} \cdot \sqrt[4]{\frac{d^{*3} + d_5^3}{0.17 I_{yy} l_p^3}} \cdot p'$$

Maxwell's reciprocal theorem states, that the displacement at A, due to a unit load at B, is equal to the displacement at B, due to a unit load at A. When the two tandem system axes are located at A and B in longitudinal direction, the total deflection at A will be caused by the axis at B. When the tandem system is located centrically above the web, $P_d = 2Q_{1k} = 300\ kN$. When the tandem system is located eccentrically above the web, P_d will be equal to the force difference between both webs.

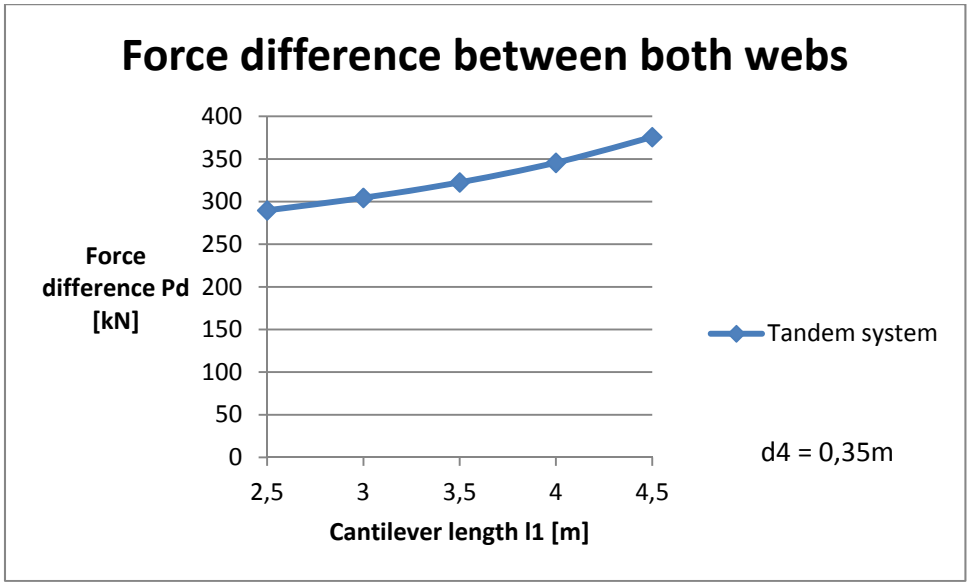

Figure 8.41: force difference between both webs

Figure 8.41 illustrates the force difference P_d between both webs, when the tandem system is applied as close to the edge as possible, for a cantilever length of 2, 2.5, 3, 3.5, 4 and 4.5 meters.

$$P_d = \frac{2Q_{1k}(l_1 - 1.41 - 0.25 - 0.2 - 1)}{l_2} + 2Q_{1k} = 2Q_{1k}\left(\frac{(l_1 - 2.86)}{l_2} + 1\right)$$

The load and bending moments caused by box girder distortion now become:

$$p' = \frac{P_d}{4} = \frac{Q_{1k}}{2}\left(\frac{(l_1 - 2.86)}{l_2} + 1\right)$$

$$m_d = \frac{d^{*3} l_p}{8\left(d^{*3} + d_5^3\right)} \cdot \sqrt[4]{\frac{d^{*3} + d_5^3}{0.17 I_{yy} l_p^3}} \cdot Q_{1k}\left(\frac{(l_1 - 2.86)}{l_2} + 1\right)$$

$$m_f = \frac{d_5^3 l_p}{8\left(d^{*3} + d_5^3\right)} \cdot \sqrt[4]{\frac{d^{*3} + d_5^3}{0.17 I_{yy} l_p^3}} \cdot Q_{1k}\left(\frac{(l_1 - 2.86)}{l_2} + 1\right)$$

These formulas only take into account the influence of the tandem system on the bending moment, since the tandem system is responsible for almost the entire bending moment in the deck. Figure 8.42 illustrates the bending moment in the deck and floor and the shear force in the floor caused by box girder distortion.

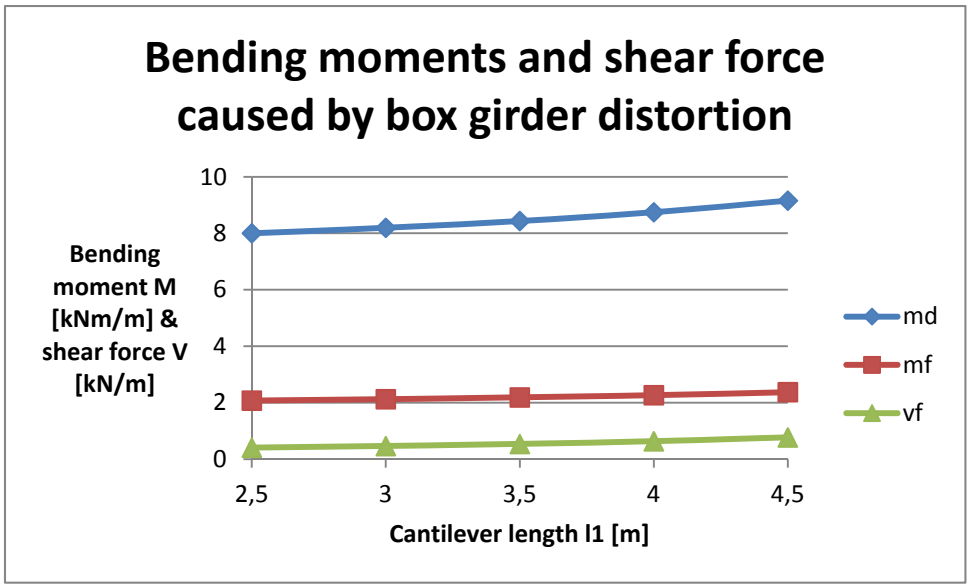

Figure 8.42: bending moments and shear force caused by box girder distortion

8.11.1 Force distribution in the floor caused by box girder distortion

Design value of the bending moment and shear force at the floor-web connection, according to NEN-EN 1990: equations 6.10a & 6.10b:

$$M_{Ed,ULS} = max\begin{cases}\gamma_G M_{G,SW} + \gamma_Q \psi_0 M_{Q,vehicle} + \gamma_Q \psi_0 M_{Qk,TS} \\ \zeta \gamma_G M_{G,SW} + \gamma_Q M_{Q,vehicle} + \gamma_Q M_{Qk,TS}\end{cases} \rightarrow$$

$$M_{Ed,ULS} = max\begin{cases}-1.4 \cdot 19 - 1.65 \cdot 1.0 \cdot 15 - 1.5 \cdot 0.8 \cdot 2 = -54\ kNm/m \\ -1.25 \cdot 19 - 1.65 \cdot 15 - 1.5 \cdot 2 = -52\ kNm/m\end{cases}$$

$$V_{Ed,ULS} = max\begin{cases}\gamma_G V_{G,SW} + \gamma_Q \psi_0 V_{Q,vehicle} + \gamma_Q \psi_0 V_{Qk,TS} \\ \zeta \gamma_G V_{G,SW} + \gamma_Q V_{Q,vehicle} + \gamma_Q V_{Qk,TS}\end{cases} \rightarrow$$

$$V_{Ed,ULS} = max\begin{cases}1.4 \cdot 14 + 1.65 \cdot 1.0 \cdot 12 + 1.5 \cdot 0.8 \cdot 1 = 41\ kN/m \\ 1.25 \cdot 14 + 1.65 \cdot 12 + 1.5 \cdot 1 = 39\ kN/m\end{cases}$$

Unity check ultimate bending moment (Appendix 22): $M_{Ed,ULS}/M_{Rd} = 54/63 = 0.86$

Unity check ultimate shear force (Appendix 22): $V_{Ed,ULS}/V_{Rd} = 41/892 = 0.05$

9 Longitudinal direction

In this chapter the loads, which occur during launch and service life, are investigated to determine the amount of prestressing that is required and the tendon arrangement. It also contains an optimization study of the steel nose.

9.1 General properties

Total length of the approach bridge: $l_{tot} = 550\ m$.

Number of spans: $n = 10$.

Intermediate span length: $l_{mid} = 57.9\ m$.

End span length: $l_{end} = 43.4\ m$.

Segment length: $l_s = 29.0\ m$.

Box girder depth: $h = 3.2\ m$.

Box girder width: $l_b = 15.5\ m$.

Slenderness: $l/h\ = 18$.

Box girder cross-section: A_c

Box girder moment of inertia: I_c

Distance neutral axis to top fiber: z_{top}

Distance neutral axis to bottom fiber: z_{bot}

Box girder moment of resistance top part: W_{top}

Box girder moment of resistance bottom part: W_{bot}

9.2 Extreme bending moments at support and span during launch

9.2.1 Self-weight

The bending moments due to the self-weight of the box girder and the steel nose, are equal to:

$$M_{Gk,SW,SUP} = -\frac{1}{12}\gamma A_c l_{span}^2$$

$$M_{Gk,SW,SPAN} = +\frac{1}{24}\gamma A_c l_{span}^2$$

$$M_{Gk,SW,CANT} = -\frac{1}{2}\gamma A_c \left(l_{span} - l_{nose}\right)^2 + M_{nose} + V_{nose} l$$

9.2.2 ULS design

Design value of the bending moment according to NEN-EN 1990: equations 6.10a & 6.10b:

$$M_{Ed,ULS} = \gamma_G M_{Gk} = 1.2 M_{Gk,SW}$$

9.2.3 SLS design

Design value of the bending moment according to NEN-EN 1990: equation 6.15b:

$$M_{Ed,SLS} = M_{Gk,SW}$$

9.3 Central prestressing

The amount of central prestressing that is required follows from the following requirement:

The maximum bending moment in the launch phase cannot exceed the maximum bending moment in the use phase in serviceability limit state.

The maximum concrete tensile stress in serviceability limit state at the support:

$$\sigma_{c,sup} = \frac{M_{Ed,SLS,sup}}{W_{top}}$$

The number of required prestressing tendons n follows from:

$$n = \frac{A_c \sigma_c}{A_{strand} n_{strand} \sigma_{p\infty}}$$

The prestressing tendons should be arranged over the top and bottom section of the box girder in such a way, that the resulting prestressing force will be introduced at the box girder's neutral axis:

$$n_0 \cdot e_0 = n_b \cdot e_b$$

with n_0, n_b the number of tendons above and beneath the neutral axis and e_0, e_b their eccentricities.

The maximum eccentricity of the upper tendons is given by:

$$e_0 = z_0 - d_3 - \frac{1}{2}\emptyset_{anchor}$$

The eccentricity of the lower tendons will become:

$$e_b = \frac{n_0}{n_b} e_0$$

9.3.1 The initial prestressing force

The value of the initial prestressing force P_{m0} immediately after tensioning and anchoring is obtained by subtracting the immediate losses $\Delta P_i(x)$ from the force at tensioning P_{max} and should not exceed the following value:

$$P_{m0} = A_p \sigma_{pm0}$$

with $\sigma_{pm0} = \min\left(0.75 f_{pk}, 0.85 f_{p0,1k}\right) = \min(0.75 \cdot 1860, 0.85 \cdot 1674) = 1395\ N/mm^2$

9.3.2 The working prestressing force

The working prestressing force is equal to:

$$P_{m\infty} = P_{m0} - \Delta P_{c+s+r}$$

with ΔP_{c+s+r}: the losses due to time-dependent behavior.

9.3.3 Shrinkage

UHPFRC shrinkage is mainly autogenous. When it has been heat treated, UHPFRC has no further shrinkage (Association Francaise de Génie Civil, 2013). Therefore, time-dependent losses due to concrete shrinkage will be neglected and will not be taken into account.

9.3.4 Creep

Heat treatment significantly reduces creep. The creep coefficient φ is 0.2 instead of 0.8 without heat treatment (Association Francaise de Génie Civil, 2013). For the calculation of the losses due to concrete creep, the concrete compressive stress in serviceability limit state must be used. As the centre of gravity of the tendons in the launch phase is alternating between the deck and the floor, the centre of gravity of the central prestressing may be chosen equal to the neutral axis of the box girder cross-section.

The concrete compressive stress at the neutral axis of the box girder cross-section:

$$\sigma_{cc} = -\frac{P_{m0}}{A_c}$$

The creep deformation of the concrete:

$$\varepsilon_{cc} = \varphi \frac{\sigma_{cc}}{E_c}$$

The loss in prestress due to creep:

$$\Delta\sigma_{pc} = E_p \varepsilon_{cc}$$

9.3.5 Relaxation

The relaxation of the prestressing steel can be determined with NEN-EN 1992-1-1 3.3.2. The prestressing steel is classified into relaxation class 2. The loss in prestress due to relaxation:

$$\Delta\sigma_{pr} = 0.66\rho_{1000}e^{9.1\mu}\left(\frac{t}{1000}\right)^{0.75(1-\mu)} \cdot 10^{-5} \cdot \sigma_{pm0}$$

with:

$\rho_{1000} = 2.5$: the value of relaxation loss at 1000 hours after tensioning and at a mean temperature of 20°C.

$$\mu = \frac{\sigma_{pm0}}{f_{pk}} = 0.75$$

t: the time after tensioning. When the launch phase is assumed to last half a year, $t = 4380$ hours.

9.3.6 The required amount of central prestressing

The required amount of central prestressing can be determined with the following procedure:

1. Determine the maximum bending moment in the use phase in SLS.
2. Assume a certain amount of prestressing steel and arrange them such that the resulting prestressing force will be introduced at the box girder's neutral axis.
3. Calculate the time-dependent losses.
4. Check if there will not occur any tensile stresses in the concrete with the equation below:

$$\sigma_{c,SLS} - \frac{A_p \sigma_{p\infty}}{A_c} \leq 0$$

9.3.7 The ultimate bending moment capacity

In the launch phase, the box girder and central prestressing should provide sufficient ultimate bending moment resistance. For this calculation the following simplifications are made:

1. A mean deck thickness d^* over the whole box girder.
2. Cross-sectional properties: A_c, z, I_c, W_c of the initial box girder are used.
3. The prestressing steel working at the compressed area of the cross-section will be neglected in force and moment equilibrium, i.e. at mid span the upper tendons are neglected and at the support the lower tendons are neglected.
4. The moment-strain diagram is valid for a simply supported prestressed box girder subjected to pure bending. The box girder is compressed at the top, while under tension at the bottom. The diagram will be used for the ultimate bending moment capacity at mid span. At the support, the top section is under tension, while the bottom section is compressed. Therefore in order to use the same diagram, the box girder needs to be reversed $\left(b_f = 0, b = b_{in} + 2b_w, t_d = t_f, t_f = d^*, z = z_b\right)$.

9.3.8 The maximum compressive stress

The compressive stress in the concrete should be limited to $0.6f_{ck}$ during construction, reduced to $0.55f_{ck}$ if the element is less than 3 days old (Association Francaise de Génie Civil, 2013). The maximum compressive stress will occur at the support when the box girder cantilever length reaches its maximum just before the steel nose reaches the next support.

9.4 Nose optimization

The steel nose will be fabricated from an IPE-profile. The profile must be diagonally cut to form two tapered steel profiles. The height of the profile should be: $h = l/10$ with $l = 2l_{nose}$. The weight of the steel nose will cause a shear force V_{nose} and a bending moment M_{nose} at the end of the cantilever part.

$$V_{nose} = \gamma A l_{nose}$$

$$M_{nose} = \gamma A l_{nose} \cdot \frac{1}{2} l_{nose}$$

$$\gamma = 78.5\ kN/m^3$$

$$A_{nose} = 2bt_f + (h - 2t_f)t_w$$

$$b = \frac{2}{5}h, t_f = h/25\ \&\ t_w = h/50$$

9.4.1 Central prestressing and nose length

In this paragraph the maximum box girder cantilever length will be studied for different levels of central prestressing and nose lengths.

$$\boldsymbol{l_{nose} = 0\ m}$$

Table 9.1 shows the maximum box girder cantilever length l_{cant} that can be reached for different levels of central prestressing P without the use of a steel nose. M is the maximum cantilever moment.

P (N/mm^2)	M (Nmm)	lcant (mm)	ltot (mm)
0	0	0	0
5	4,38E+10	22418	22418
10,17	8,90E+10	31967	31967
15	1,31E+11	38829	38829
20	1,75E+11	44836	44836

Table 9.1: maximum cantilever length without a steel nose

The bending moment capacity for a certain level of central prestressing:

$$-P + \frac{M}{W_{top}} \leq 0 \rightarrow M = PW_{top}$$

Without a steel nose l_{cant} becomes:

$$M = \frac{1}{2} q l_{cant}^2 + V_{nose} l_{cant} + M_{nose} \rightarrow M = \frac{1}{2} q l_{cant}^2 \rightarrow l_{cant} = \sqrt{\frac{2M}{q}}$$

When a steel nose will be used, the following quadratic equation must be solved for l_{cant}:

$$M = \frac{1}{2} q l_{cant}^2 + V_{nose} l_{cant} + M_{nose} \rightarrow \frac{1}{2} q l_{cant}^2 + V_{nose} l_{cant} + M_{nose} - M = 0$$

$\boldsymbol{l_{nose} = 10\ m}$

Table 9.2 shows the maximum box girder cantilever length l_{cant} that can be reached for different levels of central prestressing P and a 10 meters long steel nose.

P (N/mm^2)	M (Nmm)	lcant (mm)	ltot (mm)
0	0	0	0
5	4,38E+10	21325	31325
10,17	8,90E+10	30929	40929
15	1,31E+11	37815	47815
20	1,75E+11	43836	53836

Table 9.2: maximum cantilever length with a 10 m long nose

$\boldsymbol{l_{nose} = 15\ m}$

Table 9.3 shows the maximum box girder cantilever length l_{cant} that can be reached for different levels of central prestressing P and a 15 meters long steel nose.

P (N/mm^2)	M (Nmm)	lcant (mm)	ltot (mm)
0	0	0	0
5	4,38E+10	18521	33521
10,17	8,90E+10	28324	43324
15	1,31E+11	35290	50290
20	1,75E+11	41361	56361

Table 9.3: maximum cantilever length with a 15 m long nose

$\boldsymbol{l_{nose} = 20\ m}$

Table 9.4 shows the maximum box girder cantilever length l_{cant} that can be reached for different levels of central prestressing P and a 20 meters long steel nose.

P (N/mm^2)	M (Nmm)	lcant (mm)	ltot (mm)
0	0	0	0
5	4,38E+10	12983	32983
10,17	8,90E+10	23218	43218
15	1,31E+11	30353	50353
20	1,75E+11	36526	56526

Table 9.4: maximum cantilever length with a 20 m long nose

Table 9.1 - Table 9.4 show that, when the maximum cantilever bending moment in the launch phase and the serviceability limit state bending moment in the use phase ($8.90 \cdot 10^{10}\ Nmm$) are equal, the maximum cantilever length, including l_{nose}, will never reach l_{span}. This means, that more central prestressing is required to be able to launch the box girder to the next support. The cost for fabrication of the steel nose and the application of central prestressing will decide whether one should use higher levels of central prestressing or a longer steel nose.

Figure 9.1 shows that a steel nose of 15 and 20 meters nearly give the same reach. This means that for lengths over 15 meters, the steel nose becomes too heavy and loses its purpose.

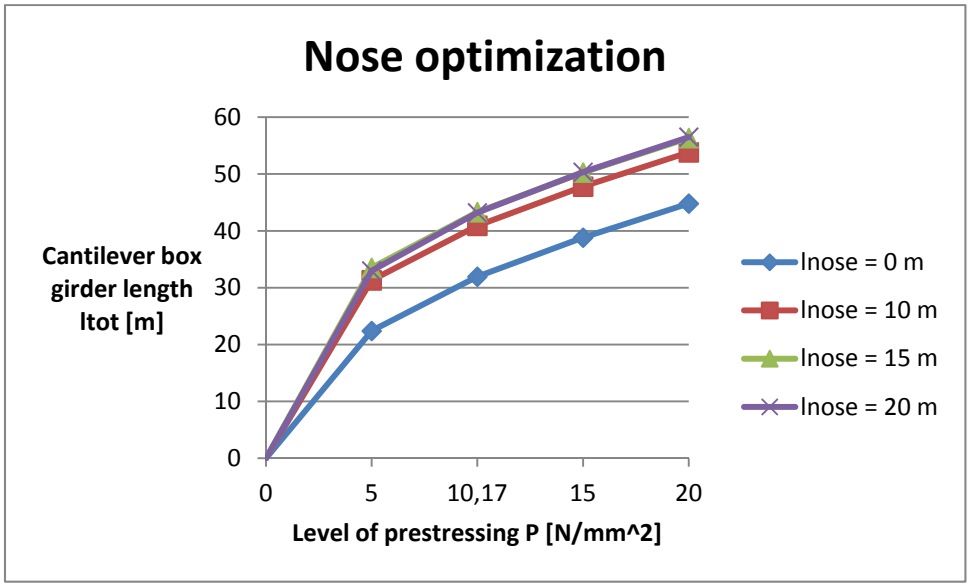

Figure 9.1: maximum cantilever box girder length for different levels of prestressing and nose lengths

The cost for fabrication of the steel nose are €3/kg. The cost for central prestressing, including the anchors are €2.5/kg.

The cross-sectional area of the steel nose can be expressed in l through the following equation:

$$A_{nose} = 2bt_f + \left(h - 2t_f\right)t_w = \frac{63}{31250}l^2$$

Figure 9.2 illustrates the price for fabrication of the steel nose for different nose lengths.

For a certain nose length the cantilever bending moment will become:

$$M = \frac{1}{2}q(l - l_{nose})^2 + V_{nose}(l - l_{nose}) + M_{nose}$$

With the cantilever bending moment known, the required amount of central prestressing can be determined:

$$-\frac{A_p\sigma_{pm\infty}}{A_c} + \frac{M}{W_{top}} \leq 0 \rightarrow A_{p,req} = \frac{A_c\frac{M}{W_{top}}}{\sigma_{pm\infty}}$$

For a certain nose length the required amount of central prestressing will be the lowest. By choosing another nose length an additional amount of central prestressing will be required: ΔA_p. Since (Iversen, et al., 1993) showed that peak moments developed during launch over approximately the first two spans, the total quantity of extra prestressing ΔQ_p will only be required for the first two spans. Figure 9.2 illustrates the cost for this additional central prestressing. The green line represents the total cost, that is the cost for the steel nose and the additional central prestressing.

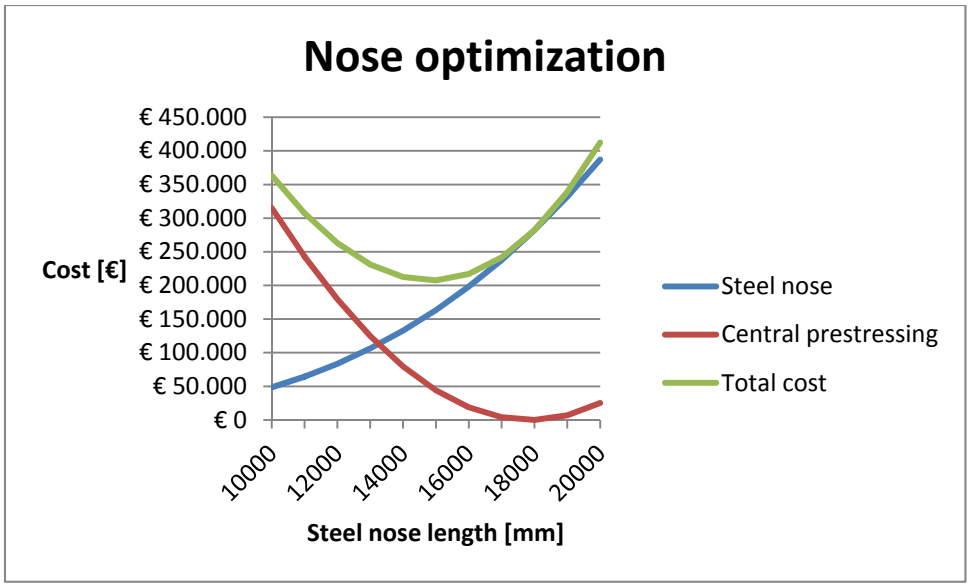

Figure 9.2: cost vs. steel nose length

9.4.2 The required amount of central prestressing for the cantilever bending moment

Figure 9.2 shows that a steel nose length of 15 meters gives the lowest total cost. The required amount of central prestressing $A_{p,req}$ for the cantilever bending moment can be determined with the formula from paragraph 9.4.1. This amount of prestressing steel is not required for the entire box girder. The rear deck sections require less prestressing (Table 9.5).

9.4.3 The ultimate bending moment capacity

During launch, the box girder and central prestressing should provide sufficient ultimate bending moment resistance. Table 9.5 shows the required amount of central prestressing for the ultimate limit state.

	M (Nmm)	tendons	Ap (mm^2)
cantilever bending moment SLS	-1,87E+11	16 49/16 mm	117600
bending moments rear deck sections SLS	-4,87E+10	4 49/16 mm	29400
cantilever bending moment ULS	-2,25E+11	2 x 6 49/16 mm	88200
bending moment rear deck sections ULS	-5,84E+10	2 x 2 49/16 mm	29400

Table 9.5: central prestressing to withstand the bending moments during launch

9.5 Extreme shear forces at the support during launch

9.5.1 Self-weight

The shear forces at the supports, due to the self-weight of the box girder and the steel nose, are equal to:

$$V_{Gk,SW,SUP} = \frac{1}{2}\gamma A_c l_{span}$$

$$V_{Gk,SW,CANT} = \gamma A_c\left(l_{span} - l_{nose}\right) + V_{nose}$$

9.5.2 ULS design

Design value of the shear force according to NEN-EN 1990: equations 6.10a & 6.10b:

$$V_{Ed,ULS} = \gamma_G V_{Gk} = 1.2V_{Gk}$$

9.5.3 Ultimate shear capacity

The ultimate shear capacity is given by (Association Francaise de Génie Civil, 2013):

$$V_u = V_{Rb} + V_f + V_s$$

When $V_{Ed} > V_{Rb} \rightarrow V_u = V_f + V_s$.

In case of prestressed concrete, the participation of the concrete will be:

$$V_{Rb} = \frac{1}{\gamma_E}\frac{0.24}{\gamma_b}\sqrt{f_c'}bz$$

with:

$\gamma_E\gamma_b$: a safety coefficient.
$b = 2d_4$: the total web thickness.
$z = d_p - \frac{1}{3}d_n$: the internal lever arm.

The contribution of the fibers can be expressed by:

$$V_f = \frac{S_{eff}\sigma(w0{,}3)_k}{\gamma_{bf}\tan\beta_u}$$

with:

$S_{eff} = bz$: the area of fiber effect.
$\sigma(w0{,}3)_k$: the characteristic post cracking stress for a crack width of 0.3 mm.
γ_{bf}: a material factor.
β_u: the angle of the compression struts.

The shear reinforcement:

$$V_s = \frac{A_{sw}}{s} z f_{ywd}\, cot\, \beta_u$$

with:

A_{sw}: the area of shear reinforcement.
s: the spacing.

The angle of the compression struts β_u should be limited to 30° as opposed to 21,8°, which NEN-EN 1992-1-1 prescribes.

Table 9.6 shows the maximum shear force during launch and the ultimate shear capacity.

VEd	9,61E+06	N
VRb	3,65E+06	N
Vf	1,14E+07	N
Vs	0	N
Vu	1,14E+07	N

Table 9.6: shear force and capacity in the launch phase

Unity check ultimate shear capacity: $V_{Ed} < V_u = 9.61/11.4 = 0.84 \rightarrow$ no shear reinforcement required.

9.6 The Use Phase

9.6.1 Self-weight

The self-weight causes a uniformly distributed load equal to:

$$q_{G,SW} = \gamma A_c = 26 \cdot A_c = 26 \cdot 6.70 \cdot 10^6 = 174\ kN/m$$

9.6.2 Super imposed dead load

The super imposed dead load combines the loads caused by the asphalt layer, the footpath and edge element, the parapet and the safety barrier. The asphalt layer causes a uniformly distributed load $q_{G,A} = 3.5\ kN/m^2$ up to 1.41 m from the cantilever's edge, the footpath and edge element cause line loads $p_F = 3.9\ kN/m$ and $p_E = 3.1\ kN/m$ at 0.8 m and 0.15 m from the cantilever's edge, the parapet causes a line load $p_P = 0.75\ kN/m$ at 0.15 m from the cantilever's edge and the safety barrier causes a line load $p_{SB} = 1\ kN/m$ at 1.41 m from the cantilever's edge.

$$q_{G,SIDL} = q_{G,A} + p_F + p_E + p_P + p_{SB} = 3.5(l_b - 2 \cdot 1.41) + 2(3.9 + 3.1 + 0.75 + 1)$$
$$= 3.5(15.5 - 2 \cdot 1.41) + 2(3.9 + 3.1 + 0.75 + 1) = 62\ kN/m$$

9.6.3 Traffic loading

The traffic loading consists of a uniformly distributed load (UDL) and a tandem system (TS), that need to be applied at the most unfavorable locations.

The uniformly distributed load works up to 1.41 m from the cantilever's edge:

$$q_{Q,UDL} = \alpha_{q1} q_{1k} \cdot 3 + \alpha_{qo} q_{ok}(l_b - 3 - 2 \cdot 1.41) = 10.35 \cdot 3 + 3.5(15.5 - 3 - 2 \cdot 1.41)$$
$$= 65\ kN/m$$

In order to determine the longitudinal bending moment due to the tandem system, the double axle loads should be split up into a symmetrical and asymmetrical part. The symmetrical part affects the bending moment, while the asymmetrical part has an impact on the torsional moment. The result for the symmetrical part will become:

$$\frac{Q_{1k} + Q_{2k} + Q_{3k}}{6} = \frac{300 + 200 + 100}{6} = 100\ kN$$

per axle.

9.7 Extreme bending moments for a bridge with multiple spans

The governing bending moments for a bridge with multiple spans can be determined with the force method for analysis of indeterminate structures. For a governing span, adjacent spans will be modeled as a rotational spring with a certain stiffness, to be able to calculate the bending moments at the supports and in the span.

9.7.1 Calculation of the extreme bending moments at the supports

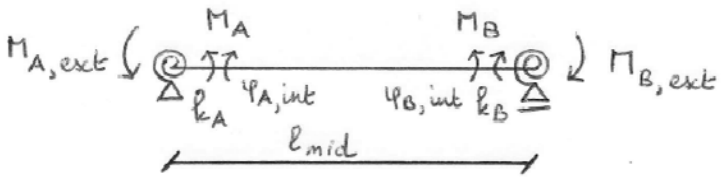

Figure 9.3: forces acting on governing span (van der Meulen, 1992)

Figure 9.3 illustrates the forces that act on the governing span, with:

M_A, M_B: bending moments at support A and B.

k_A, k_B: rotational spring stiffnesses.

$M_{A,ext}, M_{B,ext}$: external bending moments caused by adjacent spans.

$\varphi_{A,int}, \varphi_{B,int}$: rotation caused by loads on span.

The bending moments at the supports M_A and M_B can be calculated using forget-me-nots:

$$\varphi_{A,L} = \frac{M_A}{k_A} + \frac{M_{A,ext}}{k_A}$$

$$\varphi_{A,R} = -\frac{M_A l}{3EI} - \frac{M_B l}{6EI} - \varphi_{A,int}$$

$$\varphi_{B,L} = \frac{M_A l}{6EI} + \frac{M_B l}{3EI} + \varphi_{B,int}$$

$$\varphi_{B,R} = -\frac{M_B}{k_B} - \frac{M_{B,ext}}{k_B}$$

By equalizing $\varphi_{A,L} = \varphi_{A,R}$ and $\varphi_{B,L} = \varphi_{B,R}$ the following equations arise:

$$\frac{M_A}{k_A} + \frac{M_{A,ext}}{k_A} = -\frac{M_A l}{3EI} - \frac{M_B l}{6EI} - \varphi_{A,int} \rightarrow \left(2 + \frac{k_0}{k_A}\right) M_A + M_B = -k_0 \varphi_{A,int} - \frac{k_0}{k_A} M_{A,ext}$$

$$\frac{M_A l}{6EI} + \frac{M_B l}{3EI} + \varphi_{B,int} = -\frac{M_B}{k_B} - \frac{M_{B,ext}}{k_B} \rightarrow M_A + \left(2 + \frac{k_0}{k_B}\right) M_B = -k_0 \varphi_{B,int} - \frac{k_0}{k_B} M_{B,ext}$$

with:

$$k_0 = \frac{6EI}{l}$$

These equations can be solved for M_A and M_B:

$$M_A = \frac{k_0 \varphi_{B,int} + \frac{k_0}{k_B} M_{B,ext} - \left(2 + \frac{k_0}{k_B}\right)\left(k_0 \varphi_{A,int} + \frac{k_0}{k_A} M_{A,ext}\right)}{\left(2 + \frac{k_0}{k_A}\right)\left(2 + \frac{k_0}{k_B}\right) - 1}$$

$$M_B = \frac{k_0 \varphi_{A,int} + \frac{k_0}{k_A} M_{A,ext} - \left(2 + \frac{k_0}{k_A}\right)\left(k_0 \varphi_{B,int} + \frac{k_0}{k_B} M_{B,ext}\right)}{\left(2 + \frac{k_0}{k_A}\right)\left(2 + \frac{k_0}{k_B}\right) - 1}$$

In order to be able to calculate the bending moments at the supports M_A and M_B, the rotations $\varphi_{A,int}$ and $\varphi_{B,int}$, due to the load on the span that is concerned, are required.

For rotation φ_{int} the following equation applies:

$$\varphi_{int} = \varphi_{SW} + \varphi_{SIDL} + \varphi_{UDL} + \varphi_{TS}$$

For a point load F on a distance a from support A, the rotation becomes:

$$\varphi_{A,F} = \frac{Fa(a^2 - 3al + 2l^2)}{6EIl}$$

$$\varphi_{B,F} = \frac{Fal}{2EI} - \frac{Fa(a^2 + 2l^2)}{6EIl} = \frac{Fa}{6EI}\left(3l - \frac{(a^2 + 2l^2)}{l}\right)$$

For the tandem system with the first double axle F on a distance a from support A, the rotation becomes:

$$\varphi_{A,TS} = \frac{Fa(a^2 - 3al + 2l^2) + F(a + 1.2)((a + 1.2)^2 - 3(a + 1.2)l + 2l^2)}{6EIl}$$

$$\varphi_{B,TS} = \frac{Fa}{6EI}\left(3l - \frac{(a^2 + 2l^2)}{l}\right) + \frac{F(a + 1.2)}{6EI}\left(3l - \frac{((a + 1.2)^2 + 2l^2)}{l}\right)$$

For an uniformly distributed load q over the whole beam length, the rotation becomes:

$$\varphi_{A,q} = \varphi_{B,q} = \frac{ql^3}{24EI}$$

The rotations $\varphi_{A,int}$ and $\varphi_{B,int}$ need to be inserted in the formula for M_A to find distance a, which corresponds with the maximum value for M_A. For this purpose, the following condition should be met:

$$\frac{dM_A}{da} = 0$$

This gives the following quadratic equation that needs to be solved for a (Appendix 24.4):

$$6\left(3 + \frac{k_0}{k_B}\right)a^2 + 6\left((1.2)\left(3 + \frac{k_0}{k_B}\right) - \left(2 + \frac{k_0}{k_B}\right)2l\right)a + 2\left(3 + 2\frac{k_0}{k_B}\right)l^2 - 6(1.2)\left(2 + \frac{k_0}{k_B}\right)l$$
$$+3(1.2)^2\left(3 + \frac{k_0}{k_B}\right) = 0$$

9.7.2 Extreme bending moment for an intermediate beam in the span

The extreme bending moment for an intermediate beam is located at mid span and can be expressed by:

$$M_{span} = \frac{|M_A + M_B|}{2} - M_{int}$$

$$M_{int} = M_{TS} + M_q$$

For a point load F on a distance a from support A, the bending moment at mid span becomes:

$$a \leq \frac{1}{2}l \rightarrow M = \frac{1}{2}Fa$$

$$a > \frac{1}{2}l \rightarrow M = \frac{1}{2}F(l-a)$$

The extreme bending moment at mid span due to the tandem system can be found when the first axle is located at mid span:

$$M_{TS} = \frac{1}{2}F \cdot \frac{1}{2}l + \frac{1}{2}F\left(l - \left(\frac{1}{2}l + 1.2\right)\right) = \frac{1}{2}F(l-1.2)$$

For an uniformly distributed load q over the whole beam length, the bending moment at mid span becomes:

$$M_q = \frac{1}{8}ql^2$$

The internal bending moment:

$$M_{int} = \frac{1}{2}F(l-1.2) + \frac{1}{8}ql^2$$

In order to determine bending moments M_A and M_B, the rotations $\varphi_{A,int}$ and $\varphi_{B,int}$, which correspond with the position of the tandem system that was mentioned before, are required.

By substituting $a = \frac{1}{2}l$ in the formulas for $\varphi_{A,TS}$ and $\varphi_{B,TS}$, the rotations at support A and B can be obtained:

$$\varphi_{A,TS} = \frac{F \cdot \frac{1}{2}l \cdot \left(\left(\frac{1}{2}l\right)^2 + 3 \cdot \frac{1}{2}l \cdot l + 2l^2\right) + F\left(\frac{1}{2}l + 1.2\right)\left(\left(\frac{1}{2}l + 1.2\right)^2 + 3\left(\frac{1}{2}l + 1.2\right)l + 2l^2\right)}{6EIl}$$

$$\varphi_{B,TS} = \frac{F \cdot \frac{1}{2}l}{6EI}\left(3l - \frac{\left(\left(\frac{1}{2}l\right)^2 + 2l^2\right)}{l}\right) + \frac{F\left(\frac{1}{2}l + 1.2\right)}{6EI}\left(3l - \frac{\left(\left(\frac{1}{2}l + 1.2\right)^2 + 2l^2\right)}{l}\right)$$

9.7.3 Extreme bending moment for an end beam in the span

The extreme bending moment for an end beam is located at a distance 0.4l from the end support and can be expressed by:

$$M_{span} = 0.4|M_B| - M_{int}$$

$$M_{int} = M_{TS} + M_q$$

For a point load F on a distance a from support A, the bending moment at a distance 0.4l from the end support becomes:

$$a \leq \frac{2}{5}l \rightarrow M = \frac{3}{5}Fa$$

$$a > \frac{2}{5}l \rightarrow M = \frac{2}{5}F(l-a)$$

The extreme bending moment in the span due to the tandem system can be found when the second axle is located at $a = 0.4l$:

$$M_{TS} = \frac{3}{5}F\left(\frac{2}{5}l - 1.2\right) + \frac{3}{5}F \cdot \frac{2}{5}l = \frac{3}{5}F\left(\frac{4}{5}l - \frac{6}{5}\right) = \frac{1}{25}F(12l - 18)$$

For an uniformly distributed load q over the whole beam length, the bending moment at $a = 0.4l$ becomes:

$$M_q = \frac{3}{25}ql^2$$

The internal bending moment:

$$M_{int} = \frac{1}{25}F(12l - 18) + \frac{3}{25}ql^2$$

In order to determine bending moment M_B, the rotation $\varphi_{B,int}$, which corresponds with the position of the tandem system that was mentioned before, is required:

By substituting $a = 0.4l - 1.2$ in the formula for $\varphi_{B,TS}$, the rotation at support B can be obtained:

$$\varphi_{B,TS} = \frac{F(0.4l - 1.2)}{6EI}\left(3l - \frac{((0.4l - 1.2)^2 + 2l^2)}{l}\right) + \frac{F \cdot 0.4l}{6EI}\left(3l - \frac{((0.4l)^2 + 2l^2)}{l}\right)$$

The bending moment M_B can be determined with the following equation:

$$M_A + \left(2 + \frac{k_0}{k_B}\right) M_B = -k_0 \varphi_{B,int} - \frac{k_0}{k_B} M_{B,ext} \rightarrow M_B = -\frac{k_0 \varphi_{B,int} + \frac{k_0}{k_B} M_{B,ext}}{2 + \frac{k_0}{k_B}}$$

9.7.4 Calculation of the external bending moments for a bridge with multiple spans

The maximum bending moments at the support and in the span for a continuous beam due to live loading can be determined with influence lines. The maximum support moment is found when two adjacent spans are fully loaded and the remaining spans are not. The maximum bending moment in the span is found when a single span is loaded and the other spans are not.

The calculation of the external bending moments $M_{A,ext}$ and $M_{B,ext}$ requires the contribution of every other loaded span to these moments. For the maximum bending moment in the span, all adjacent spans are subject to dead loading. For the maximum support moment, the directly adjacent span is subject to live loading as well. Table 9.7 reviews the contribution of a number of adjacent spans to the external bending moment, by assuming the left support to be fixed and $l_{end} = 0.75 l_{mid}$. For the complete calculation, see Appendix 24.5 & 24.6.

number of adjacent spans n	contribution n spans to M_{ext} (ql^2)	contribution adjacent span to M_{ext} (ql^2)
1	9/128	9/128
2	133/1536	5/48
3	95/1152	19/180
4	599/7168	71/672
5	6683/80256	265/2508
6	4993/59904	989/9360

Table 9.7: contribution of adjacent spans to the external bending moment

9.7.5 Rotational spring stiffness for a beam with multiple spans

The resistance of the adjacent spans can be modeled as a rotational spring with stiffness k_r. The stiffness can be calculated with forget-me-nots (Figure 9.4 & Appendix 24.7).

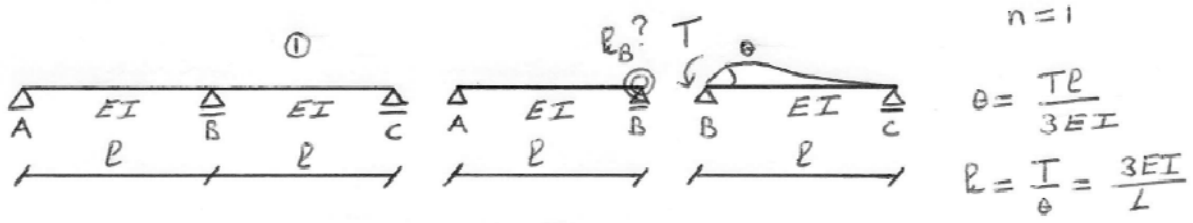

Figure 9.4: procedure of finding the rotational spring stiffnesses

Table 9.8 reviews the stiffness obtained for a number of spans and $l_{end} = 0.75 l_{mid}$.

number of adjacent spans n	rotational spring stiffness k_r $[EI/l]$
1	4
2	7/2
3	52/15
4	97/28
5	724/209
6	1351/390

Table 9.8: rotational spring stiffness for a number of spans

9.8 Calculation of the required amount of continuity prestressing

The amount of continuity prestressing that is required will be determined in serviceability limit state. In the use phase, the joints always need to be fully compressed.

The maximum concrete tensile stresses in serviceability limit state at the support and mid span:

$$\sigma_{c,sup} = \frac{M_{Ed,SLS,sup}}{W_{top}}$$

$$\sigma_{c,span} = \frac{M_{Ed,SLS,span}}{W_{bot}}$$

When the continuity tendons are two spans long and anchored at the zero bending moment points, i.e. at about one-fifth of the span length, one-and-a-half times the amount of prestressing steel in the span, will be present at the support.

The following requirements should be met:

$$-\frac{3}{2}\frac{P_{m\infty}}{A_c} + \sigma_{c,sup} - \frac{M_p}{W_{top}} \leq 0$$

$$-\frac{P_{m\infty}}{A_c} + \sigma_{c,span} - \frac{M_p}{W_{bot}} \leq 0$$

The maximum tendon eccentricities:

$$e_0 = z_0 - d_3 - \frac{1}{2}\emptyset_{anchor}$$

$$e_b = z_b - d_5 - \frac{1}{2}\emptyset_{anchor}$$

9.8.1 Tendon arrangement

The tendon lay-out and bending moment by prestressing (Figure 9.5):

$$\tan\theta = \frac{e_0 + e_b}{a} \rightarrow \theta = \tan^{-1}\left(\frac{e_0 + e_b}{a}\right)$$

$$F_v = P_{m\infty}\sin\theta$$

$$M_{p,sup} = \frac{F_v a(l-a)}{l}$$

$$M_{p,span} = \frac{F_v a^2}{l}$$

The distance a from the deviator to the support can be varied in order to obtain either a higher bending moment at the support or in the span. When $a = l/3$, the bending moment by prestressing at the support is twice the bending moment by prestressing in the span, which is beneficial for a continuous beam under a uniformly distributed load: $M_{sup} = \frac{1}{12}ql^2$ & $M_{span} = \frac{1}{24}ql^2$ (Appendix 24.8).

However, when the same tendon arrangement is used when the box girder is also subject to live loading (tandem system), the compressive stresses at mid span become almost tensile stresses and deviators at $a = l/2$ will form a better solution (Appendix 24.8). Finally, the best solution is given by the tendon arrangement, which is used for traditional incrementally launched bridges, where the tendons continue over the supports and are anchored at the zero bending moment points, resulting in an amount of prestressing at the support that is one-and-a-half times the amount of prestressing in the span (Appendix 24.8).

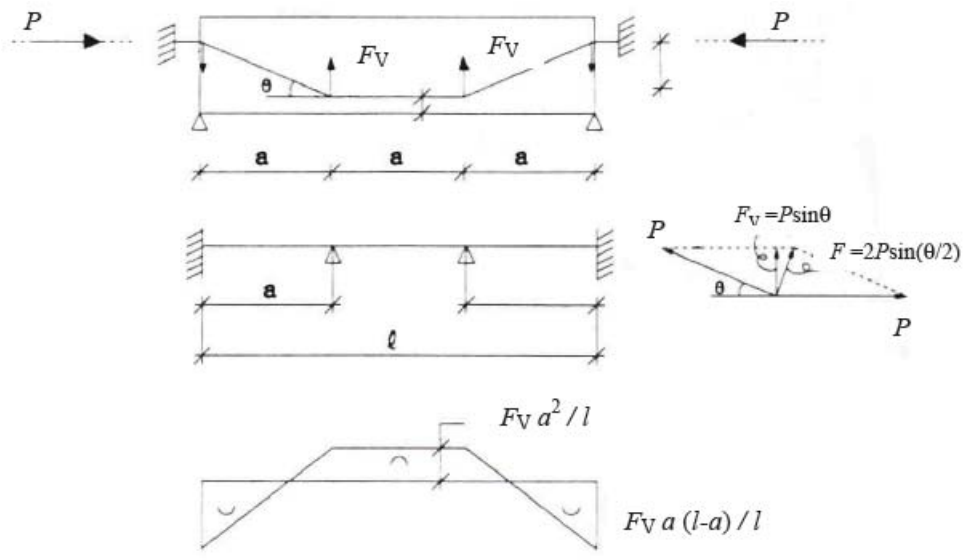

Figure 9.5: the prestressing load and bending moment (Walraven & Braam, 2011)

9.8.2 Creep

The concrete compressive stress at the support at the lowest level of the tendons:

$$\sigma_{cc} = -\frac{3}{2}\frac{P_{m0}}{A_c} - \frac{M_{sup}e_{bot}}{I_c}$$

The creep deformation of the concrete:

$$\varepsilon_{cc} = \varphi\frac{\sigma_{cc}}{E_c}$$

The loss in prestress due to creep:

$$\Delta\sigma_{pc} = E_p\varepsilon_{cc}$$

9.8.3 Relaxation

The loss in prestress due to relaxation:

$$\Delta\sigma_{pr} = 0.66\rho_{1000}e^{9.1\mu}\left(\frac{t}{1000}\right)^{0.75(1-\mu)} \cdot 10^{-5} \cdot \sigma_{pm0}$$

with: $t = 876000$ hours (100 years).

9.8.4 The required amount of continuity prestressing

The required amount of continuity prestressing can be determined with the following procedure:

1. Determine the maximum concrete tensile stress at support and mid span in SLS.
2. Determine the maximum tendon eccentricities, prestressing load and bending moment (Figure 9.5).
3. Assume a certain amount of prestressing steel and estimate the time-dependent losses.
4. Calculate the real time-dependent losses.
5. Check if there will not occur any tensile stresses in the concrete with the equations below:

$$-\frac{3}{2}\frac{P_{m\infty}}{A_c} + \sigma_{c,sup} - \frac{M_p}{W_{top}} \leq 0$$

$$-\frac{P_{m\infty}}{A_c} + \sigma_{c,span} - \frac{M_p}{W_{bot}} \leq 0$$

The requirements above result in four tendons with 49 strands per tendon $\left(A_p = 29400\ mm^2\right)$. For full calculations see Appendix 24.1.

9.8.5 The ultimate bending moment capacity

In the use phase, the box girder and continuity prestressing should provide sufficient ultimate bending moment resistance. For this calculation, the following simplifications are made:

1. A mean deck thickness d^* over the whole box girder.
2. Cross-sectional properties: A_c, z, I_c, W_c of the initial box girder are used.
3. The moment-strain diagram is valid for a simply supported prestressed box girder subjected to pure bending. The box girder is compressed at the top, while under tension at the bottom. The diagram will be used for the ultimate bending moment capacity at mid span. At the support, the top section is under tension, while the bottom section is compressed. Therefore in order to use the same diagram, the box girder needs to be reversed $\left(b_f = 0, b = b_{in} + 2b_w, t_d = t_f, t_f = d^*, z = z_b\right)$.

At mid span, six tendons with 49 strands per tendon $\left(A_p = 44100\ mm^2\right)$ are required to provide sufficient bending moment resistance (Appendix 24.2). That means, there will be nine tendons with 49 strands per tendon $\left(A_p = 66150\ mm^2\right)$ present at the supports that suffice as well (Appendix 24.3).

9.9 Extreme shear forces at the supports in the use phase

The maximum shear force in the use phase can be found when the first axle is located above the support:

$$V_A = \frac{|M_A - M_B|}{l} + \frac{1}{2}ql + F\left(1 + \frac{l - 1.2}{l}\right)$$

In order to determine bending moments M_A and M_B, the rotations $\varphi_{A,int}$ and $\varphi_{B,int}$, which correspond with this position of the tandem system, are required. The rotations can be determined with the formula's from paragraph 9.7.1 and $a = 0$. $|M_A - M_B|$ reaches its maximum when the directly adjacent span from support A is subject to both dead load and live load.

9.9.1 Ultimate shear capacity

The ultimate shear capacity is given by (Association Francaise de Génie Civil, 2013):

$$V_u = V_{Rb} + V_f + V_s$$

When $V_{Ed} > V_{Rb} \rightarrow V_u = V_f + V_s$.

Table 9.9 shows the maximum shear force in the use phase and the ultimate shear capacity.

VEd	1,36E+07	N
VRb	3,38E+06	N
Vf	1,84E+07	N
Vs	0	N
Vu	1,84E+07	N

Table 9.9: shear force and shear capacity in the use phase

Unity check ultimate shear capacity: $V_{Ed} < V_u = 1.36/1.84 = 0.74$.

There is no shear reinforcement required to withstand the shear forces in the use phase.

9.10 The length of a segment

The optimum length of the mould can be found when assembly cost and launching cost are at their minimum (van den Broek & van den Hoonaard, 1975).

$$K = B \times K_b + \frac{L}{B} \times K_v + C$$

B: length of the mould (m).
K_b: cost per meter of formwork.
L: total length of launching part (m).
K_v: cost per launching operation.
L/B: number of launching operations.
C: cost independent on B.

K is at its minimum when $dK/dB = 0$.

$$\frac{dK}{dB} = K_b - \frac{LK_v}{B^2} = 0 \rightarrow K_b = \frac{LK_v}{B^2} \rightarrow B^2 = \frac{LK_v}{K_b} \rightarrow B = \sqrt{\frac{LK_v}{K_b}}$$

For “the new bridge crossing the IJssel near Zutphen” the following cost applied:

Total cost for purchase and assemblage of the mould including foundation: $f\ 300.000,-$.

For a mould of 20 meters this will result in : $K_b = f\ 15.000,-$.

The launching cost per unit: $K_v = f\ 5.000,-$.

However, these cost will nowadays not apply anymore. Gerard Filé, cost engineer at Royal HaskoningDHV, and Jan Schenk, cost engineer at Van Hattum en Blankevoort, suggest that for a mould with dimensions similar to the mould of “the new bridge” (van den Broek & van den Hoonaard, 1975), the cost will be $€\ 300.000 - 350.000$ and the cost for the foundation will be $€\ 150.000 - 200.000$, resulting in total cost of about $€\ 500.000,-$. The cost per launching operation based on the production of a single unit per week and the presence of twelve workmen will be $€\ 20.000,-$. These twelve men lift and lower the formwork, assemble the prestressing and cast the concrete. They also carry out the launching itself. However, additional manpower is required to control the launch process and to insert the temporary sliding bearings.

For:

$K_v = €\ 20.000,-$

$K_b = €\ 25.000,-$

The optimum length of the mould becomes:

$$B = \sqrt{\frac{L \cdot 20000}{25000}} = 0.89\sqrt{L} = 0.89\sqrt{550} = 20.1\ m$$

Thus, the span will be ideally cast in three segments of 19.3 meters. Then the total cost will be equal to:

$$K = B \times K_b + \frac{L}{B} \times K_v + C = 20 \cdot 25000 + 27 \cdot 20000 + C = €\ 1.040.000 + C$$

However, three segments per span will jeopardize the structural safety of the bridge. Figure 9.6 illustrates the ideal tendon arrangement for the use phase. The anchor zones are located at one fifth of the span length. Deviators can be found above the supports and at mid span. As maximum bending moments occur at the supports we should avoid joints at these locations. Unfortunately, when a span is divided in three segments, moving the joints by one sixth of the span length means creating joint positions at mid span and near the anchorage zone. Positions where the fiber continuity is needed the most, since there is no continuous longitudinal reinforcement present in the box girder. For structural safety it is better to work with segments that have one fourth or half of the span length.

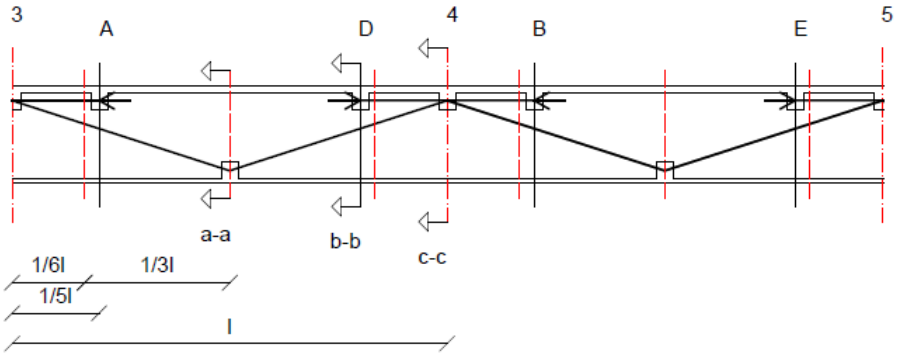

Figure 9.6: continuity tendon arrangement and joint positions for three segments per span

The total cost for two and four segments per span:

$$K = B \times K_b + \frac{L}{B} \times K_v + C = 30 \cdot 25000 + 19 \cdot 20000 + C = € 1.130.000 + C$$

$$K = B \times K_b + \frac{L}{B} \times K_v + C = 15 \cdot 25000 + 37 \cdot 20000 + C = € 1.115.000 + C$$

As shown in the calculation above, the total cost for two and four segments per span are nearly the same. In order to avoid as many weak points in the structure as possible, the bridge will be designed with two segments per span. Figure 9.7 illustrates the continuity tendon arrangement and joint positions when two segments are used per span.

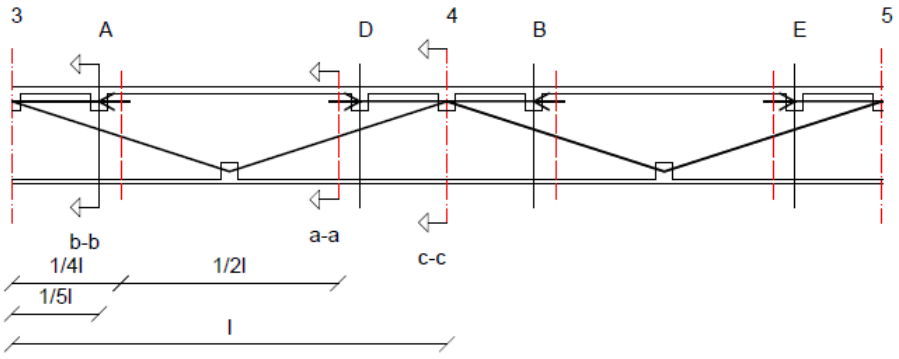

Figure 9.7: continuity tendon arrangement and joint positions for two segments per span

9.11 The final box girder design

Figure 9.8 shows the final box girder design and its dimensions and the transverse prestressing that will be applied internally in the deck and floor. Because of the presence of the fibers, conventional reinforcement and shear reinforcement will not be necessary. The absence of conventional reinforcement is not just positive. Since there is no continuous reinforcement in the joints, tensile stresses will force the joints to open. To prevent this, the cross-section must always remain compressed and the tensile capacity of the concrete cannot be used to generate savings in the amount of prestressing that is required.

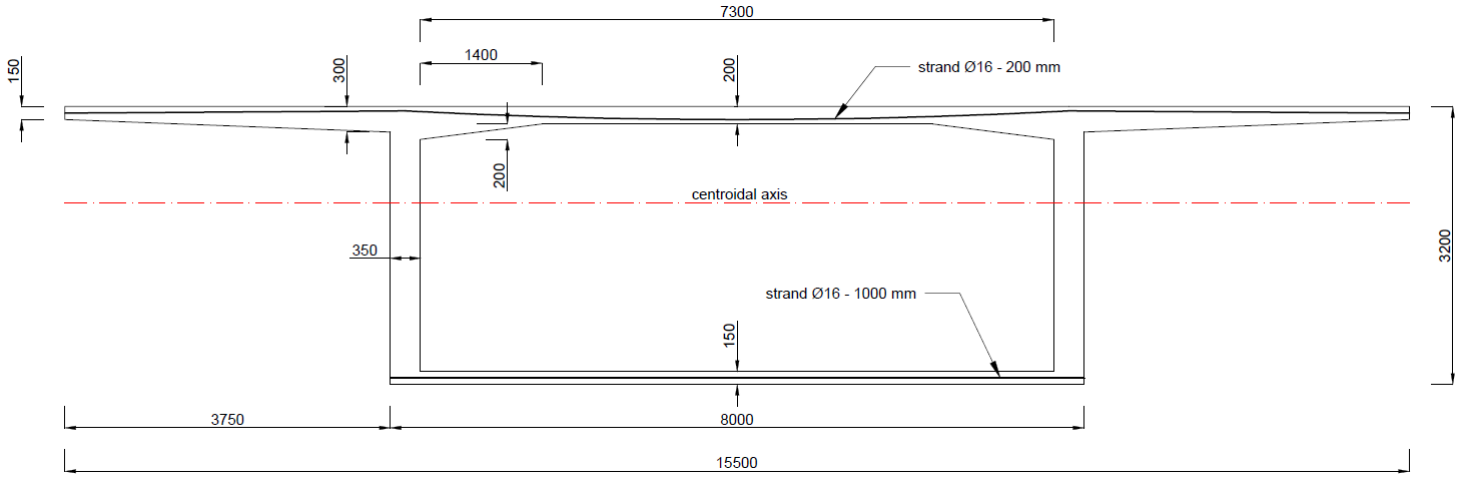

Figure 9.8: the final box girder design

9.11.1 Reduction of web thickness

The webs will be 350 mm thick. However, Appendix 25 shows that for a web thickness of 300 mm their capacity is still sufficient to carry the shear forces during launch and in the use phase. This reduction will change other box girder dimensions and thus will influence the force distribution in transverse direction. In order to check if the capacity in transverse direction is still sufficient, the procedure in Chapter 8 needs to be followed again.

9.11.2 Maximum span length

Increasing the span length by using one permanent bridge pier less, i.e. ten instead of eleven, and keeping all the box girder dimensions constant at the same time, appears to be possible (Appendix 26). However, in order to provide sufficient bending moment capacity, a lot of prestressing tendons would be required, which could give problems with force introduction and execution.

10 Execution

Now that we know the final box girder design the execution plan must be established. The construction of the incrementally launched bridge will be carried out in the following phases:

1. preparation of the construction site.
2. installation of the fabrication yard with a solid foundation.
3. construction of the substructure, i.e. permanent bridge piers and abutments.
4. assembling the nose and formwork system.
5. construction cycle of the deck segments.
6. installation of the continuity prestressing.

10.1 The construction site and fabrication yard

The box girder will be executed from the eastern, lower, abutment near Zevenaar. Launching from the lower abutment makes a braking system unnecessary. At first, the construction site should be prepared. The site infrastructure, accommodations and auxiliaries must be taken care of. The site infrastructure is important to transport materials to the construction site. The site infrastructure can be divided into an access road, roads at the site itself and the use of space.

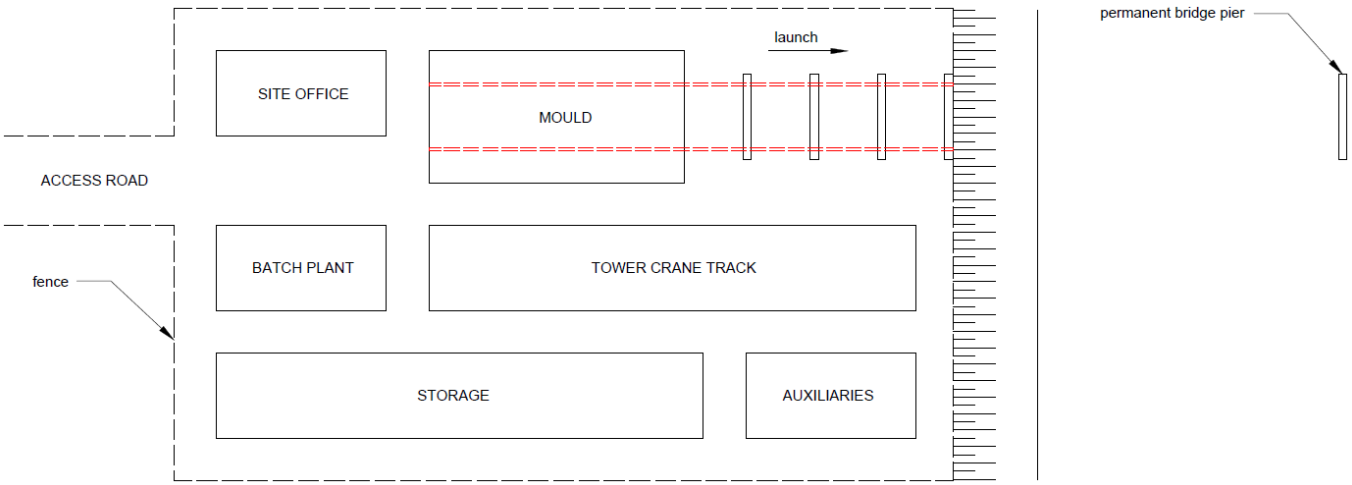

Figure 10.1: plan of the construction site

Traditionally, a temporary fabrication yard will be installed behind the abutment, arranged with separate areas to accommodate for the tower crane and concrete batch plant, to preassemble and store the reinforcement and prestressing, to cast the concrete and to launch the deck (Figure 10.1). As nearly all activities are concentrated here, transport distances are, therefore, very short.

However, at less than 5 km away, there is a big concrete plant facility owned by a company called “Cementbouw BV” (Figure 10.2). As shown in paragraph 10.4, the total volume of concrete per segment is only 194 m^3. It may, therefore, be cheaper to use the facilities of “Cementbouw BV”, instead of installing a temporary batch plant on site. Especially since the transport distance is very short. The concrete would then be batched in the central mix plant and brought to the construction site with truck mixers. It is very important, that the time between batching of the concrete and completion of placement is consistent and short, since hydration begins at the plant. Since the mixture contains fibers we would need permission to use one of the company’s batch plants; regular concrete does not use steel fibers and some fibers may remain and get stuck in the plant, which would then have to be removed. This option also has a big impact on the construction cycle of the deck segments. We need to make sure that the company can provide sufficient capacity at the scheduled days of placement.

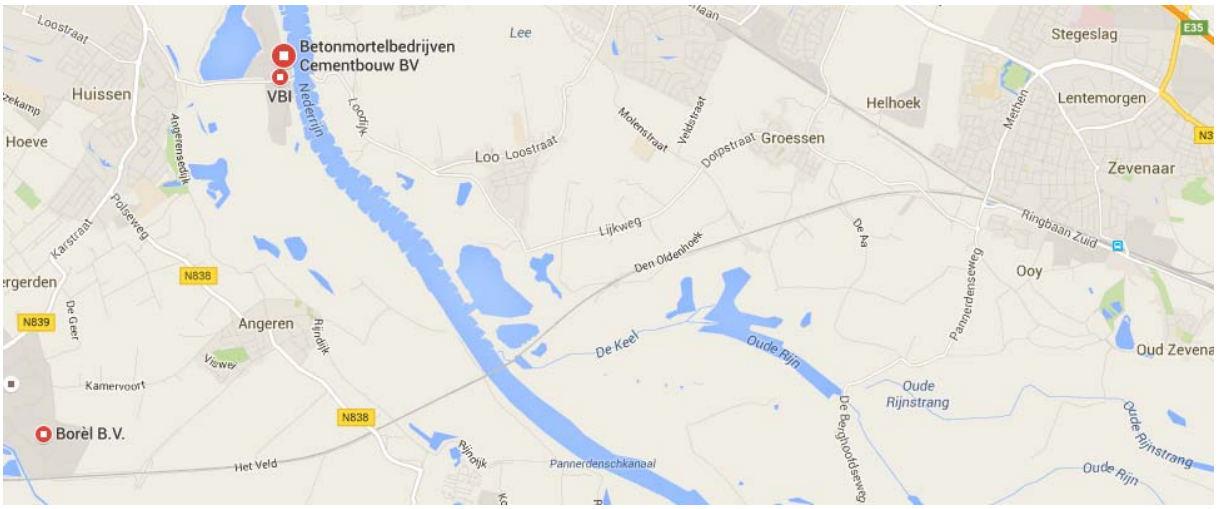

Figure 10.2: “Betonmortelbedrijf Cementbouw BV” close to the construction site

The fabrication yard requires a solid foundation to provide sufficient resistance against the very large horizontal forces during the launch operation. The whole area should be completely covered, so factory-like conditions independent of the weather are created and concrete can be produced of high quality. When the casting area has a length of 73.4 meters, that is the length of the first span plus the length of the nose, the weight of the cantilever will be secured in the initial stages of launch (Figure 10.3 second and third picture).

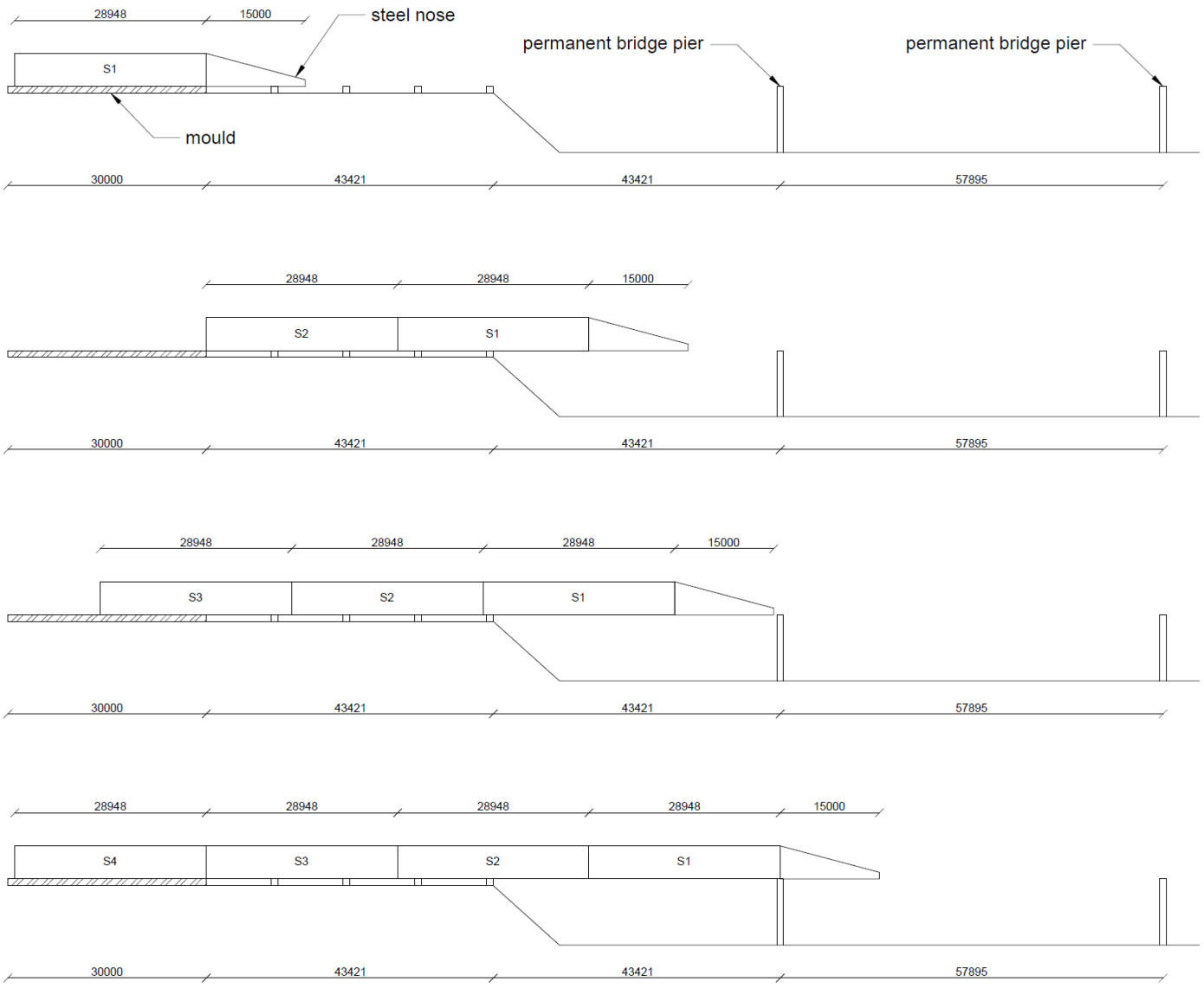

Figure 10.3: the launch process

10.2 The steel nose

After the construction site, the infrastructure, the equipment and accommodations are ready, the steel nose can be assembled in position at the front of the casting yard at the beginning of the construction of the bridge deck (Figure 10.3 top).

10.3 The formwork system

The next step is the fabrication of the mould. A hydraulic steel formwork system is supported by two skidding beams located directly under the webs. The bottom and outer side shutters can be stripped downwards and sideways, whereas the internal shutters can be lifted and collapsed (Figure 10.4).

This formwork system is based on the formwork system that was used in the execution of the Zeeburgerbrug (Lugthart, 1987). The big difference between both systems is a strip at the web-floor connection, of at least one meter width. This strip must prevent the fresh concrete in the floor from rising, because of the large pressure that is exerted by the weight of the concrete being poured in the web sections. The internal shutters rest on cones that are mounted on the floor shutters. At the top, the cones are provided with rollers in order to be able to move the internal shutters from the fabricated unit. The deck will be pushed from the rear by hydraulic jacks, which are clamped to the sides of the skidding beams.

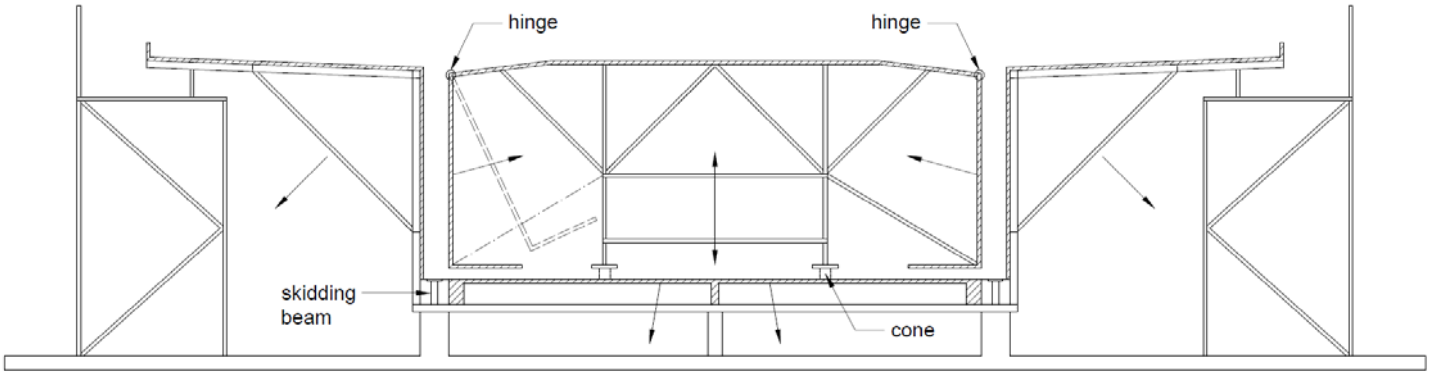

Figure 10.4: cross-section of the box girder formwork

10.4 Casting of concrete

At this moment, the actual construction cycle of a deck segment can begin. A complete section will be cast in a single pour to ensure fiber continuity by avoiding a cold joint in the box girder cross-section, and to take an activity away from the cycle to speed up production. The total volume of concrete per segment is equal to: $A_c \cdot l_s = 6.70 \cdot 28.9 = 194\ m^3$. When a complete segment should be cast in a single day, the concrete batch plant should be able to produce and the workmen should be able to pour 194 m^3 concrete per day.

As any flow tends to align fibers in the direction of flow, care should be taken during concrete pouring. In order to obtain the highest tensile and flexural properties, one should pour the concrete in layers (Figure 10.5). Such an optimum fiber orientation may probably be difficult to achieve as the presence of prestressing ducts and the complex shuttering for the box girder have an additional influence on the flow of the fiber concrete.

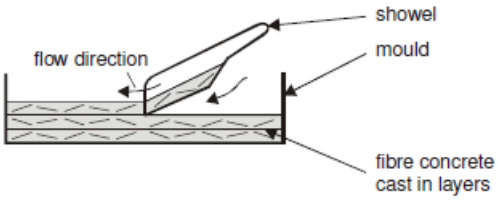

Figure 10.5: pouring process of fiber concrete (Markovic, 2006).

It is important to achieve a homogeneous fiber distribution in all parts of the box girder. Too large spaces without fibers, as well as fiber segregation should be avoided. The best possible solution is to use self-compacting concrete. This concrete flows under its own weight and fibers therefore may orient in appropriate directions during flowing in the formwork. As no additional compaction is required, fibers will remain in their original positions (Markovic, 2006).

10.5 Curing of concrete and heat treatment

Curing of concrete is essential for optimum hardening conditions. Optimum hardening will result in optimum strength development and durability. Normal curing at 20℃ produces $f_{ck} > 30\ MPa$ at 24 hours after initial set and $f_{ck} > 150\ MPa$ at 28 days. A thermal treatment of 90℃ at 90% relative humidity produces $f_{ck} > 180\ MPa$ at 48 hours after final set (Lafarge Ductal, 2009). An early strength development is vital in order to be able to begin with the launch operation quickly. In order to qualify the increase in strength of UHPFRC maturity monitoring can be envisaged.

The compressive stress in the concrete should be limited to $0.6f_{ck}$ during construction, reduced to $0.55f_{ck}$ if the element is less than 3 days old (Association Francaise de Génie Civil, 2013). The central prestressing consists of 16 tendons with 49/16 mm cables and will introduce a compressive stress in the concrete:

$$\sigma_c = -\frac{P_{m0}}{A_c} = -\frac{A_p \sigma_{pm0}}{A_c} = -\frac{117600 \cdot 1395}{6.70 \cdot 10^6} = -24\ N/mm^2$$

The central prestressing will be applied when the box girder is still supported by the skidding beams, so no external additional compressive stresses will be present in the concrete. Since normal curing at 20℃ already produces $f_{ck} > 30\ MPa$ at 24 hours after initial set, prestressing can start after the concrete has hardened for a full day.

When we assume a linear strength development, the concrete compressive strength $f_{ck} \approx 60\ MPa$ a week later. The maximum concrete compressive stress will occur at the support when the cantilever length reaches its maximum just before the steel nose reaches the next support and is equal to (Appendix 23.1):

$$\sigma_c = -\frac{P_{m\infty}}{A_c} + \frac{M_{cant}}{W_{top}} = -64\ N/mm^2$$

However, Figure 10.3 points out that it will take more than one week to reach the maximum cantilever length. This means, that normal curing provides an early strength development, which is sufficient to withstand the compressive forces during launch. Heat treatment is not required for strength development.

10.6 Anchors and deviators

The central and continuity tendons will be applied outside the concrete cross-section. They are typically two spans long. Anchors and deviators will be positioned outside the concrete cross-section as well. However, the inside of the box girder needs to remain uniform in order to be able to use the inner mould properly. Provisions for anchoring and deviating the tendons as shown in Figure 9.7 are not possible. Provisions for anchors and deviators can be applied outside the cross-section, but only after the complete segment is cast and the inner mould is moved to the next segment.

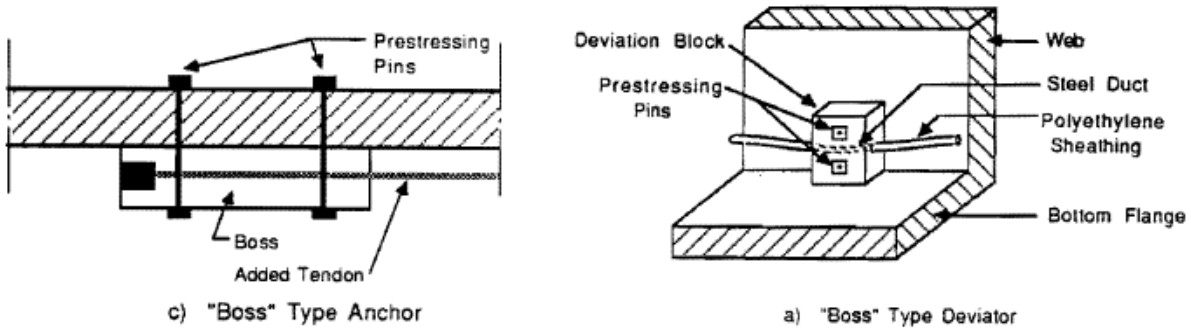

Figure 10.6: a boss type anchor and deviator (Powell, et al., 1988)

Figure 10.6 shows the principle of a boss type anchor. This solution is used for bridge strengthening and repair by adding external prestressing tendons to the existing bridge. Anchors and deviators are prestressed to the existing webs or flanges. This system is advantageous, since the additional prestress force can be distributed over a fairly long part of the structure. However, localized stresses will still arise, which are additive to the existing state of stress.

Experience has shown that the clamping force should be at least two times the prestressing force to create a good force transmission and bond between the boss and the structure (Powell, et al., 1988). Additionally, if necessary, the surface could be slightly roughened. The same system could be used for deviating devices (Figure 10.6 right).

Figure 10.7: ankerbus

Instead of drilling holes in the concrete cross-section and using prestressing pins for the connection, it might be better to make use of cast-in provisions in the concrete: so-called *ankerbussen* (Figure 10.7) and bolts. When the segment is finished and the concrete has set, a steel plate can be bolted to the box girder section to form a base for a steel construction that accommodates for the anchor or deviator (Figure 10.8). The steel construction must have sufficient strength to transfer the prestressing force to the concrete. The force will be transmitted by shear. The fiber concrete should be perfectly able to distribute the localized stresses that will occur during this force transmission, and no heavy ordinary reinforcement would be required. The bolts will be loaded in shear and must provide resistance against slip.

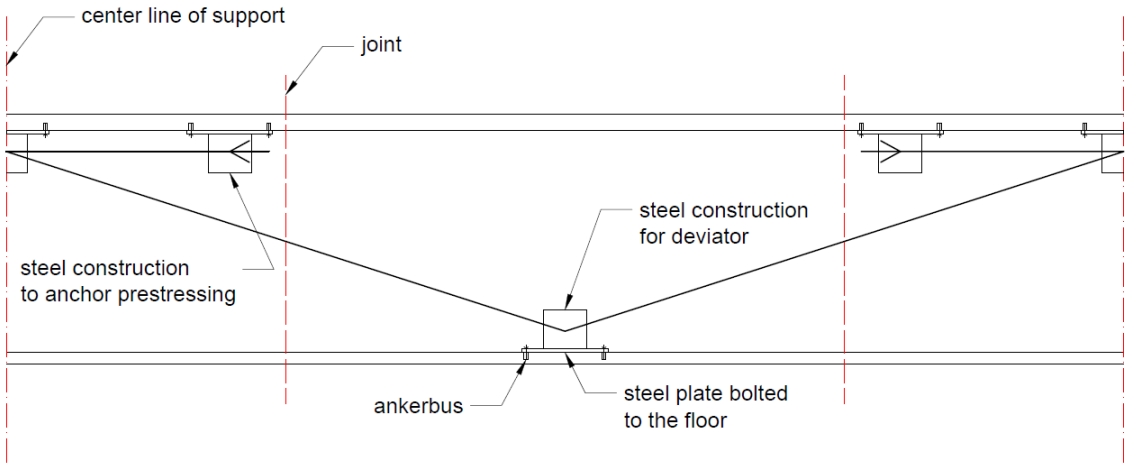

Figure 10.8: provisions to anchor and deviate the tendons

The complete central and continuity tendon arrangement is shown in detail in Appendix 27 and 28.

10.7 Temporary launch bearings and launch procedure

The box girder slides over the bridge piers on temporary launch bearings, made of a high strength concrete block covered with a stressed chrome-steel plate. On top of these elements, steel reinforced neoprene sliding plates, with a Teflon coating on one face, are inserted in a repeating cycle to reduce friction during launch.

Every bridge pier requires a platform, which provides the necessary access to insert the sliding plates and to position the jacks in order to remove the temporary bearings when the bridge is transferred onto the permanent bearings. It would be obvious to use the platform of the bridge pier formwork.

The platforms on the bridge piers that are located on solid ground can be accessed by temporary scaffolding. The access of the parts of the structure positioned above water depends on the chosen method of execution for the substructure, that is with a temporary gangway (Figure 10.9) or with floating equipment (Figure 10.10). During launch the launch operator is in contact with the personnel on every bridge pier. They all have a kill switch to stop the launch operation in case of emergencies.

10.8 Sequence of work

Because no conventional reinforcement and shear reinforcement are required and prestressing will be applied outside the concrete cross-section, the production cycle of an ultra-high performance fiber-reinforced concrete box girder will deviate from a conventional concrete box girder. The sequence of work to cast the complete section in a single pour will be as follows:

1. Positioning all the shutters.
2. Assembling the tendon ducts at the deck and floor for the transverse prestressing and assembling the cast-in provisions for the anchors and deviators.
3. Casting the complete deck section over the full segment length.
4. Curing of concrete and carrying out heat treatment.
5. Installation of the transverse and central prestressing.
6. Lowering of the formwork.
7. Launching the deck forward by one increment.

Figure 10.9: a temporary gangway, which gives safe and reliable access to the substructure

Figure 10.10: bridge piers can only be accessed by boats

For The Zeeburgerbrug, a segment was constructed in a weekly cycle (Figure 10.11). Two and a half days were available to assemble reinforcement and prestressing ducts. The weekends were necessary for the concrete to develop sufficient strength to be able to apply the prestressing on Mondays. Launching one segment of 29 meters long took approximately four hours (Lugthart, 1987).

tasks	mo		tu		we		th		fr		sa		su		mo	
prestressing	■														■	
lowering of formwork		■														■
launching by one segment		■														■
positioning of formwork			■													
assembling reinforcement and prestressing ducts			■	■	■	■	■	■								
casting of complete section									■	■						
hardening of concrete											■	■	■	■		

Figure 10.11: the traditional weekly cycle, which was used for The Zeeburgerbrug

The use of UHPC enables a quicker cycle to shorten the total construction time. Instead of using the weekends, just one full day of hardening should be enough for the concrete to develop sufficient strength. Since conventional and shear reinforcement are not required, one day should be enough to assemble the tendon ducts and cast-in provisions. This leaves a full day to cast the complete section, another full day to install the auxiliary steel construction to anchor or deviate the tendons and, lastly, a full day to install the transverse and central prestressing and launch the bridge by one segment. This will result in a five day cycle (Figure 10.12). However, when we adopt this five day cycle, there is no room for errors. Each activity can only take place when the previous one is finished. They all form one big critical path, and since this cycle includes shifts during the weekends, disturbance of the cycle will immediately have consequences for the entire building schedule.

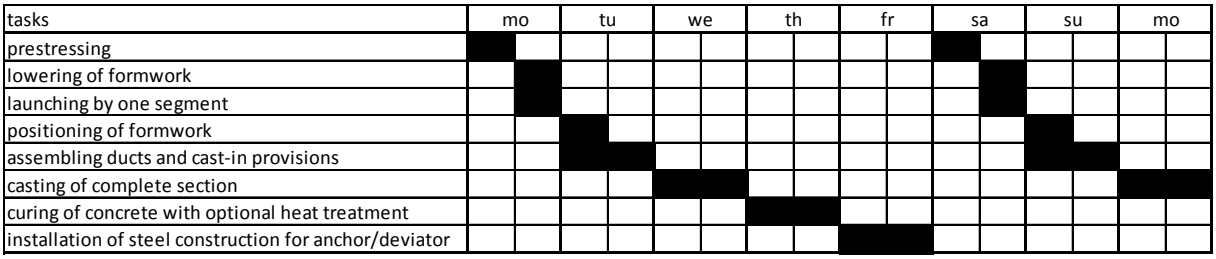

Figure 10.12: a five day cycle

With this in mind, it is better to use the weekly cycle of Figure 10.13, where the complete section is cast on Thursday, curing of concrete takes place on Friday and the weekends remain empty and can be used in case of an unexpected delay, for instance in the event of any problems with supply of concrete. Heat treatment is not required for early strength development but may be carried out on Friday to reduce any delayed time-dependent deformations and to improve durability. The auxiliary steel construction is connected to the inside of the box girder on Monday, and prestressing, lowering of formwork and launching happens on Tuesday. On Wednesday the cycle starts again with positioning of formwork and assembling ducts and cast-in provisions.

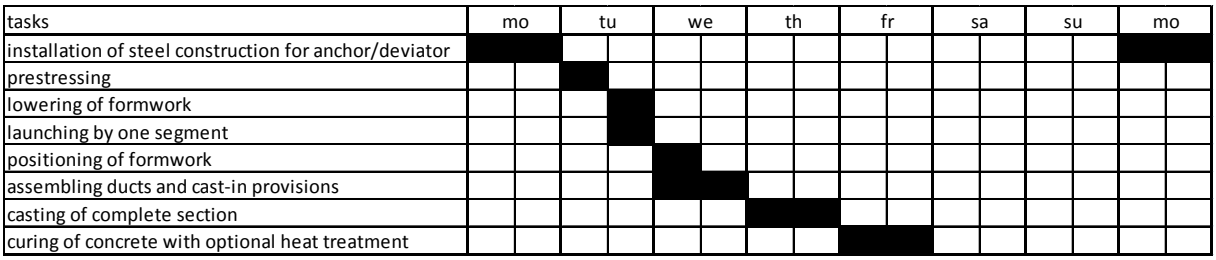

Figure 10.13: a weekly cycle for the use of UHPC

11 Cost

This chapter provides the cost to produce and launch the UHPFRC box girder and compares them to the cost of the design of The Zeeburgerbrug, which is an incrementally launched bridge built with normal strength concrete.

11.1 Cost of production of UHPC and NSC

The cost of production of UHPC are many times higher than the cost of production of traditional reinforced or prestressed concrete. Table 11.1 lists the cost of production of one cubic meter unreinforced UHPC. These are the cost just after leaving the batch plant when the concrete is ready to be cast in the box girder mould. As transportation distances are very short they are not taken into account. The cost have been provided by Gerard Filé, cost engineer at Royal HaskoningDHV. The quantities of the mixture components have been determined with Figure 5.2, which presents the typical composition of Ductal UHPC.

UHPFRC B150					
material	quantity		ppu (€)	total (€)	
cement	705	kg	0,120	84,60	
sand/gravel	1010	kg	0,018	18,18	
crushed quartz	210	kg	0,030	6,30	
silica fume	230	kg	0,300	69,00	
superplasticizer	17	kg	0,500	8,50	
reinforcing steel	0	kg	1,000	0,00	
steel fibers	190	kg	1,500	285,00	
prestressing steel	0	kg	2,500	0,00	
manufacture	1		30,00	30,00	
transport	0		-	-	
assembly	0		-	-	
				€ 502	cost per m^3 concrete

Table 11.1: cost of production of UHPC

Table 11.2 lists the cost of production of one cubic meter normal strength unreinforced concrete. The cost of manufacture of normal strength concrete $(€15/m^3)$ are considerably lower than for UHPC $(€30/m^3)$, because there are no fibers present in the mixture.

NSC B45					
material	quantity		ppu (€)	total (€)	
cement	350	kg	0,12	42,00	
gravel	1200	kg	0,018	21,60	
sand	600	kg	0,012	7,20	
filler	25	kg	0,15	3,75	
plasticizer	1	kg	0,5	0,50	
reinforcing steel	0	kg	1	0,00	
prestressing steel	0	kg	2,5	0,00	
manufacture	1		15	15,00	
transport	0		-	-	
assembly	0		-	-	
				€ 90	cost per m^3 concrete

Table 11.2: cost of production of normal strength concrete

As shown in Table 11.1 & Table 11.2 the cost of production of UHPC are approximately five times higher than of normal strength concrete. The question is: can these investments somehow be recovered in the longer term to make a profitable design in UHPC? To answer this question, the design of the UHPC box girder will be compared to the design of The Zeeburgerbrug by using them for the case study and then integrating all cost into a price per cubic meter of concrete.

11.1.1 General properties of The Zeeburgerbrug

The Zeeburgerbrug has a total length of 1,182 meters. The launched part consists of two double cell box girders of 864 meters long and has a typical span length of 58 meters. The spans are divided in two segments with joints at one fourth of the span length. The bridge is designed with concrete strength class B45. Auxiliary bridge piers were used to reduce peak bending moments during launch.

11.2 Cost components

11.2.1 Formwork

The cost per meter of formwork have been determined in paragraph 9.10. As both designs have nearly the same span length and each span is cast in two segments, the length of the formwork will be the same. The concrete cross-section of The Zeeburgerbrug has about twice the area of the cross-section of the design in UHPC. Therefore, the cost of the formwork and foundation will be a lot higher. The total cost of the formwork and foundation need to be divided by the total volume of concrete to find the cost of formwork per cubic meter of concrete.

11.2.2 Reinforcement and prestressing

The Zeeburgerbrug contains 110 kg reinforcing steel, 15.6 kg central prestressing steel and 21.2 kg continuity prestressing steel per cubic meter of concrete (van der Meulen, 1991).

The design in UHPC contains no ordinary reinforcing steel, 15 kg transverse prestressing steel, 140 kg central prestressing steel for the first two spans, 35 kg central prestressing steel for the rear spans and 53 kg continuity prestressing steel per cubic meter of concrete (Appendix 29).

11.2.3 Launching

Since the span length for both designs is almost equal and both designs have two segments per span, the number of launch operations will be the same. However, the cost per launch operation may differ. For traditional reinforced and prestressed concrete, the cost per launch operation have been already discussed in paragraph 9.10. The weight of the UHPC box girder is fairly lower than of The Zeeburgerbrug, which should benefit the launch process. For the design in UHPC, no longitudinal and shear reinforcement are required, which should simplify execution. However, the casting and curing of UHPC must be carefully carried out and may be time-consuming. The total cost for all launch operations should be divided by the total volume of concrete to find the launch cost per cubic meter of concrete.

11.2.4 Nose

The steel nose that was used for the execution of The Zeeburgerbrug had a length of 18 meters. The steel nose that will be used for the design in UHPC has a length of 15 meters. The cost of the steel nose must be divided by the total volume of concrete to find the cost of the steel nose per cubic meter of concrete.

11.2.5 Auxiliary bridge piers

During the execution of The Zeeburgerbrug, auxiliary bridge piers were used to control the bending moments. The total cost for all auxiliary bridge piers need to be divided by the total volume of concrete to find the cost of the auxiliary bridge piers per cubic meter of concrete.

11.3 Price index

The cost of all auxiliary bridge piers for The Zeeburgerbrug were $f\ 2{,}650{,}000.-$ in 1985. These cost must be multiplied by the price index over the period 1985 – 2015 to find cost that will apply nowadays. Table 11.3 presents the price index for the construction cost of a bridge over the period 1995 – 2015.

Index 1995-2015 (GWW 1995)					
cost component	estimated part (%)	t = 0 (nov 95)	t = 1 (jan 15)	cost t = 0 (€)	cost t = 1 (€)
personnel	40	100	171,5	40	68,60
fuel	1	100	223,1	1	2,23
steel	18	100	176,8	18	31,82
concrete	26	100	126,6	26	32,92
equipment	15	100	105,4	15	15,81
total	100			100	151,38

Table 11.3: price index construction cost 1995 – 2015

The price index for construction cost over the period 1985 – 1991 is 1.16 (van der Meulen, 1991). When this development is extrapolated until 1995 a price index of 1.29 is found. Combining both periods will give a price index of 1.96 for the period 1985 – 2015.

11.4 Comparing the designs in UHPC and NSC

When not just the cost of production, but also the cost of bridge execution are integrated in the price, the outcome is completely different. Table 11.4 & Table 11.5 show that the cost per cubic meter of UHPC have dropped from five times to twice the cost per cubic meter of NSC. The difference in cost per square meter of bridge deck is even smaller: just 30 %. The complete calculation can be found in Appendix 29. It should be said, however, that the cost per meter of formwork and the cost per launch operation were held the same for both designs, and that possible re-use of central prestressing in the UHPC box girder design was not taken into account. Which means, that a further reduction in cost per cubic meter of UHPC may be accomplished.

Incrementally launched UHPFRC box girder					
material	quantity		ppu (€)	total (€)	
cement	705	kg	0,120	84,60	
sand/gravel	1010	kg	0,018	18,18	
crushed quartz	210	kg	0,030	6,30	
silica fume	230	kg	0,300	69,00	
superplasticizer	17	kg	0,500	8,50	
reinforcing steel	0	kg	1,000	0,00	
steel fibers	190	kg	1,500	285,00	
prestressing steel	124	kg	2,500	309,10	
manufacture	1		30,00	30,00	
formwork	1			203,49	
launching	1			103,10	
nose	1			44,32	
				€ 1.162	cost per m^3 concrete
				€ 502	cost per m^2 bridge deck

Table 11.4: integral cost of the incrementally launched UHPFRC box girder

As can be seen in Table 11.1, steel fibers are a major cost factor in the cost of production of UHPC. There might be temptations to reduce the quantities. However, modifications in the fiber content will induce drastic changes in material behavior. The higher cost of production need to be compensated in a different way. The improved durability properties of UHPC compared to conventional concrete could be a solution, because they can reduce the maintenance cost of the structure significantly. Furthermore, the lower self-weight of the UHPC box girder should enable the engineer to design the substructure lighter to save more cost.

Design Zeeburgerbrug					
material	quantity		ppu (€)	total (€)	
cement	350	kg	0,12	42,00	
gravel	1200	kg	0,018	21,60	
sand	600	kg	0,012	7,20	
filler	25	kg	0,15	3,75	
plasticizer	1	kg	0,5	0,50	
reinforcing steel	110	kg	1	110,00	
prestressing steel	37	kg	2,5	92,09	
manufacture	1		15	15,00	
formwork	1			100,49	
launching	1			50,91	
nose	1			38	
auxiliary bridge piers	1			101	
				€ 582	cost per m^3 concrete
				€ 394	cost per m^2 bridge deck

Table 11.5: integral cost of The Zeeburgerbrug design

12 Conclusion

The main goal of this research project was to determine whether UHPFRC can increase the application range of incremental bridge launching and whether the combination results in an economical bridge design in The Netherlands. To answer this question a case study approach was used.

The following conclusions are based on the analysis of the cross-sectional capacity, in longitudinal direction, of simply supported concrete beams, which are loaded in pure bending.

- An increase in concrete compressive strength only leads to a small increase in bending moment capacity. The shear capacity is increased much more due to stronger concrete compression struts. The higher strength of the concrete can only be utilized when the amount of reinforcement or prestressing is increased.
- (Ultra) High strength concrete box girders can hold such large prestressing forces that it may not be possible to fit anchors and ducts inside the cross-section, so prestressing needs to be applied externally.
- Fibers have a huge contribution to the total shear capacity of UHPFRC. Absence of fibers in the concrete mixture or an unfavorable fiber orientation would have a detrimental effect on the shear capacity.
- Using very-high performance fiber-reinforced concrete instead of UHPFRC barely reduces the longitudinal bending moment and shear capacity of the box girder.

The following conclusions are based on the prestressed UHPFRC single cell box girder design that is used in the case study. This design is compared to the design of The Zeeburgerbrug, which used NSC, by using them at the location of the case study.

- Transverse prestressing is required to use UHPFRC efficiently and to transmit the mobile loads through the webs to the substructure. In contrast to conventional concrete box girders, transverse and shear reinforcement are not necessary.
- The fibers make shear reinforcement unnecessary and therefore allow very thin web design.
- The box girder can be launched without auxiliary supports.
- A steel nose longer than approximately one fourth of the span length already becomes too heavy and loses its purpose, and therefore is less effective than for traditional incrementally launched bridges.
- The required amount of central and continuity prestressing does not fit in the cross-section.

- Anchors and deviators do not fit in the concrete cross-section and need to be positioned outside the cross-section as well. As the inside of the box girder needs to remain uniform in order to be able to use the inner mould properly, anchors and deviators can only be installed after the complete segment is cast and the inner mould is moved to the next segment.
- As the box girder is designed without continuous longitudinal reinforcement, joints must always remain compressed and positioned at locations where peak moments will not develop.
- A complete section can be cast in a single pour, which ensures fiber continuity by avoiding a cold joint between the floor and the webs, and an activity can be taken away from the cycle.
- Pouring concrete in layers may result in an optimum fiber orientation to obtain the highest tensile and flexural properties.
- Prestressing can start after the concrete has hardened for just one day when a normal curing procedure is carried out. Heat treatment is not required for early strength development.
- The traditional weekly cycle can be accelerated to a five day cycle to shorten the total construction time. However, when we adopt this five day cycle, disturbance of the cycle will immediately have consequences for the entire building schedule.
- The cost of production of one cubic meter of UHPFRC, just after batching, are approximately five times higher than the cost of producing the same amount of NSC. When execution cost are integrated in the price, the cost per cubic meter of UHPFRC are reduced to approximately twice the cost per cubic meter of NSC. The difference in cost per square meter of bridge deck is even smaller: just 30 %.
- The remaining part of the higher cost of production of UHPFRC need to be recovered in a different way, for instance by savings in maintenance cost due to better durability properties or by a lighter substructure as we are able to save a lot of weight in the superstructure.

When the superstructure is considered only, it may be hard to design and execute an UHPFRC box girder, which is more economical than the design of The Zeeburgerbrug, which used NSC. However, when the total bridge (including the substructure) is considered over the entire service life we might have a competitive design.

13 Discussion

13.1 General remarks

Longitudinal reinforcement has proved to be unnecessary. However, the absence of reinforcement is not just positive. Since there is no continuous reinforcement in the joints, tensile stresses will force the joints to open and thus cannot occur. This means, that the tensile capacity of the concrete cannot be used to generate savings in the amount of prestressing that is required.

The length of a segment is very important for the structural safety of the bridge. Joints should be positioned away from locations where peak moments develop. For structural safety, it is best to work with two segments per span. Even though this might not be the cheapest option, it creates the least weak points in the structure.

It may be difficult to achieve an optimum fiber orientation, as the presence of prestressing ducts and the complex shuttering for the box girder have an additional influence on the flow of the fiber concrete. Since fiber orientation defines the mechanical behavior of UHPFRC it should be monitored closely. In addition, it is important to achieve a homogeneous fiber distribution in all parts of the box girder. Too large spaces without fibers and fiber segregation should be avoided. Self-compacting concrete can be an outcome, as it flows under its own weight and fibers therefore may align in appropriate directions during flow. And since additional compaction is unnecessary, fibers will remain in their original positions.

13.2 Limitations

While this study has tried to assess whether application of UHPFRC in incremental bridge launching can result in economical bridge designs, the study itself was not completely free from limitations. For one, there are still no (inter)national acknowledged regulations for designing with UHPFRC, making it hard to prove that a structure has sufficient reliability. Work towards such regulations has recently been conducted. (Association Francaise de Génie Civil, 2013) have developed recommendations for designing with UHPFRC. This document is compatible with the Eurocode, the regulation document for conventional concrete. (VSL Australia, 2000), the Australian office of the producer of Ductal UHPFRC, has developed a design guideline for Ductal prestressed concrete beams, which is based on the AFGC recommendations. These two documents are used for the design of the UHPFRC box girder, however as these documents are not finalized it is hard to get an UHPFRC structure approved by the authorities.

Another limitation of this study is the result of the limited literature available on box girder distortion. This study has shown that bending moments in the deck and floor due to box girder distortion are negligible. However, due to the limited literature available, the moment values are based on a box girder with other dimensions than the UHPFRC box girder. This means that there might be a slight deviation in the outcome.

Finally, for the launch phase, only the critical load case, where the box girder cantilever is maximum and the steel nose ends just before the next support, has been addressed. The load case where the steel nose has passed the next bridge pier was not considered.

13.3 Recommendations for further research

The analysis of the cross-sectional capacity of a simply supported UHPFRC prestressed box girder, loaded in pure bending, has revealed that a design in very-high performance fiber-reinforced concrete will hardy affect the bending moment and shear capacity in longitudinal direction, just 3% and 1% respectively. However, since there is no datasheet with the mechanical properties of a VHPFRC mixture available, they have been obtained by reducing the mechanical property values of UHPFRC by 20%. As the UHPFRC box girder can easily handle all compressive forces during launch and lifetime and early strength development is not an issue, further work on using VHPFRC in the design and execution, to save in cost of production, would be beneficial.

Until now, UHPFRC has not been applied on a large scale in The Netherlands. Due to strict rules regarding quality control, UHPFRC is usually produced in a factory. To guarantee the reliability of the material, one could investigate a different concept where the segments are precast in a factory, then transported to the construction site and connected by external prestressing.

The optimization study of the nose has identified that a nose, which is longer than approximately one fourth of the span length, becomes too heavy and loses its purpose, whereas for incrementally launched bridges, designed in conventional concrete, the steel nose has usually a length of 60% of the span length. In order to reach longer spans, and to save in the amount of central prestressing that is required, further studies regarding possible weight reduction of the steel nose would be worthwhile. Perhaps, a truss girder can provide the answer. Maybe it is even possible to reduce the cantilever moment by combining a nose with guying from a mast. This, however, requires constant adjustment to the forces in the cables during launch.

This study has shown that UHPC can easily handle the high prestressing forces, even after just one full day of hardening. However, since the prestressing tendons are applied outside the concrete cross-section, the prestressing forces must be transferred to the concrete from steel auxiliary constructions that are connected to the concrete with bolts and cast-in provisions. The connection might be a source of weakness, which has not been evaluated in the study. More research is required to determine the limitations and failure mechanisms of this solution. If it proves to be able to transfer such high prestressing forces into the concrete, even longer spans will be possible and bridge spans that are build with precast elements, and therefore have limited span length due to crane capacity and transport, can be outreached.

UHPC enables the box girder to be designed with light and slender elements. Due to the absence of auxiliary supports, the first segments will be subject to very high compressive forces exerted by the huge amount of central prestressing that is required to balance the massive cantilever bending moment. This study does not include a check on buckling of the thin-walled box girder. Further research on the buckling capacity of an UHPC box girder needs to be carried out to determine whether these high compressive forces will not cause instability.

The cost comparison has shown that the cost per cubic meter of UHPC are only twice the cost per cubic meter of NSC when the cost of execution are also integrated in the price. However, the cost per meter of formwork and the cost per launch operation were held the same for both designs, although the superstructure of The Zeeburgerbrug is a lot heavier than the UHPC box girder, uses auxiliary supports that need to be staffed during launch and possible reuse of central prestressing was not taken into account. Therefore, further compensation of the higher cost of production of UHPC is likely. More research is required to determine under what circumstances central prestressing may be reused as continuity prestressing.

14 References

Association Francaise de Génie Civil, 2013. *Ultra high performance fibre-reinforced concretes - recommendations.* revised ed. Paris: AFGC.

Behloul, M., 1999. *Design rules for DUCTAL prestressed beams,* s.l.: s.n.

Bogue, R. & Lerch, W., 1934. Hydration of Portland Cement Compounds. *Industrial & Engineering Chemistry,* 26(8), pp. 837-847.

Bourne, S., Minto, B., Platt, F. & Slater, D., 2009. Design and construction of Clackmannanshire Bridge, Scotland. *Proceedings of the institution of Civil Engineers - Bridge Engineering,* 162(BE4), pp. 167-187.

Burge, T. A., 1982. 14,000 psi within 24 hours. *Concrete International ,* 5(9), pp. 36-41.

CAE Nederland B.V., 2011. Rekenmodel VVUHSB. *Cement,* 60(3), pp. 50-57.

Caffrey, J., Burton, T. & Higgins, J., 2003. *Broadmeadow Estuary Bridge: Integration of Design and Construction,* Dublin: The Intitution of Engineers of Ireland - Civil Division.

Cement, 1966. Access viaducts. *Cement,* 18(4-5), pp. 225-228.

Cement, 1990. Ringweg om Amsterdam voltooid. *Cement,* 42(10), pp. 8-12.

Cement, 2012. Ultra hogesterktebeton. *Cement,* 64(6).

de Ridder, J., de Clercq, E. & Vanhaleweyk, J., 2003. Schuiven en vijzelen binnen de perken. *Cement,* 55(4), pp. 44-47.

Dywidag-Systems International, 2015. *Dywidag Bonded Post-Tensioning Systems using Strands.* [Online]
Available at: http://www.dywidag-systems.com/

Eberwijn, J., 1984. Tendenzen in de bruggenbouw. *Cement,* 36(2), pp. 88-93.

G.tecz Engineering, 2015. *Quantz technology, the next generation of UHPC.* [Online]
Available at: http://www.gtecz-engineering.com/concrete-technologies/quantz-uhpc-technology/performance/

Hewson, N., 2003. Incrementally launched box girder bridges. In: *Prestressed Concrete Bridges: Design and Construction.* London: Thomas Telford, pp. 262-281.

Hofstede, K., Hok-Bhe, T., Licht, R. & van Waarde, F., 2014. Van spoorstaafspanning naar betonspanning. *Cement,* 66(6), pp. 45-51.

Homberg, H. & Ropers, W., 1965. *Fahrbahnplatten mit veränderlicher dicke.* Berlin - New York: Springer - Verlag.

Iversen, N., Faulds, J. & Rowley, F., 1993. Design and construction of the Dornoch Firth Bridge. *Proceedings of the Institution of Civil Engineers - Transport,* 100(3), pp. 133-144.

Krebs, A. & Lindlar, H.-G., 1988. Zur Profilverformung einzelliger Kastenträger. *Beton- und Stahlbetonbau,* 83(1), pp. 13-18.

Kuiper, B., 2003. Een reuze viaduct voor een wereldgigant. *Cement,* 55(6), pp. 24-27.

Lafarge and Bouygues, 2015. *Ductal.* [Online]
Available at: http://www.ductal.com/wps/portal/ductal/2-Structural

Lafarge Ductal, 2009. *Technical Datasheet Ductal FM Grey,* s.l.: Lafarge Ciments.

Lau, C., Hul, C., Wong, K. & Leung, Y., 2000. Prestressed concrete application in bridges in the Hong Kong Airport Core Programme projects. *Structural Concrete,* 1(1), pp. 27-45.

Leonhardt, F., 1979. *Vorlesungen über Massivbau - Sechster Teil: Grundlagen Des Massivbruckenbaues.* Berlin: Springer-Verlag.

Locher, F., Richartz, W. & Sprung, S., 1976. Erstarren von Zement Toil 1: Reaktionen und Gefugeentwicklung. *Zement-Kalk-Gips,* 29(10), pp. 435-442.

Lugthart, J., 1987. Uitvoeringstechnische aspecten Zeeburgerbrug. *Cement,* 39(8), pp. 51-55.

Mandic Ivankovic, A., Kresimir, I. & Martinkovic, B., 2014. Competitiveness and progress in application of incremental bridge launching. *37th Madrid IABSE Symposium 2014,* pp. 3-10.

Markovic, I., 2006. *High-Performance Hybrid-Fibre Concrete - Development and Utilisation - ,* Delft: DUP Science.

Markovic, I., 2006. *High-Performance Hybrid-Fibre Concrete: development and utilisation,* Delft: DUP Science.

Meester, H., 1979. Schuiven - viaductenbouw zonder verkeersstremmingen. *Cement,* 31(5), pp. 215-219.

Nelissen, M., 1987. Doorbraak in toepassing van uitwendige voorspankabels. *Cement,* 37(12), pp. 56-59.

Oostra, A. J., 2014. *Literature Review MSc Thesis: UHPFRC in incremental bridge launching,* Delft: s.n.

Oostra, A. J., 2014. *Literatuurstudie MSc Thesis - UHPC in schuifbruggen,* Amsterdam: s.n.

Powell, L., Breen, J. & Kreger, M., 1988. *State of the art externally post-tensioned bridges with deviators,* Austin: Center for transportation research, Bureau of engineering research, The university of Texas at Austin.

Projectbureau ViA15, 2015. *Doortrekkingsalternatief A15.* [Online]
Available at: http://via15.nl/kaart/trace-verlegde-bocht.html

Projectbureau ViA15, 2015. *ViA15.* [Online]
Available at: http://www.via15.nl/

Quartel, K., 1989. Tweede van Brienenoordbrug snel klaar dankzij prefabricage. *Cement,* 39(3), pp. 10-20.

Quartel, K., 2011. KW520: Ontwerp. *Cement,* 63(6), pp. 38-44.

Reinhardt, H., 1985. *Beton als constructiemateriaal - eigenschappen en duurzaamheid.* Delft: Delftse Universitaire Pers.

Rijkswaterstaat, 2011. *Richtlijnen Vaarwegen.* Delft: RWS Dienst Verkeer en Scheepvaart.

Rijkswaterstaat, 2013. *Richtlijnen Ontwerpen Kunstwerken.* 1.2 ed. s.l.:RWS Dienst Infrastructuur.

Rijkswaterstaat, 2013. *ViA15 Werktekening, Voorlopig Ontwerp.* s.l.:s.n.

Rijkswaterstaat, 2015. *A27: verbreding traject Houten - Hooipolder.* [Online]
Available at: http://www.rws.nl/wegen/plannen_en_projecten/a_wegen/a27/houten_hooipolder/

Rijkswaterstaat, 2015. *Bezoekerscentrum Schiphol - Amsterdam - Almere.* [Online]
Available at: http://bezoekerscentrum.rijkswaterstaat.nl/SchipholAmsterdamAlmere/?work=tweede-hollandse-brug

Rosignoli, M., 1997. Influences of the incremental launching construction method on the sizing of prestressed concrete bridge decks. *Proceedings of the Institution of Civil Engineers - Structures & Buildings,* 122(3), pp. 316-325.

Savor, Z., 2008. *Croatian Bridges designed by Structural department of Zagreb Civil Engineering Faculty utilizing Sofistik software,* Zagreb: University of Zagreb.

Schlaich, J. & Scheef, H., 1982. *Concrete Box Girder Bridges.* Stuttgart: International Association for Bridge and Structural Engineering.

ten Voorde, A., Barten, P., Jansen, R. & Laurijsen, H., 2011. Brugligger zonder druklaag. *Cement,* 63(7), pp. 78-82.

Thomaes, T., Janssen, H., Maas, P. & Robaard, M., 1974. Viaduct Ravensbosch; eerste toepassing schuifmethode in Nederland. *Cement,* 26(3), pp. 102-121.

van Breugel, K., 2013. *Course CIE5110 - Concrete, Science & Technology,* s.l.: TU Delft.

van den Broek, H. & van den Hoonaard, J., 1975. De nieuwe brug over de IJssel bij Zutphen. *Cement,* 27(5), pp. 187-197.

van der Horst, A. et al., 2012. Fietsbrug over de Deltawerken. *Cement,* 64(2), pp. 70-73.

van der Horst, A. et al., 2012. Geribbelde en gelijmde moten. *Cement,* 64(5), pp. 56-60.

van der Horst, A. et al., 2012. Voorspanning in fietsbrug. *Cement,* 64(3), pp. 18-23.

van der Meulen, C., 1991. *Optimalisering kokerbrug: voorstudie afstudeeropdracht,* Tilburg: TU Delft, Faculteit der Civiele Techniek, Vakgroep Mechanica en Constructies, Sectie Betonconstructies.

van der Meulen, C., 1992. *Algemene ontwerpberekening prismatische kokerbruggen - eindstudie,* Tilburg: s.n.

van der Veen, C., 2014. *Course CIE5127 - Concrete Bridges,* s.l.: TU Delft.

van der Veen, C., 2014. *Course CIE5127 - Concrete Bridges,* Delft: TU Delft.

Vermeulen, G., Kaptijn, N. & van der Veen, C., 1993. Uitwendige voorspanning in schuifbruggen. *Cement,* 45(12), pp. 46-51.

Virlogeux, M., 1993. Normandie Bridge Design and construction. *Proceedings of the Institution of Civil Engineers - Structures & Buildings,* 99(3), pp. 281-302.

Virlogeux, M., 2002. New trends in prestressed concrete bridges. *Structural Concrete,* 3(2), pp. 67-97.

Völkers, E., 2012. Nieuwe tuibrug in A50. *Cement,* 64(3), pp. 12-17.

Vriend, H. d., 1975. Prefabricage of ter plaatse storten. *Cement,* 27(6), pp. 317-320.

VSL Australia, 2000. *Design guidelines for Ductal prestresed concrete beams,* Sydney: School of Civil and Environmental Engineering, The University of New South Wales.

VSL International LTD., 1977. *The incremental launching method in prestressed concrete bridge construction,* Bern: Gerber AG, Schwarzenburg.

Walraven, J. C. & Braam, C. R., 2011. *Course CIE4160: Prestressed Concrete - Textbook,* Delft: s.n.

Zellner, W. & Svensson, H., 1983. Incremental Launching of Structures. *Journal of Structural Engineering,* 109(2), pp. 520-537.